Seismic hazard of the Izmir region, Turkey, based on a probabilistic seismic hazard assessment and stochastic ground motion simulations

Krister Moberg

Master of Science Thesis

Department of Earth Science

University of Bergen

June 2015

"*Whatever you do, work at it with all your heart,*
as working for the Lord, not for human masters"
Colossians 3:23

Abstract

The purpose of this thesis is to conduct a seismic hazard analysis of the region surrounding Izmir. The chosen area is located in a very active seismic region with a high seismicity due to large amount of earthquakes. In the past, several destructive and deadly earthquakes have affected this region. These destructive earthquakes can potentially be very dangerous and affect millions of people, especially in densely populated coastal areas close to Izmir. Due to previous severe earthquakes, the public awareness of potential new destructive earthquakes in the region is high. In this thesis, an analysis of the seismic hazard in a broad region surrounding Izmir is performed.

Two ground motion methods are conducted in order to measure the maximum ground motion in terms of acceleration of gravity. One of the methods is a probabilistic seismic hazard assessment, computing ground motion values by using different return periods for a fixed probability of exceedance. The second method includes stochastic ground motion simulations, giving maximum possible ground motion values from several large faults by using a reference earthquake, such as the Izmir fault, the Manisa fault, the Karaburun fault, the Seferihisar fault, the Tuzla fault or the Samos fault.

Three areas are identified with a significant hazard. These areas include the Izmir metropolitan, the area between the cities of Manisa, Akhisar and Salihli, and the northern part of the Karaburun Peninsula. The highest identified PGA values, by using the PSHA, are found in the area between the cities of Manisa, Akhisar and Salihli. This area have a PGA of up to 0.33g, by using a return period of 475 years. In the Izmir metropolitan, the highest PGA values using the PSHA with a return period of 475 years is 0.27g. By using the stochastic simulation, a maximum PGA value of 0.3g was found at the Izmir fault, using a reference earthquake of M_W = 6.8. A maximum PGA value of 0.5g was found using a reference earthquake of M_W = 6.9 on both the Karaburun and the Tuzla fault. A maximum PGA value of 0.6g was found using a reference earthquake of M_W = 6.6 on the Seferihisar fault. Other high PGA values between 0.2g and 0.3g were found by using stochastic simulations on the Manisa and the Samos fault.

Foreword

This master's thesis is carried out at the Department of Earth Science, University of Bergen, in the period from August 2014 to June 2015.

I would like to thank my supervisors Mathilde Sørensen, Kuvvet Atakan and Lars Ottemöller for being helpful and supporting throughout my time as a master student. It has always been a pleasure to meet you for discussions and guiding.

I specially want to thank Mathilde Sørensen and Kuvvet Atakan. You have spent much of your time discussing, guiding, providing literature, and helping me through difficulties during the last two years. I also want to thank you all for taking the time to read parts of my thesis during the last year, and giving me helpful suggestions for improvement.

Furthermore, I would like to thank Lars Ottemöller for always having an open door if I needed help or had problems of any kind. You were always happy to help, which I appreciate. I am also thankful for you reading parts of my thesis.

I would further like to thank Tuğbay Kiliç for providing me seismic data from AFAD, as well as Jens Havskov for helping me with errors in Seisan.

Finally, I would like to thank my family for the continuous support and encouragement, and Jan Ketil Moberg for reading through the thesis.

June 2015
Krister Moberg

Table of contents

1. Introduction

The area surrounding Izmir is located in a seismically very active region, which poses a likelihood for having destructive earthquakes in the future based on the seismicity and past historical destructive events. The area around Izmir is located within the western part of the Anatolian plate, and yet is close to several plate boundaries, such as the African plate in south, the Arabian plate in southeast, the Eurasian plate in north as well as some minor continental blocks, indicating high seismicity in the study area, which can provide a high seismic hazard (Taymaz et al., 1991).

It is important to conduct seismic hazard analyses in this region, simply because public awareness is critical for the threat that this region faces. Destructive events can potentially be very dangerous and affect millions of people, especially in densely populated coastal areas close to Izmir. Destruction from historical as well as recent earthquakes in Turkey has increased the interest for seismic hazard and risk assessments in urban areas mainly for the metropolitan area of Istanbul, but also for other major cities such as Izmir. The fact that this area is exposed for such high hazard makes this topic of great importance (Deniz et al., 2010).

A problem with earthquakes is the fact that they often occur unexpectedly. Currently there is not any scientific consensus on predicting earthquakes in short time scales, even though earthquake early warning based on a set of precursory phenomena such as foreshocks or changes in deformation rates is to some extent possible. Although seismic hazard can not be reduced in a given area, the vulnerability of the buildings to ground shaking can be reduced lowering the risk. Therefore, any mitigation measure applied in a region plays an important role in reducing the level of risk. Seismic hazard mapping conducted in this thesis may help government authorities in implementing proper risk reduction measures taking into account the ground motion levels.

In historic times (i.e. pre-instrumental period), there have been several large destructive earthquakes in the region. In 1688, there was a great event in Izmir, and in 1739, another destructive event occurred in Foça. The latest significant earthquake was in 1778 and destroyed large parts of the city of Izmir (Ambrayseys and Finkel, 1995). In total 237 years have passed

since the last catastrophic earthquake, indicating that stresses have been building up and thus increase the likelihood of an upcoming destructive earthquake in the future.

During the instrumental period, several larger events have occurred in the area around Izmir. Some of the largest events during the last 70 years are the M_S = 6.8 large earthquake that occurred near the Gulf of Edremit, the M_S = 7.2 large earthquake that occurred 170 km north of Izmir back in 1953, the M_S = 5.2 large earthquake that occurred in Izmir in 1974, the M_S = 6.2 large earthquake that occurred 50 km SSW of Izmir in 1992, the M_W = 5.8 large earthquake that occurred 50 km southwest of Izmir in 2003, and the most recent sequence of three earthquakes in the bay of Sığacık in 2005, with M_S = 5.5, 5.9 and 5.9 (Deniz et al., 2010). Some of the important locations are shown in fig.1.1.

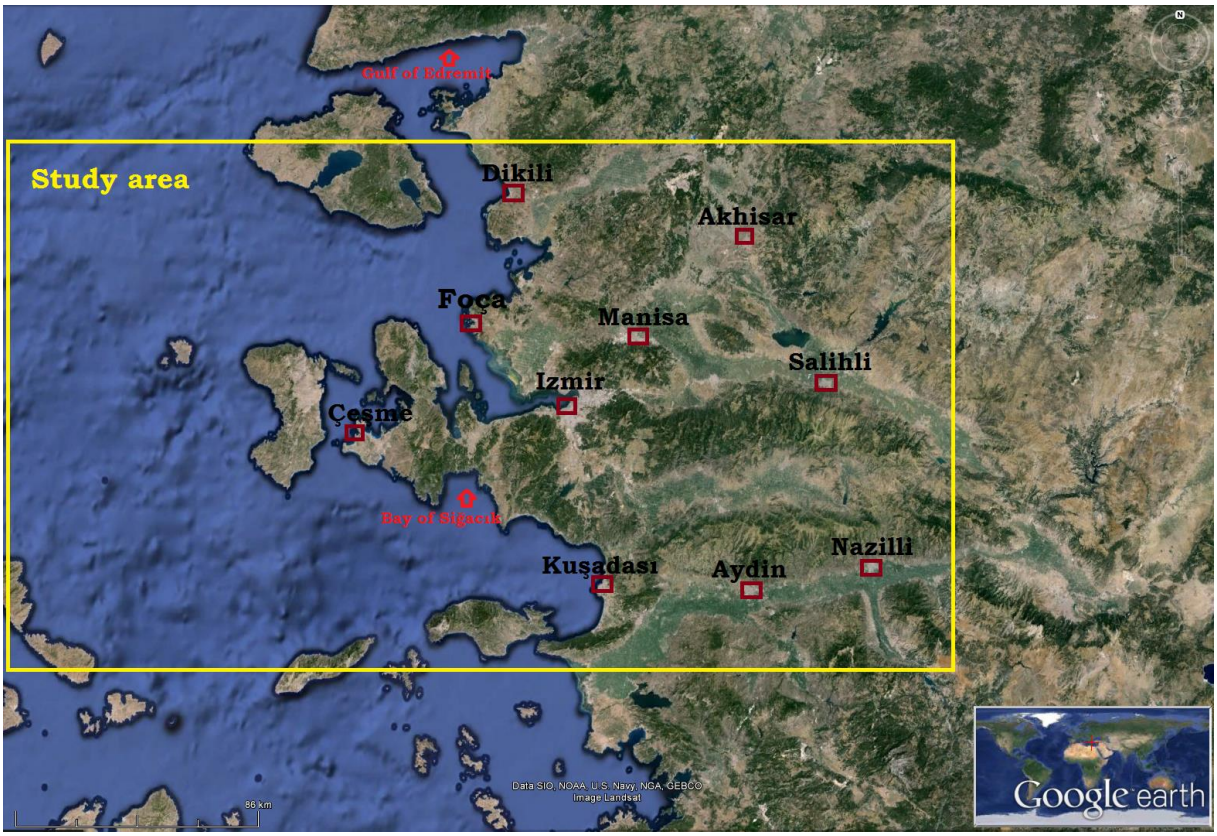

Fig.1.1. Map of the study area and other important places.

There have been several analyses carried out to estimate the seismic hazard in Izmir and its vicinity. Both Emre et al. (2005), RADIUS (1997), Akinci et al. (2013) and Korkmaz et al. (2009) have in recent years carried out seismic hazard assessments in the area around the Aegean microplate (Deniz et al., 2010). Some other important studies are the master plan

developed for the Metropolitan Municipality of Izmir (MMI, 2000), Bjerrum et al. (2013), Bjerrum et al. (2014a) and Bjerrum et al., (2014b).

In addition, a regional seismic hazard map for the Mediterranean in terms of peak ground acceleration was conducted as a part of the GSHAP (Global Seismic Hazard Assessment Program) project. Later, GSHAP has been used in order to carry out a newer and more detailed hazard map from the Mediterranean region named the SESAME (Seismotectonics and Seismic Hazard Assessment of the Mediterranean Basin) project (Jimenez et al., 2001). The SESAME project use the attenuation relationship from Ambrayseys et al. (1995) in terms of PGA and absolute spectral acceleration, and they measured PGA values of about 0.20g to 0.40g in the western part of Turkey for bedrock, stiff soil, soft soil, and very soft soil conditions. The EFEHR portal also have updated seismic hazard results from the SHARE project (EFEHR, 2015). This portal access data, models, tools and expertise for an assessment of the seismic hazard in Europe. They indicate PGA values of about 0.30g to 0.35g for the city of Izmir.

The study by Deniz et al. (2010) mainly focuses on a probabilistic seismic hazard analysis for Izmir. It also looks at earthquake statistics and employs a logic tree procedure in order to account for uncertainties. The different source zones are considered separately in order to calculate the hazard, by using two ground motion estimation models, expressed in peak ground acceleration, in g. From this study, a PGA value of 0.34g was estimated in Izmir for a return period of 475 years.

Another probabilistic seismic hazard assessment for Izmir was conducted in 2000, the so-called "the Izmir Earthquake Master Plan" (MMI, 2000) and it reports PGA values of about 0.2g - 0.4g for a return period of 475 years for bed rock conditions, and a bit higher values for soft soil conditions.

Korkmaz et al. (2009) studied the seismic risk in Izmir on reinforced concrete buildings. There were several estimation approaches used in order to study how the buildings react to heavy ground shaking. The results indicate that most of the buildings in Izmir can face heavy damage or even collapse, during possible strong future events.

RADIUS (1997) was a risk assessment for different cities, including the city of Izmir. The main goal was to give assessment tools for urban areas. There are also some studies done on ground

motion simulations, such as Akinci et al. (2013) and Bjerrum and Atakan (2008). The study from Akinci et al. (2013) provide a description of ground motion characteristics of the western parts of the Anatolian region.

The study by Bjerrum and Atakan (2008) conducted ground motions from different scenarios on important faults near Izmir. They found a worst case scenario for Izmir with peak ground accelerations of 291 cm/s^2. On the Tuzla and the Izmir fault, the maximum peak ground accelerations were 438 and 574 cm/s^2, respectively. Bjerrum et al. (2013) carried out ground motion simulations for Izmir, exceeding 600 cm/s^2. Bjerrum et al. (2014a), and Bjerrum et al. (2014b) carried out two additional studies, which looked at the building vulnerability with a risk assessment, and simulated ground motions with site effects potential, respectively.

In this thesis, the aim is to do a more broad analysis of the seismic hazard, including a larger region surrounding Izmir, than earlier carried out. Probabilistic seismic hazard analyses are conducted by computing the maximum ground motions from different return periods for a fixed probability of exceedance. In this approach, several steps are followed, starting with the definition of study area. An earthquake catalogue is then compiled as complete as possible. The next step is to map the earthquake sources in the area, both in order to use them in the zonation part and in the ground motion simulations. The second part of the study includes stochastic ground motion simulations, modelling large faults in the study area.

2. Background

2.1 Tectonic setting

Izmir (fig.2.1.1) is the third largest city in Turkey with approximately four million inhabitants, and it is located at the west coast of the Aegean Sea. Izmir is located in one of the most seismically active regions in the world, owing to the fact that this region is located close to three large plate boundaries that are in constant movement (Taymaz et al., 1991). Izmir has in recent history been subjected to several large destructive earthquakes. These events have several times destroyed the city, latest back in 1778, and because of this long and calm period there is reason to believe that stress has been building up in the area close to Izmir (Bjerrum and Atakan, 2008).

The Mediterranean Sea is the remaining's of the Tethys Ocean, which, separated Europe from Africa/Arabia prior to the lower Jurassic. Since lower Jurassic, the Tethys Ocean has been smaller and smaller due to the collision between the present African and the Eurasian plate. There was in Jurassic an Euler pole situated near Morocco, which migrated further west into the Atlantic Ocean. This provoked an anticlockwise rotation of the African plate and surroundings which is the reason for larger plate velocities in the eastern parts of the present Mediterranean (Duval et al., 1977).

The kinematics of the regional deformation of the Aegean-Anatolian region is controlled by three important factors seen in fig.2.1.1. These are the westward motion of the Anatolian microplate relative to the Eurasian plate, the collision between northwest Greece-Albania and the Apulia-Adriatic platform, and the presence of the Hellenic subduction zone to the south of the Aegean province (Taymaz et al., 1991).

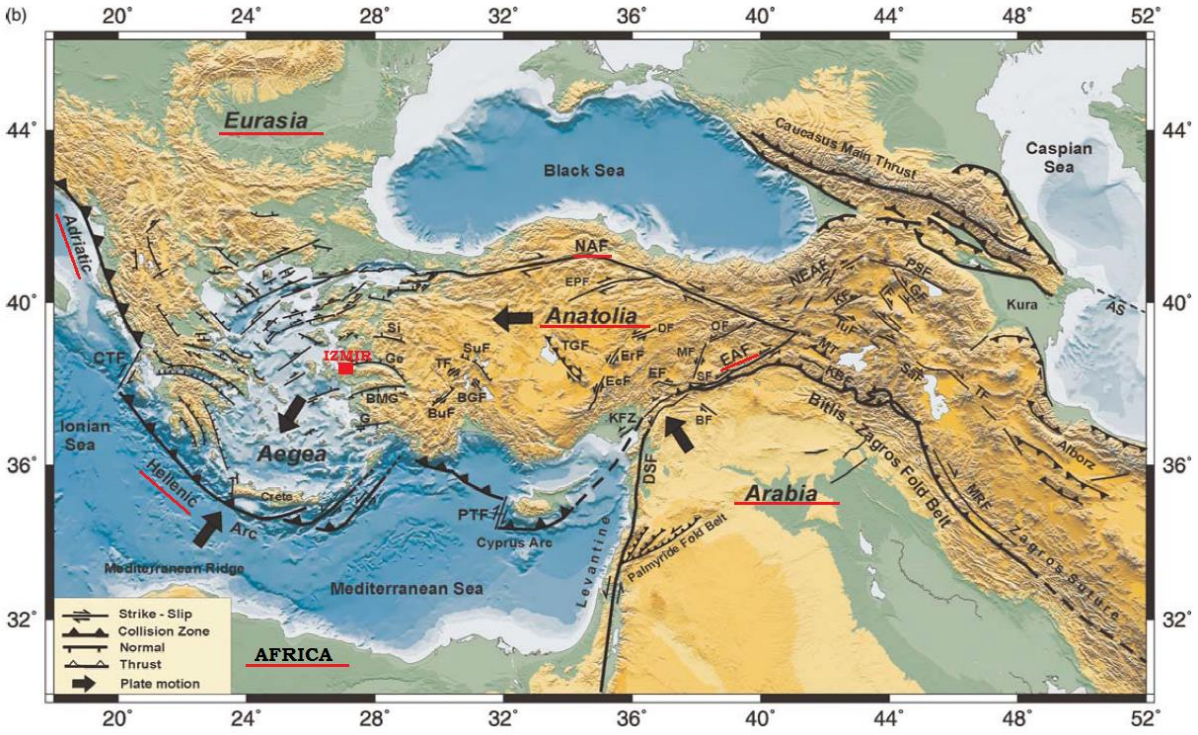

Fig. 2.1.1. The eastern Mediterranean region, including faults and relative motions between plates/microplates. Large black arrows show relative plate motions with respect to the "stable" Eurasia. Izmir is in the red box. Solid black lines show faults and plate boundaries. The Arabian plate is located in southeast (red underline), the Eurasian plate is located in northwest (red underline), the Anatolian microplate (red underline) is located between Eurasia and the Arabian plate, and the African plate is located south (red underline) in the figure. The Adriatic plate is located in west (red underline) and the Aegean microplate (red underline) is located in the Aegean Sea. The North Anatolian Fault and the Eastern Anatolian Fault is marked with a red underline. (Taymaz et al., 2007).

The westward motion of the Anatolian microplate is related to a collision in eastern parts of Turkey and in Caucasus between the Arabian plate in southeast and the Eurasian plate in northwest. This motion is accommodated along two large well known strike-slip faults (Taymaz et al., 1991). One of them is situated north in Turkey and is called "the North Anatolian Fault" (NAF). It has a right lateral displacement and the other one is situated to the southeast and is called "the East Anatolian Fault" (EAF) which has left lateral displacement as seen in fig.2.1.1 (Taymaz et al., 2007). The collision between the Arabian and the Eurasian plate causes a crustal thickening, and the effect of the crustal thickening provides a buoyancy force that drives the Anatolian plate westwards, a process which has started about 12Myr ago back in mid-Miocene (Taymaz et al., 1991).

In the Hellenic subduction zone (fig.2.1.1) the subducting slab penetrates into the mantle causing the overriding plate, in this case, the Aegean microplate to move southwards. This process generates extension together with a southward migration of the subduction zone and a corresponding slab retreat as well as volcanism in the Aegean province; (Taymaz et al., 2007; Jolivet et al., 2013). The overriding Aegean plate has since late Eocene - early Oligocene for about 35 Ma ago (the age is still under discussion) been subjected to extensional forces and the slab retreat has since then controlled the deformation of the Aegean microplate. The stretching and thinning of the crust appears stronger in central parts of Aegean compared to western Anatolia (Jolivet et al., 2013). This extension is important in understanding the focal mechanisms observed in the area around Izmir. The relative motion between the Africa plate and Aegean microplate (fig.2.1.1) is almost perpendicular on the location of the Hellenic arc (McClusky et al., 2000).

Today the deformation is self-sustaining, which means that the collision of the Arabian plate with the Eurasian plate is still active. This is causing accumulation of high topography in eastern Turkey and in Caucasus, driving the westward motion of the Anatolian and the Aegean plate. Continental material are still being pushed over the oceanic crust of the eastern Mediterranean forming the Hellenic subduction zone, and the subducting slab beneath the Hellenic trench thus maintain the present extension seen in the Aegean area (Taymaz et al., 1991). This extension is oriented NNE-SSW as shown in fig.2.1.2.

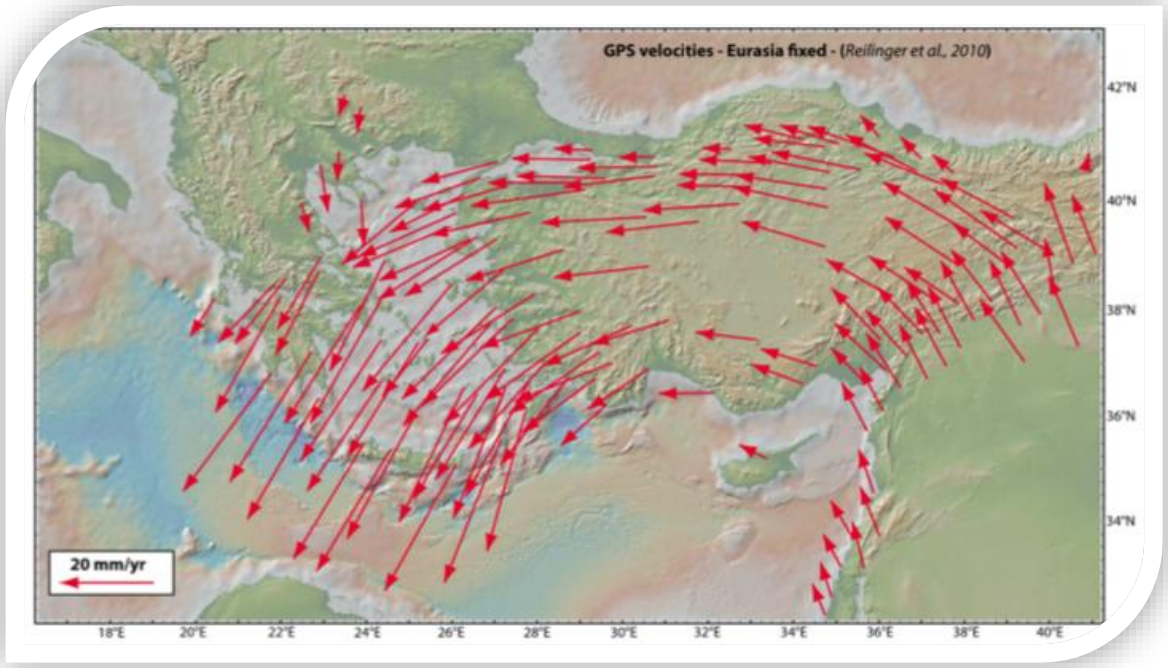

Fig. 2.1.2. Velocity map showing the relative motion of the Aegean-Anatolian region from GPS data derived by Reilinger et al. (2006), where the Eurasian plate is fixed. The Anticlockwise rotation of the Aegean microplate and the surrounding area is visible from these GPS data (Jolivet et al., 2013).

The Aegean plate moves westwards due to the crust- thickening in eastern Turkey and Caucasus and southwards because of pull from the Hellenic subduction zone. The resulting combination causes an anticlockwise rotation of the Aegean plate (fig.2.1.2), and thus a movement towards southwest (Taymaz et al., 2007). The entire region south of the North Anatolian Fault is involved in this rotational pattern as well as parts of the Arabian peninsula (Reilinger et al., 2006). The average velocity of the Aegean plate (fig.2.1.3) relative to Eurasia is 35 mm/yr, and the Anatolian microplate moves westward with a velocity of about 22-25 mm/yr relative to Eurasia (Benetatos et al., 2006). This anticlockwise rotation is visible on a velocity field map seen in fig.2.1.2, which is obtained from Global Position System- (GPS) results derived by Reilinger et al., (2006). The collision between Greece-Albania and the Apulia-Adriatic platform as seen in fig.2.1.1 leads to shortening of the continental crust, resulting in a resistance against the rotation of Greece and Albania (Taymaz et al., 1991).

From fig.2.1.3, it is seen a noticeable change in direction of the crustal part of the Aegean microplate near Izmir, where the direction changes from a SW- to a more SSW- direction (Nyst and Thatcher, 2004). It looks like the Izmir metropolitan (inside the red circle) is located at the

border between the Aegean and the Anatolian microplate, near a rotational point. This change in plate- direction also lead to reactivation of existing faults in all directions, which trigger normal faulting. The plate velocities as shown in fig.2.1.3 also increases from the Anatolian plate and south towards the Hellenic subduction zone because of the slab retreat effects (Aktuğ and Kılıçoğlu, 2006). This extension is the main driving force behind the reactivation of faults on both the Aegean microplate and at the western parts of the Anatolian microplate (Aktuğ and Kılıçoğlu, 2006).

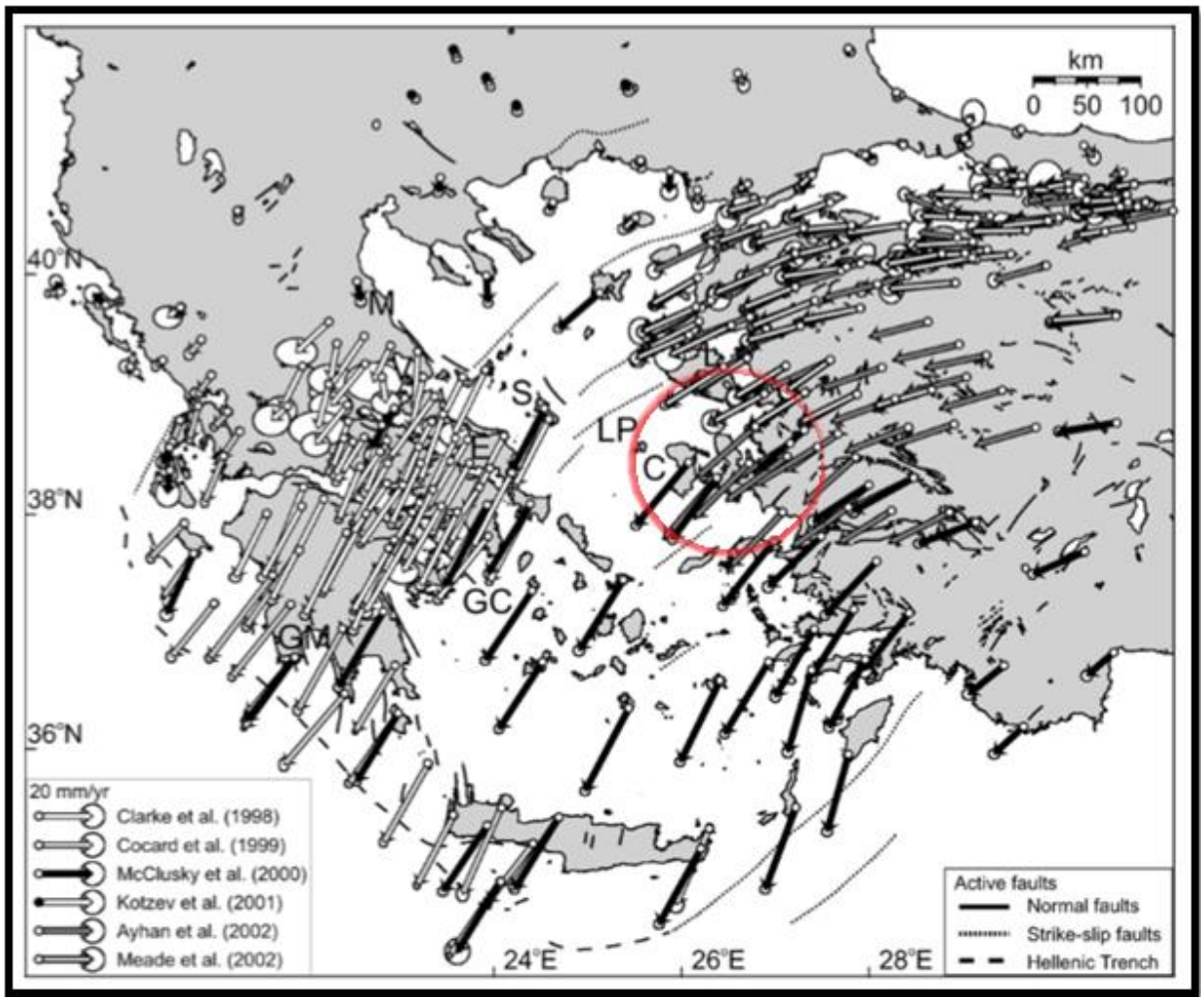

Fig. 2.1.3. GPS velocity field of the area around the Aegean Sea relative to the stable Eurasia. The Izmir metropolitan is marked by a red circle. Velocities relative to Eurasia are measured by GPS data. The length of the arrows depends on the velocity, and the shading indicate the data source (Nyst and Thatcher, 2004).

Izmir (fig.2.1.4) is located at the Aegean Sea on the west coast of Turkey and is situated at the Gulf of Izmir, which is a region dominated by north-south extension, which is expressed in E-W oriented graben structures seen in fig.2.1.5. This region belongs to the transition zone between the Anatolian microplate in east and the Aegean microplate in west. The southern part

of the Aegean microplate move with a velocity if about 35mm/yr towards south, while the African plate move with 10 mm/yr towards Eurasia. The Anatolian plate moves towards west with 22-25 mm/yr, relative to Eurasia (Benetatos et al., 2006).

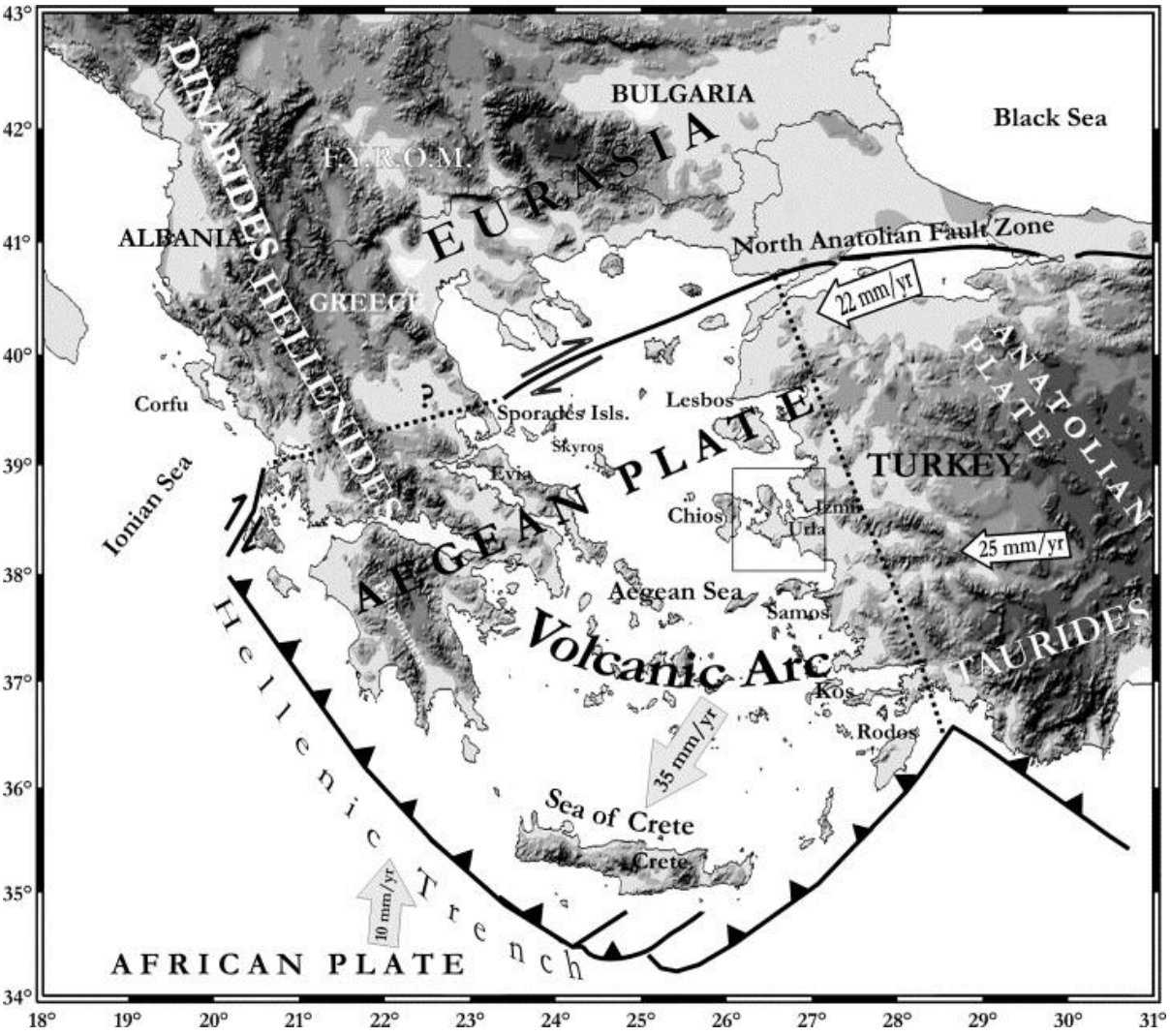

Fig.2.1.4. Important plates and their corresponding velocities relative to the stable Eurasia. Dashed lines mark the eastern and northern border of the Aegean plate. The small rectangle indicates the area surrounding Izmir (Benetatos et al., 2006).

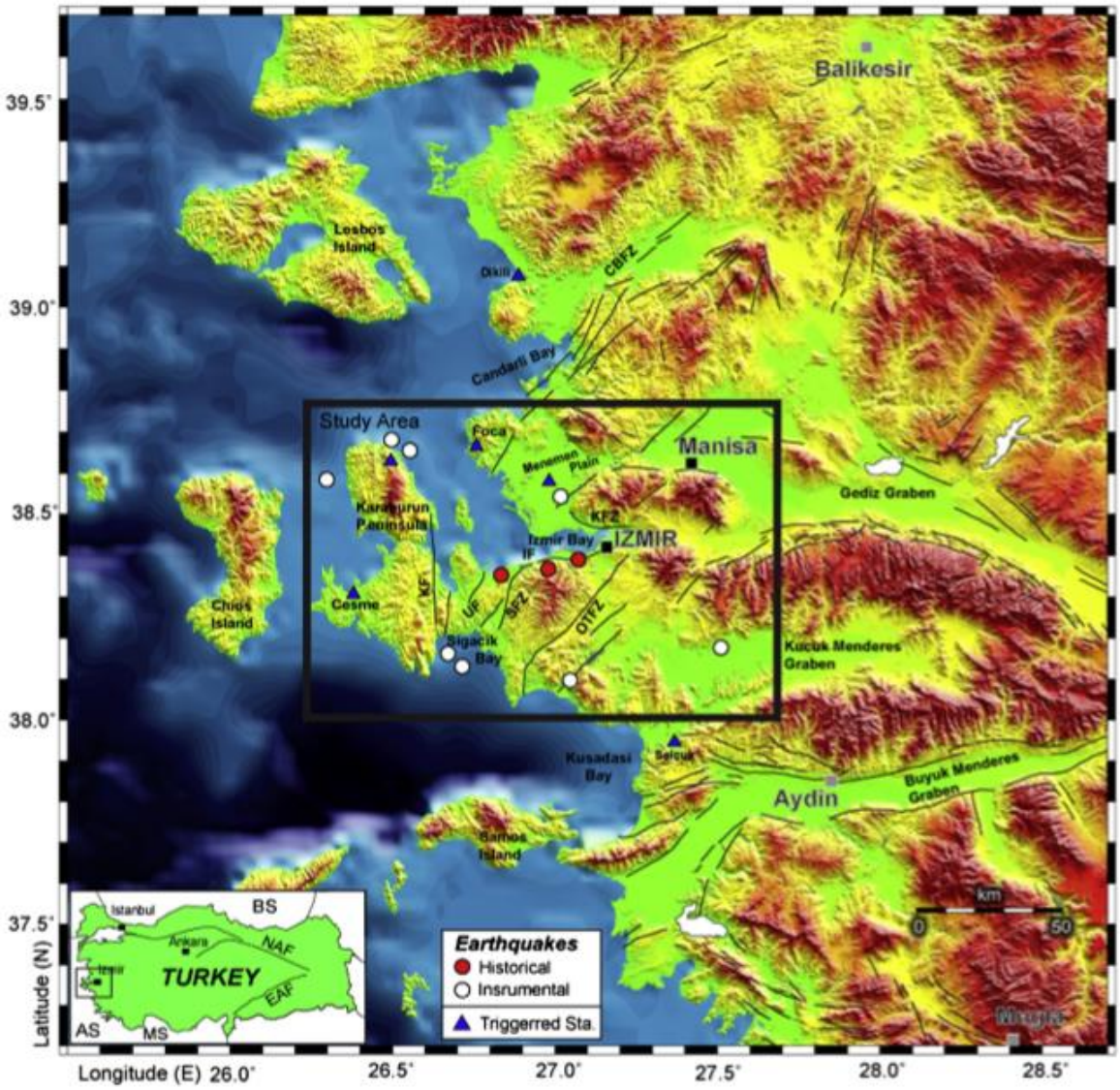

Fig.2.1.5. Topographic map showing important faults, grabens and structures in the Izmir-area. Tectonic features were compiled from Bozkurt (2001) and Emre et al. (2005). UF is the Urla fault, IF is the Izmir fault, KF is the Karaburun fault, KFZ is the Kamalpasa fault, and SFZ is Seferihisar fault. Historical earthquakes are pointed in red, instrumental in white and stations in blue. In the left corner is a map showing Turkey with Izmir in a small box, were also NAF/EAF is plotted in the small map (Gok and Polat, 2014).

In fig.2.1.5 there are several faults reactivated by extension and the anticlockwise rotation. The most prominent faults (fig.2.1.6) in the area are the Karaburun Fault (KF), the Urla Fault (UF), the Izmir Fault (IF), and the Tuzla Fault (TF) (Benetatos et al., 2006). Ocakoğlu et al. (2005) identified KF as an active revers fault, UF as an N-S trending reverse fault, IF as an E-W trending normal fault, and TF as a dextral strike-slip fault (Benetatos et al., 2006). The Tuzla Fault lies between Menderes and Doganbey Cape and is trending NE-SW with an offset of about 200-700m. In 1992, a magnitude 6.0 earthquake occurred on this fault, and the largest

extensional rate in the region occurs at parts of this fault, which confirms its active state. Further east lies another important fault, called the Manisa Fault. This is about 25 km in length and trending NW-SE. East of this fault lies the Kemalpasa fault which is a about 20 km in length and is located on the southwestern side of the Gediz graben as shown in fig.2.1.5 (Aktuğ and Kılıçoğlu, 2006). The tectonics in the area is complex, and fig.2.1.6 show the faults close to Izmir even better (Aktuğ and Kılıçoğlu, 2006).

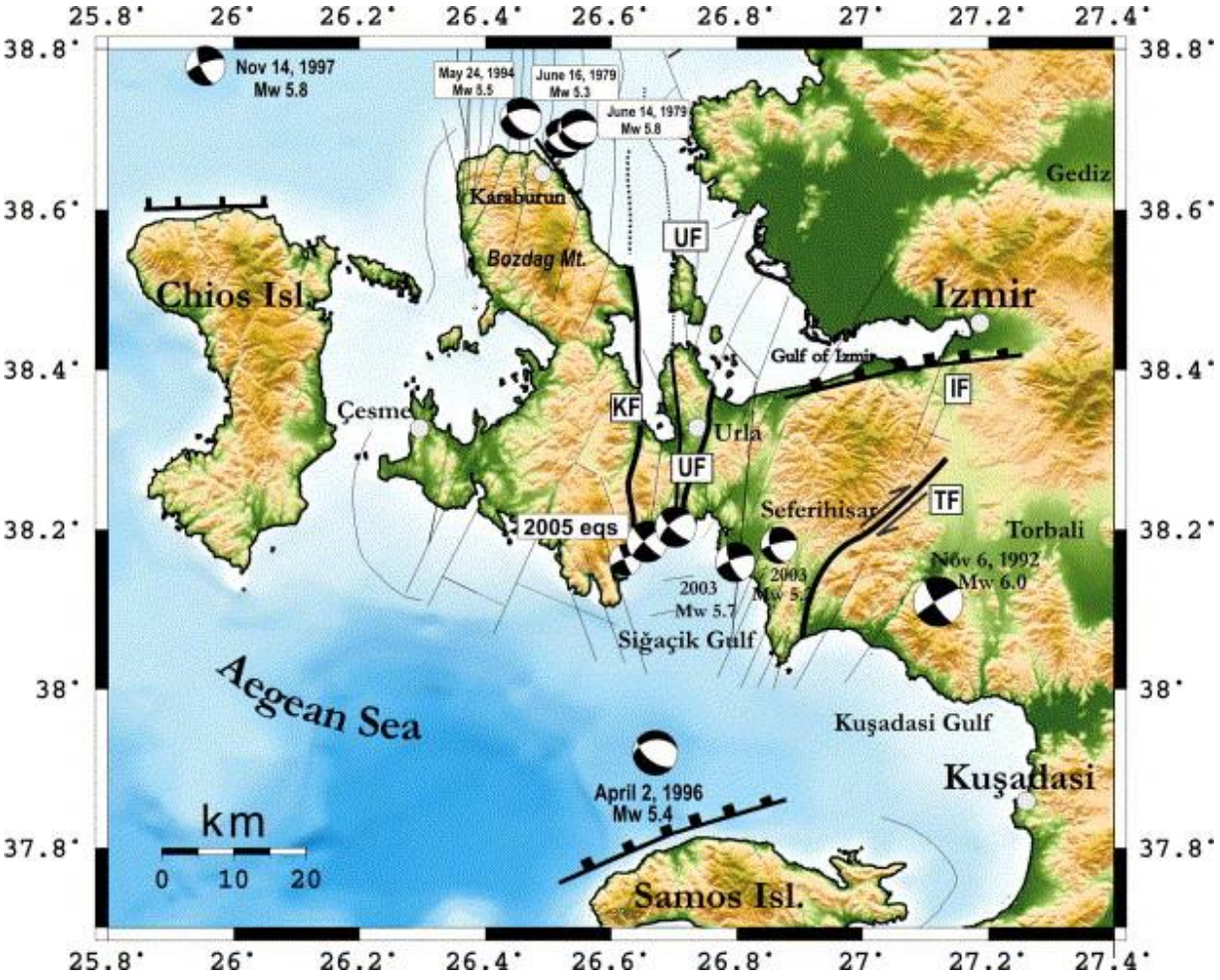

Fig.2.1.6. Focal mechanisms of previous strong earthquakes plotted at the area around Izmir. The focal mechanisms show pure strike slip motions south of Izmir and normal faulting with a clear strike slip motion north of Izmir. KF is the Karaburun Fault, UF is the Urla Fault, IF is the Izmir Fault and TF is the Tuzla Fault. In south lies Samos Island, in west the Chios Island and east of Chios is the Karaburun peninsula located. (Emre et al., 2005; Benetatos et al., 2006).

2.2 Seismicity

The seismicity in the study area is shown in fig. 2.2.1 for M_W larger or equal to 5.0, and in fig. 2.2.2 for M_W larger or equal to 4.0, from the period 1901-2015. It looks like the seismicity is rather homogeneous distributed around the study area, but it is still possible to do a zonation, choosing source zones. There are regions with very low seismicity, such as an area in southwest and in some smaller regions in east. Two places have significantly more large earthquakes, and these places are an area just west of Muğla and north on the Karaburun Peninsula.

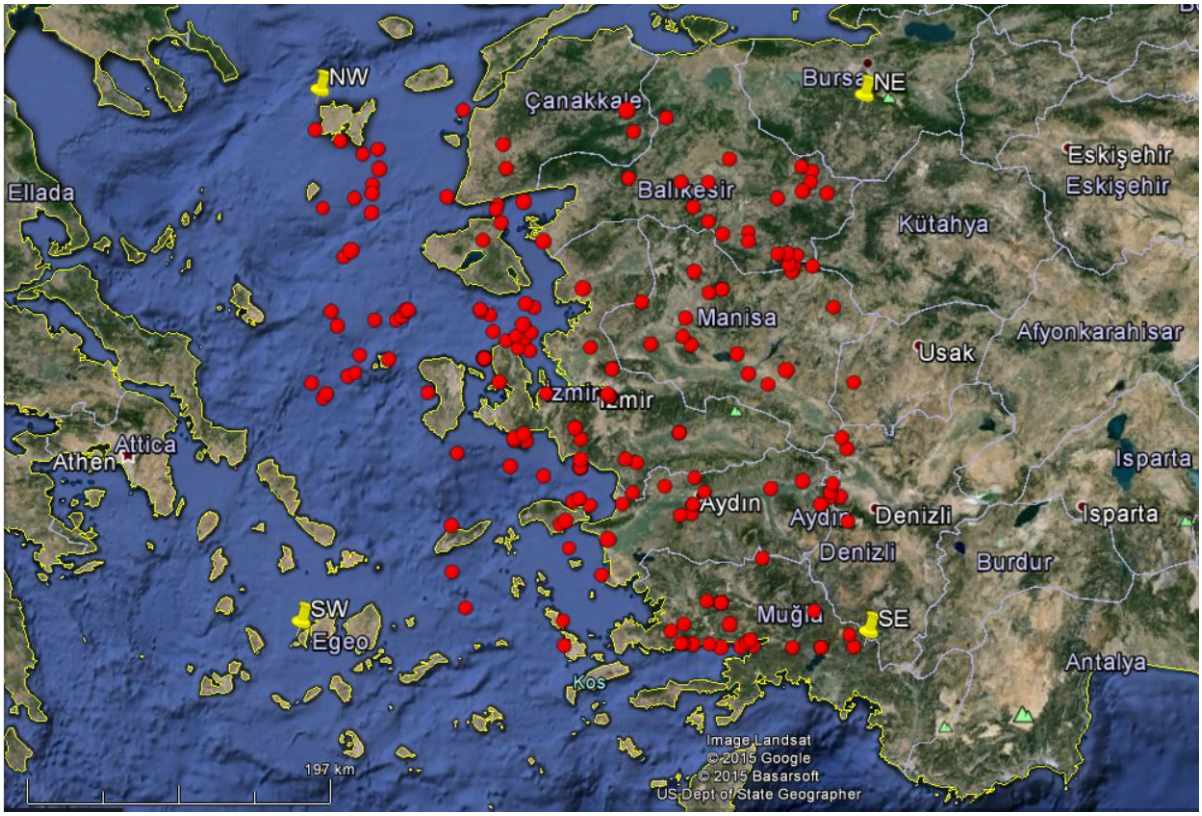

Fig. 2.2.1. All earthquakes in the study area larger or equal to M_W = 5.0, plotted in Google Earth©.

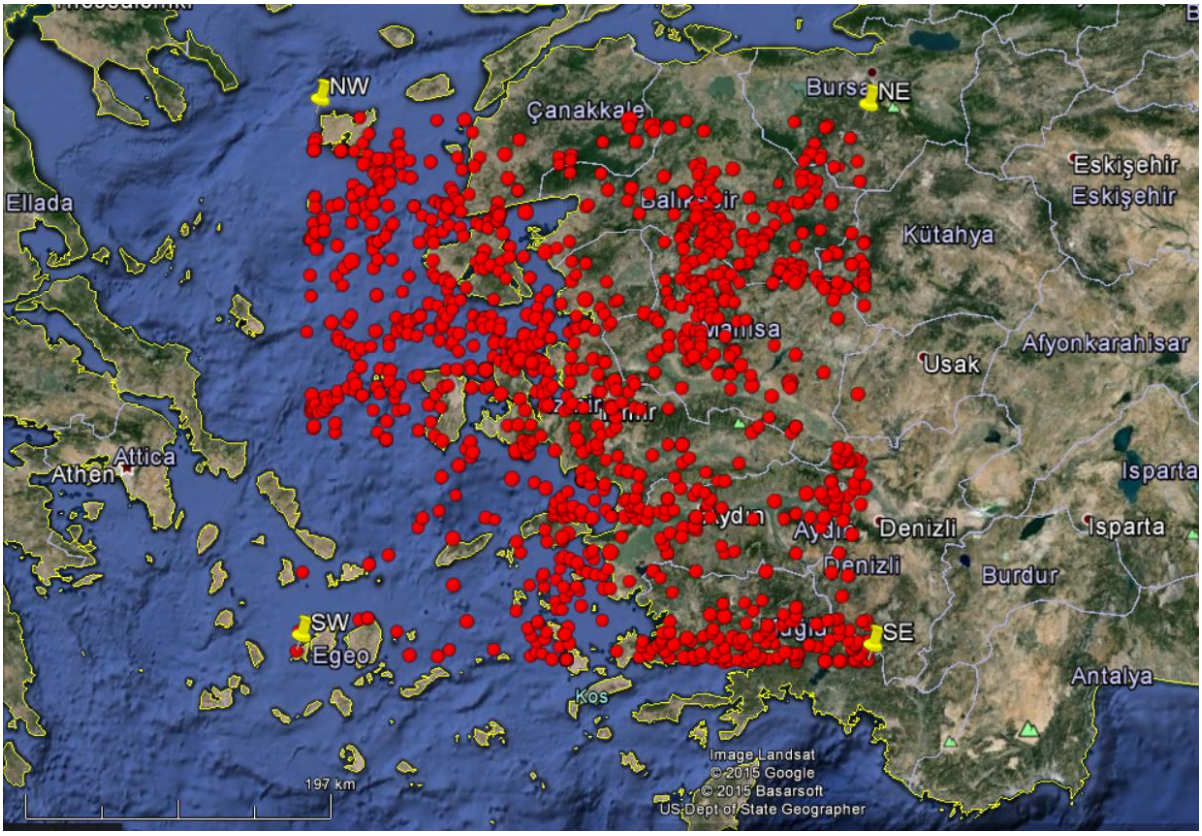

Fig. 2.2.2. All earthquakes in the study area larger or equal to M_W = 4.0, plotted in Google Earth©.

The seismicity is rather high in the study area, but it looks like the seismicity is low in eastern parts of the study area, probably due to longer distances from plate- boundaries. Another important observation, is the rather low seismicity for events with larger or equal M_W = 4 southwest of Izmir out in the Aegean Sea. However, earthquakes affect the whole study area.

There are larger historical events listed in table 4.1.2 telling that this area are highly affected by large earthquakes, even larger than what has been observed during the last 100 years from instrumental data. Izmir, Foça, and Aydın have all experienced destructive earthquakes in the past, which have been deadly and destructive events.

3. Methods

There are two fundamental types of seismic hazard analysis, which are probabilistic and deterministic. A probabilistic seismic hazard analysis (PSHA) consists of two distinctive parts. The first part characterize the source or the sources of the hazard and could for instance be the size and spatial location of the earthquakes. The second part characterizes the natural effects these sources would cause at a particular location (Reiter, 1990). The other method is a stochastic ground motion method, giving maximal ground motion from a chosen fault, using a reference magnitude. A ground motion modelling is a way of computing seismic hazard in a deterministic way.

3.1 The probabilistic approach

Cornell (1968) carried out the pioneering study on estimation of probabilistic seismic hazard and other newer studies build on this report. Seismic hazard is the probability of a certain amount of earthquake shaking to happen at a given locality and in a given time interval. Seismic hazard is not the same as seismic risk, because seismic risk describe the consequences the earthquake can cause to the society both in destruction of buildings and death to human beings (Reiter, 1990). The risk is therefore equal to hazard times the vulnerability.

A probabilistic seismic hazard analysis consists of four fundamental steps as seen in fig.3.1.1, and was defined by Carl Allin Cornell. These four steps are; the definition of earthquake sources, the definition of seismicity recurrence characteristics for each source, ground motion effects, and probability of exceeding different ground motion levels (Reiter, 1990). It is important to consider the fact that both the occurrence, magnitude and location of future earthquakes are not predetermined, so dealing with the data in a probabilistic manner is important (Deniz, 2010).

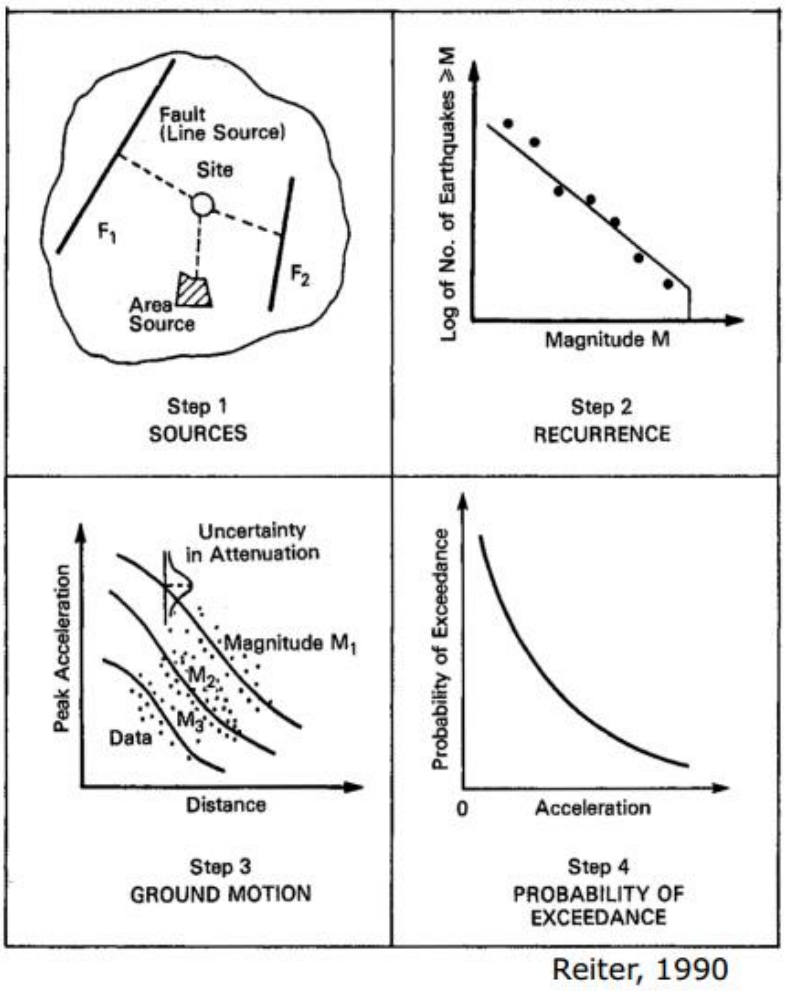

Fig.3.1.1. Step 1-4 in a probabilistic seismic hazard analysis. Step 1 is the definition of source zones, step 2 is the definition of seismicity recurrence characteristics, step 3 is the ground motion looking at the earthquake effect, and step 4 is the probability of exceedance in a given time interval, given in this thesis in peak ground acceleration. Defined by Carl Allin Cornell (Reiter, 1990).

1. Definition of earthquake sources:

The first step is to define source zones in the study area, which is the zonation. These zones can be defined as a point, a line, an area or as a volume, and they are assumed to be homogeneous when considering the seismicity. In this study, all sources are areas defined based on the seismicity, the morphology and faults.

An important fact regarding the standard probabilistic seismic hazard analysis is the assumption that earthquakes do not have any "memory". This statement originate from the "Poisson model" and means that each earthquake occur independently from other earthquakes in a given zone. Therefore, the earthquake catalogues used in the computations need to be cleaned up from

dependent events. These include both aftershocks and foreshocks, which often occur right after and right before the main shock. In addition, the "Poisson model" does not consider the time dependency of stress build-up and stress release such as the seismic gap theory (Reiter, 1990).

There can be three types of sources to earthquakes, which is faults, localizing structures or seismotectonic provinces (Reiter, 1990). In this thesis, faults are used in the zonation process.

A fault (fig.3.1.2) can be divided into normal faults, reverse faults and strike slip faults. In nature, there are a combination of movements occurring in different directions, and such faults are called oblique faults (Stein and Wysession, 2003).

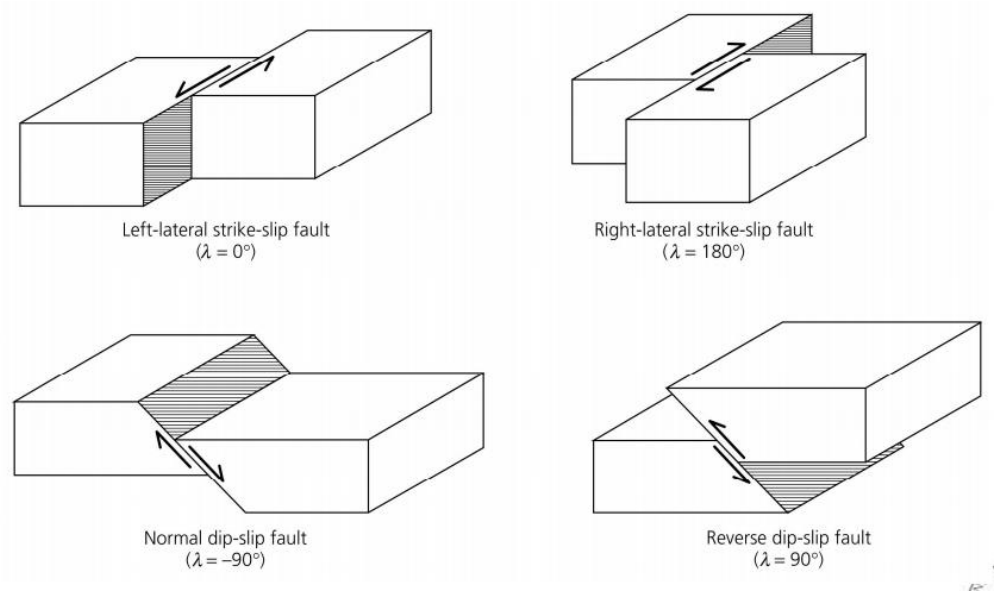

Fig. 3.1.2. Four figures showing a left-lateral strike slip fault, a right-lateral strike slip fault, a normal dip-slip fault, and a reverse dip-slip fault. The relative motion between the hanging wall and footwall decides if it is a normal or reverse fault (Stein and Wysession, 2003).

Localizing structures are identifiable geological structures, which are assumed to generate or localize earthquakes in areas such as subduction zones (Reiter, 1990). Seismotectonic provinces are areas with seismic activity that have no identifiable faults or localizing structures. There are often problems associated with determining maximum earthquakes for these zones. For instance, a seismotectonic province could be located in an intraplate setting, and the earthquakes can appear in spatial clusters, such as the earthquakes, which occurred back in 1811-1812 in New Madrid, Missouri (Reiter, 1990).

2. Definition of seismicity recurrence characteristics for each source:

After defining the source zones, the next step is to compile an earthquake catalogue for each zone. This catalogue needs to be as homogeneous and complete as possible by removing dependent events (foreshocks, aftershocks and swarms), duplicates and fake events. This catalogue will be used in order to make an earthquake probability distribution. This probability represents the chance of an earthquake of a given size to occur during a given time inside a certain source zone. In this thesis, the Poisson occurrence model will be used to derive parameters used in the process of producing hazard maps.

The probability distribution or recurrence relationship for individual sources is represented with a plot showing the logarithm of the number of earthquakes of a given size (magnitude or epicentral intensity) or larger plotted against the increasing magnitude. This relation is often referred to as the Gutenberg-Richter relation and characterizes the seismicity in the region (Reiter, 1990). The recurrence curve is described by "Log N = a – b*M", where N is the number of earthquakes of a certain magnitude during a specific time- period. The a- value is the activity rate in the same time- period, which describe the seismicity in the zone. The b- value is the slope of the curve describing the relation between small to large earthquakes, and M is the magnitude used in the catalogue (Reiter, 1990). The recurrence curve from the final earthquake catalogue is shown in fig. 3.1.3, with cumulative values starting at $M_W > 3$, for the complete part.

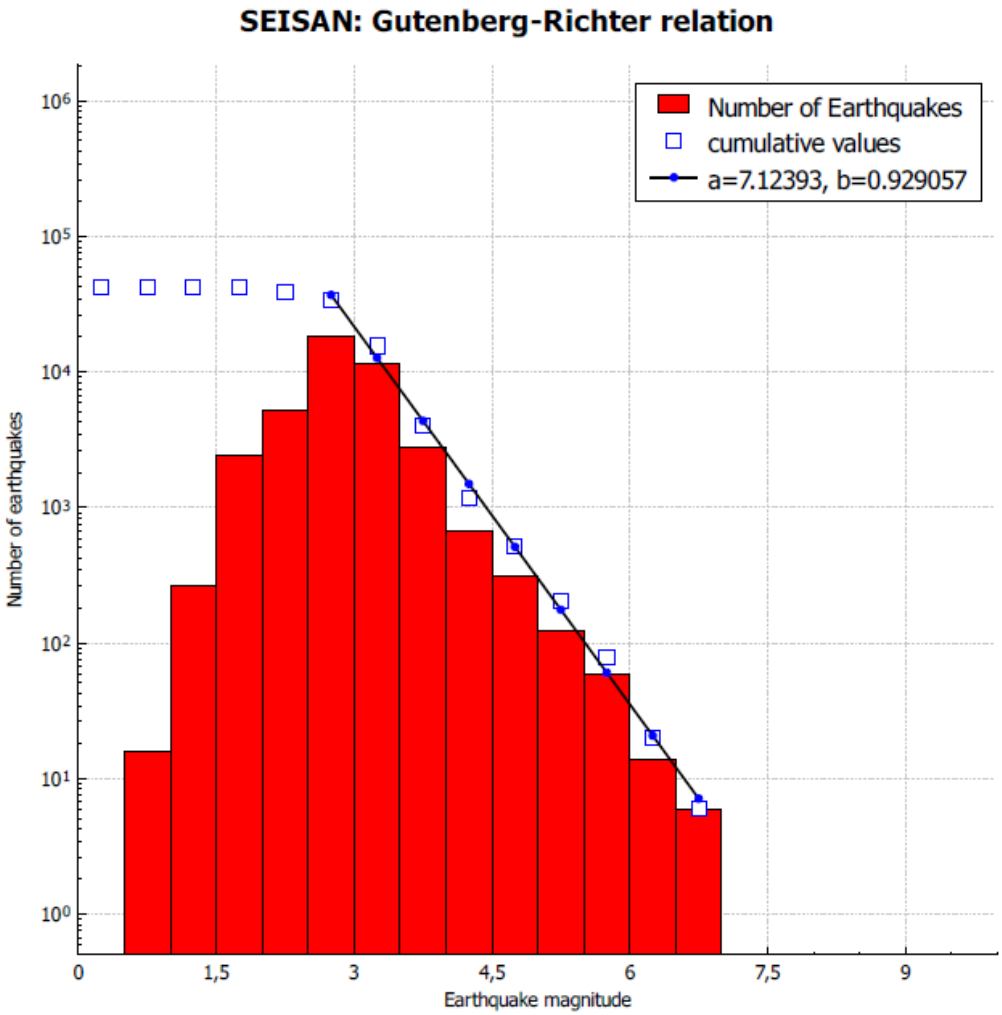

Fig.3.1.3. Gutenberg-Richter relation from the final earthquake catalogue with data from 1901-2014. The b-value looks at the proportion of small to large earthquakes. The a-value is the activity rate. These parameters are calculated for $M_W > 3$.

A maximum magnitude is chosen for each source zone to represent the maximum magnitude expected at a given source area, as well as a lower bound earthquake (Reiter, 1990). It is important to choose a reasonable value for the maximum possible magnitude, because it has a significant influence on the hazard, especially at longer return periods. However, this is not easy both because the physical understanding of the expected M_{max} is poor and because the statistics from the earthquake catalogue is limited (Wiemer et al., 2008).

The maximum expected earthquake is found by searching for the largest earthquake that has occurred in the earthquake catalogue and add this magnitude with an uncertainty of ± 0.5. In this thesis the maximum expected earthquake in any zone are set to at least $M_W = 6.0 \pm 0.5$, because all source zones have the possibility of experiencing such a large earthquake. The lower bound earthquake in most probabilistic seismic hazard analysis is set to $M_W = 4.5$. This is based on the expected damage to engineering structures.

3. Ground motion prediction equations (GMPE's):

This step looks at the prediction of the resulting ground motion on the surface (site) from an earthquake at depth (source), due to the attenuation of seismic waves in a heterogeneous crust (path). The ground motion prediction equations (GMPE's) are determined for every source and is presented as curves in fig. 3.1.4 defining the change of ground motion in distance, relating ground motion such as peak ground acceleration (g) to the distance, for an earthquake with a certain magnitude (Reiter, 1990). In this thesis, the GMPE from Boore and Atkinson (2008), and Campbell and Bozorgnia (2008) will be applied. It is important to apply a GMPE because level of ground motion depends on both magnitude and distance to source. The attenuation model compensate for the decrease of ground motion with distance. Values obtained in step 2, such as the a-value, the b-value, M_{max}, M_{min}, and some additional values will be used in the determination of the earthquake effects.

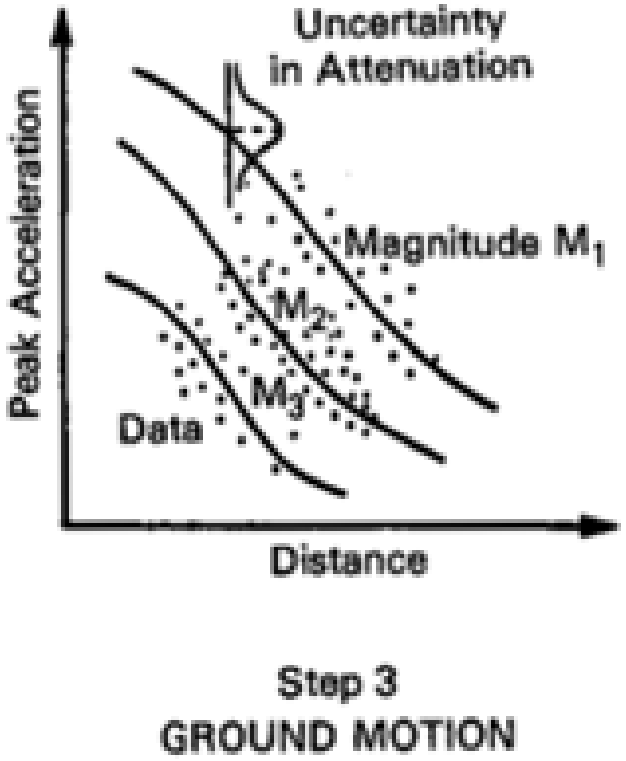

Fig.3.1.4. Step 3 in a probabilistic seismic hazard analysis. The ground motion is given in peak ground acceleration (cm/s^2) versus distance for a various amount of magnitudes (Reiter, 1990).

4. Probability of exceeding different ground motion levels:

The last step in the probabilistic seismic hazard analysis it to integrate all the effects of all the earthquakes located in all different source zones, with different sizes, and with different probabilities of occurrence into one final curve. This curve shows the probability of exceeding different levels of ground motion, in this case for peak ground acceleration at the site during a specified time- period (Reiter, 1990). With some assumptions, the hazard at site can be written as:

$$E(z) = \sum_{i=1}^{N} ai \int_{mo}^{mu} * \int_{r=0}^{r=\infty} * \; f_i(m)\, fi(r)\, P(Z>z|m, r)\, drdm \qquad (3.1.1)$$

E (z) is the expected number of exceedances of ground motion level "z" during a specific time-period "t". ai is the mean rate of occurrence of earthquakes in the i-th source between the lower, and upper magnitudes (m_0 and m_u). f_i (m) is the recurrence relationship, or the probability density distribution of magnitude within source i. f_i(r) is the probability density distribution of the source distance between the various locations within the source i and the site for which the hazard is estimated. In short words, it is the site to source distance. P (Z>z|m, r) comes from the attenuation relation and is the probability that a given earthquake of a certain magnitude, m and the epicentral distance, r will exceed the ground motion level, z (Reiter, 1990).

An alternative way to express the hazard is in terms of the return period as seen in fig. 3.1.5. The "Poisson model" describe some useful approximations and because there is no preferred occurrence in any particular year, the return period of an event exceeding a particular ground motion level is similar to its annual probability of exceedance. In a probabilistic seismic hazard analysis, the aim is to estimate the probability of exceeding a certain level of ground motion at a specific time interval, and therefore the return period, which is equivalent to that probability (Reiter, 1990), be written as:

$$\text{Return period} = -T/\ln(1 - P(Z > z)) \qquad (3.1.2)$$

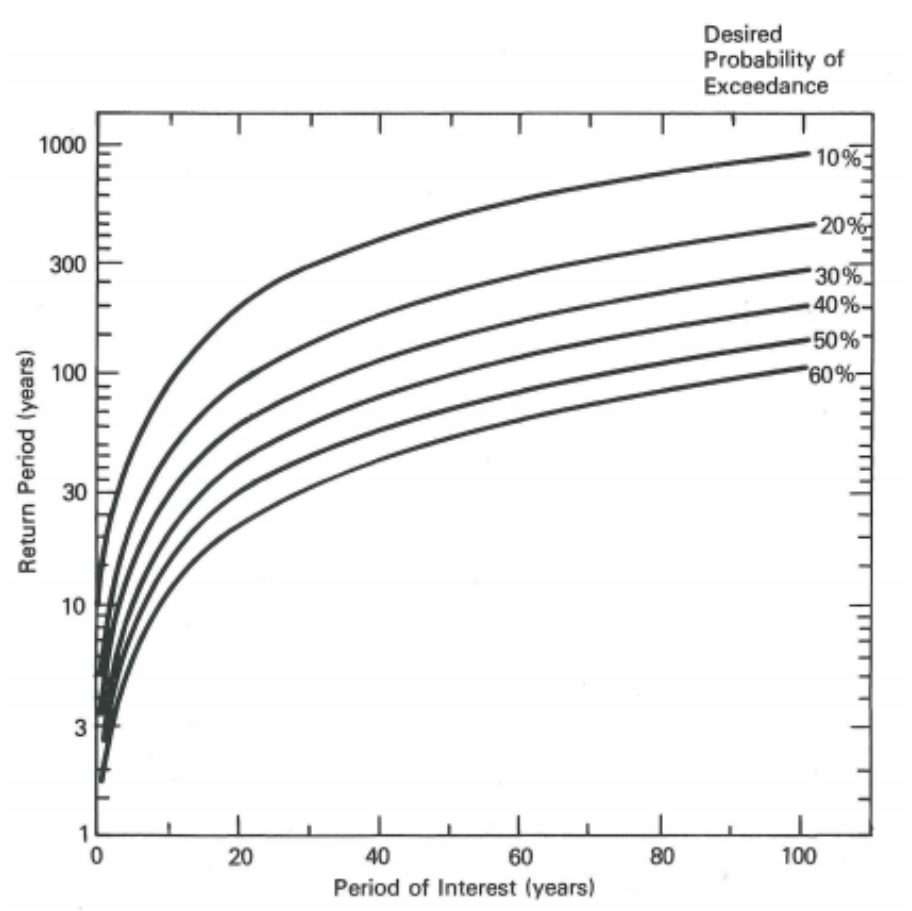

Fig.3.1.5. A relationship between the return period in years, period of interest in years and desired probability of exceedance for the Poisson model (Reiter, 1990).

3.2 Stochastic ground motion modelling as a deterministic approach

In its simplest form, a deterministic seismic hazard assessment use a single-valued event or a model to define the hazard based on some worst case scenario descriptions, and typically one or two earthquakes are specified based on magnitude and location. This analysis requires basic elements, in the form of an earthquake source, and a controlling earthquake of a certain size in order to determine the seismic hazard. Site conditions also participate in this analysis (Reiter, 1990).

There are both advantages and disadvantages by doing a deterministic seismic hazard analysis. The fact that this analysis is simple, makes it relatively easy to use. It also gives a conservative estimation of the hazard, which means that the value gives the worst case scenario. Two disadvantages with using a deterministic model are that there can be hidden faults in the study area, and the fact that the value determined is a possible, but not likely hazard, due to the

conservativism. One other important factor is that the area in a deterministic seismic hazard analysis is controlled mainly on one single fault, and therefore it is not considering possible effects from other faults. This sounds like a disadvantage, but it can also be an advantage in the way of giving a more precise maximum possible hazard (BGS, 2015).

There are four main steps in the deterministic seismic hazard analysis as seen in fig. 3.2.1. The first step is similar to the PSHA, and is a definition of an earthquake source or sources (Reiter, 1990). These sources can be faults, geological structures or seismotectonic provinces and can be measured as points, lines, areas or as volumes. In this thesis, these sources are the Izmir fault, the Karaburun fault, the Seferihisar fault, the Tuzla fault, the Samos fault, and the Manisa fault (Reiter, 1990).

Step 2 selects the controlling earthquake and is defined in terms of the maximum expected earthquake, which is reasonable to expect in the source. Earthquake magnitude or epicentral intensity are the measurements normally used, and in this thesis, the moment magnitude will be used. It is possible to have more than one controlling earthquake, for instance if two sources are evenly important in defining the largest ground motion (Reiter, 1990).

Step 3 is about determining the earthquake ground motion at the site. This step is often carried out by having a GMPE. This gives ground motion estimates of a given earthquake with a given magnitude at different distances (Reiter, 1990).

The last step defines the hazard, and is typically the output from step 3. The hazard is then given either in peak ground acceleration, in velocity or in some other measurements that describe the earthquake effect. In this thesis, this effect is given in peak ground acceleration, which is measured in acceleration of gravity (Reiter, 1990).

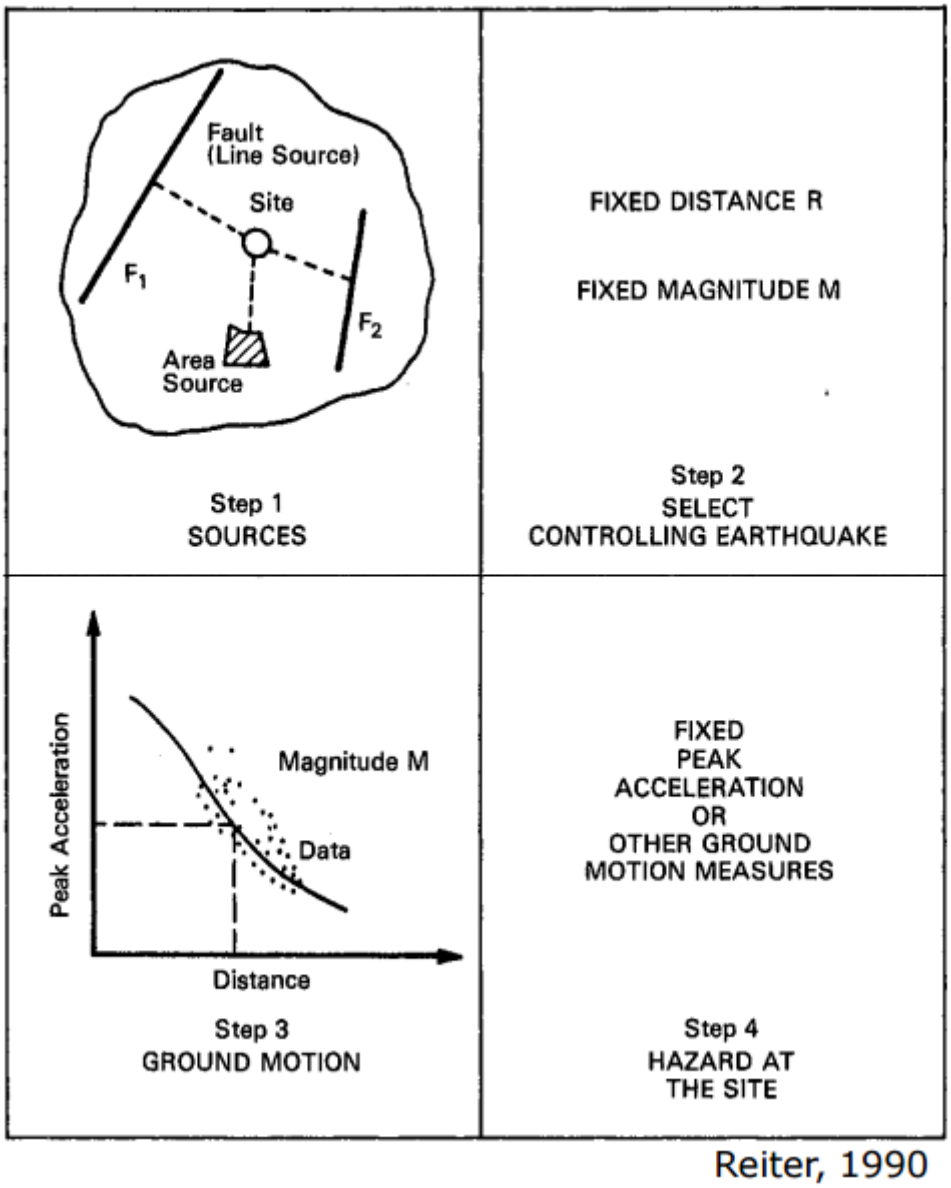

Fig. 3.2.1. All four steps in a deterministic seismic hazard assessment (Reiter, 1990).

Another more sophisticated seismic hazard analysis based on deterministic approach is to calculate synthetic ground motions based on some assumptions. Three kinds of such deterministic ground motion methods are the kinematic ground motion simulations, the dynamic ground motion simulations and the stochastic ground motion simulations. In the following, a stochastic approach is defined by Beresnev and Atkinson (1998). Later modified by Motazedian and Atkinson (2005), and Boore (2009). Both the kinematic and the dynamic method are theoretical ground motion methods (Reiter, 1990). In this thesis, a stochastic ground motion simulation will be used.

- Stochastic ground motion simulation

The stochastic method is based on observation of large parts of the strong shaking (usually from S-waves) visible on accelerograms that are associated with both an incoherent and a random appearance (Reiter, 1990). EXSIM, which will be used in this thesis, use a stochastic method to determine the ground motions from the various faults in the study area.

EXSIM is one of two stochastic finite simulation programs available. EXSIM differs from the SMSIM program in the way that, it not only looks at one point but at a whole grid. In EXSIM, the time series from each individual subfault is based on the same methods as in SMSIM (Boore, 2009). In ground motion predictions, the finite-source modelling is important to use near epicentres of very large earthquakes (Beresnev and Atkinson, 1998).

The modifications done to both SMSIM and EXSIM results in reasonably similar ground motions for near large earthquakes. At least for ground motions derived from hypocenters randomly distributed over the fault surface (Boore, 2009).

Ground motion is an output resulting from ruptures on various tectonic faults (Beresnev and Atkinson, 1998). Both SMSIM and EXSIM simulate stochastic ground motions. SMSIM is a point-source ground motion simulation program and EXSIM is a finite-source simulation program (Boore, 2009). At very large distances from the source, the faults can be considered as point sources, and at close distances, the faults can be considered as finite-sources. Both the duration as well as the amplitude of the ground motion are dependent on the observation angle. (Beresnev and Atkinson, 1998).

SMSIM works well for earthquake simulations that are far away from the source, since it only looks at one point. This simulation does not use any information about the fault geometry in the calculations because it only looks at a point-source, and therefore it is not that useful for simulations close to large earthquakes (Boore, 2009). The simulation can even break down in some cases, if the earthquakes are large and close to the source (Beresnev and Atkinson, 1997).

There are done several modifications to overcome the limitation of the point-source model, for instance, by summing up the ground motions from each subfault distributed over a fault surface (Boore, 2009). Here each subfault is treated as a point source (Beresnev and Atkinson, 1997).

One important advantage of SMSIM is the speed of the calculations. It then allows for more exploring of the input parameter effects. This program is best used for computing ground motions from finite faults with the hypocenters randomly distributed. Not for specific earthquakes (Boore, 2009).

4. Data

4.1 Earthquake catalogue

An earthquake catalogue is the most important source of information needed to make a probabilistic seismic hazard assessment (Deniz, 2010). An earthquake catalogue is a list of all earthquakes that have occurred in a specific region at a given time interval, and it consists of both historical and instrumental recorded earthquakes. An earthquake catalogue give information about the time of event, location, depth, magnitude type etc. It is also important to include historical earthquakes into the catalogue, because they make significant influences to the probabilistic seismic hazard analysis with for instance, increasing the expected maximum magnitude. The aim of the earthquake catalogue is to have a complete collection of events with both locations and magnitudes in the study area as far back as possible.

4.1.1 Databases considered

During the work with collecting data from all the databases, it is of importance to use a defined area in order to make a final comprehensive seismic database. Collected as much earthquake data as possible from as early as possible until the 31 of December 2014 in a rectangular area (37-40˚ N and 25-29˚E) surrounding Izmir. This area had to be larger than the study area in order to make the final hazard map without side- effects. In order to make the final earthquake catalogue, four different sources were used. These sources were USGS, ISC, KANDILLI and AFAD. USGS and ISC are international databases, while KANDILLI and AFAD are local databases from Turkey.

- USGS database

The U.S. Geological Survey (USGS) is a scientific agency of the United States government, and one of their major science disciplines is seismology. They have an earthquake hazard program that monitors worldwide earthquake activity from "The National Earthquake Information Center (NEIC). From the "Advanced National Seismic System" (ANSS) they have a comprehensive catalogue called ComCat, which is a long term archive of earthquake data for both domestic and worldwide earthquakes with source parameters such as hypocentres,

magnitudes and amplitudes (USGS, 2015).

Time- period, data availability, magnitude range and magnitude types for the catalogue are listed in table 4.1.1. The moment magnitude is the preferred magnitude type in the USGS database (USGS, 2015).

Table 4.1.1. The time- period, data availability, magnitude type and magnitude range for the databases from USGS, ISC, KOERI and AFAD.

Database	**USGS**	**ISC**	**KOERI**	**AFAD**
Time period		1904 to present.	1901 to present, including some historical events.	2007 to present (data available)
Data availability	1900-2007: Centennial catalogue (Based on existing data) 1923-2011: Shakemap atlas (peak ground motions and intensity) 1973-2011: Monthly data 2011-2013: Weekly data 2012-2013: Daily data 2013-present: Real- time data			
Magnitude type	M_D, M_L, M_W, M_S and M_B.	M_D, M_L, M_W, M_S and M_B.	M_D, M_L, M_W and M_S.	
Magnitude range		Larger than M = 2.5.		

- ISC database

The International Seismological Centre (ISC) is the leading database for the world's earthquake recordings and started up back in 1964. However, the calculations of M_S began in 1968 (Johnston and Halchuk, 1993). ICS is a non-governmental organization charged with a final worldwide collection of earthquake information. The main goal for ISC is to compile a complete collection of all earthquakes based on original readings (ISC, 2015).

This database is named the "Bulletin of the International Seismological Centre". The ISC Bulletin contains over 4 million seismic events, (earthquakes, explosions, mine blasts etc.) and

there are an increasing number of seismic stations built during the last years. The ISC Bulletin is typically checked by analysts at least every 24 months. The time-period, magnitude types and magnitude ranges are listed in table 4.1.1 (ISC, 2015).

- KOERI database

"Kandilli Observatory and Earthquake Research Institute" (KOERI) is a Turkish observatory institute. This observatory is specialized on earthquake research and established back in 1868. Systematic research started in 1911 and today the Kandilli Observatory consists of a number of departments, such as the "National Earthquake Monitoring Center" (KOERI, 2015). The time-period and magnitude types from the catalogue are listed in table 4.1.1.

- AFAD database

"The Disaster and Emergency Management Authority" (AFAD) is a local database from Turkey and inside this organisation lies the department of earthquakes (AFAD, 2015). Tuğbay Kiliç provided all data from AFAD in Seisan format.

4.1.2 Historical events

This earthquake catalogue consist of instrumental events and not the historical events, because the uncertainties regarding the location of the historical events are too large. However, the historical events are extremely important when dealing with maximum expected earthquakes. These will later be used in the probabilistic seismic hazard assessment.

Historical records contains events from hundreds to thousands of years ago and is mainly based on written recordings from historians, travellers and philosophers. These records show a variety in completeness and quality depending on age and population of the study area. Often only, the largest events are noticed and written down in different papers such as the work made by Ambrayseys and Finkel (1995). Based on work from Ambrayseys and Finkel, (1995) together with historical data from KOERI (2015), table 4.1.2 can be made based on historical earthquakes in the area surrounding Izmir (37-40˚N, 25-29˚E);

Table 4.1.2. All earthquakes from 26BC up to the year of 1899. These events are listed according to year, day, time, place, deaths, coordinates and strength (moment magnitude and intensity). The events are divided into four groups after the event information given. All these events are derived either from Ambrayseys and Finkel (1995) or from KOERI (2015).

Year	Date	Time	Place	Death toll	M_W	Area-felt (km^2)	Epicentral Intensity	Coordinates	Source
26 BC			Aydın	Unknown				37.85N, 27.85E	1
17 BC			Manisa, Aydın	Unknown			IX	38.40N, 27.50E	1
105			Candarli Bay	Unknown			IX	38.90N, 27.00E	1
110			Izmir, Ephesus	Unknown			IX	37.00N, 26.00E	1
177			Izmir, Sakiz, Sisam	Unknown			X	38.40N, 27.10E	1
253			Bergama	Unknown			IX	39.10N, 27.15E	1
688			Izmir	Unknown			IX	38.40N, 27.00E	1
1389			Izmir/Chios	Unknown			IX	38.40N, 26.30E	1
1546			Chios	Unknown	4.5-6.0			38.10N, 26.10E**	2
1565			Chios	Unknown	3.5-4.5	875		38.10N, 26.10E**	2
1577			Balıkesir	Unknown	>6			39.39N, 27.53E**	2
1595	22.9.	18:00	Sart-Manisa	Unknown	4.5-6.0	14395		38.29N, 28.02E**	2
1611-12			Manisa	Unknown	4.5-6.0			38.37N, 27.25E**	2
1631			Milas	Unknown	4.5-6.0			37.18N, 27.46E**	2
1645-46			Büyük Menderes valley	610	>6	1525		37.54N, 28.19E**	2
1646	31.5.		Chios	Unknown	4.5-6.0			38.10N, 26.10E**	2
1648	18.10.	evening	Chios	Unknown	3.0-3.5			38.10N, 26.10E**	2
1653	22.2.		Aydın	5000	>6	5224	IX	37.90N, 28.30E	1,2
1654	20.5.		Smyrna, Izmir	Unknown	>6			38.25N, 27.07E**	2
1664	2.6.	night	Smyrna, Izmir	Unknown	>6			38.25N, 27.07E**	2
1667	november		Smyrna, Izmir	Unknown	4.5-6.0			38.25N, 27.07E**	2
1674	23.1.	03:00	Chios	Unknown	4.5-6.0			38.10N, 26.10E**	2
1676	29.11.	14:00,18:00,22:00	Izmir	Unknown	3.0-3.5			38.25N, 27.07E**	2
1678	13.6.	02:00 and 06:00	Izmir	Unknown	3.0-3.5			38.25N, 27.07E**	2
1679	july		Izmir	Unknown	3.5-4.5			38.25N, 27.07E**	2
1680	14.2.		Izmir	Unknown	>6			38.25N, 27.07E**	2
1684			Chios	Unknown	3.0-3.5			38.10N, 26.10E**	2
1688	10.7.	11:45	Izmir	5-15000	7,1*	45069	X	38.40N, 27.20E	1,2
1688	10.9.		Balıkesir	Unknown	>6	30428		39.39N, 27.53E**	2
1690	13.1.		Izmir	Unknown	>6			38.25N, 27.07E**	2
1694	5.3.	03:00	Chios	Unknown	3.5-4.5			38.10N, 26.10E**	2
1705			Izmir	Unknown	3.5-4.5			38.25N, 27.07E**	2
1706			Izmir	Unknown	3.0-3.5			38.25N, 27.07E**	2
1708			Izmir	Unknown	3.5-4.5			38.25N, 27.07E**	2
1709	3.7.		Foça	Unknown	>6			38.41N, 26.49E**	2
1713			Izmir	Unknown	3.0-3.5			38.25N, 27.07E**	2
1716			Izmir	Unknown	3.0-3.5			38.25N, 27.07E**	2
1717	1.7.		Izmir	300+	>6			38.25N, 27.07E**	2
1718			Izmir	Unknown	3.0-3.5			38.25N, 27.07E**	2
1723	september		Izmir	400+	>6			38.25N, 27.07E**	2
1728	15.9.	12:00	Izmir	Unknown	3.0-3.5			38.25N, 27.07E**	2
1732	11.5.	01:17	Izmir	Unknown	3.5-4.5			38.25N, 27.07E**	2
1738	9.12.	23:00	Chios	Unknown	3.0-3.5			38.10N, 26.10E**	2
1738	23.12.	night	Chios	Unknown	3.0-3.5			38.10N, 26.10E**	2
1739	4.4.	04:15	Foça	80+	8*	153764	IX	38.40N, 27.20E	1,2

1745	18.3.	16:00	Izmir	Unknown	3.0-3.5			38.25N, 27.07E**	2
1751	6.7.		Sisam Island	Unknown			X	37.75N, 27.00E	1
1754	july		Izmir	Unknown	3.0-3.5			38.25N, 27.07E**	2
1763	13.1.	23:00	Izmir	Unknown	3.0-3.5			38.25N, 27.07E**	2
1765	11.7.	07:00	Izmir	Unknown	3.0-3.5			38.25N, 27.07E**	2
1767	7.2.		Chios	Unknown	>6			38.10N, 26.10E**	2
1771	8.8.		Izmir	Unknown	3.0-3.5			38.25N, 27.07E**	2
1771	24.8.		Izmir	Unknown	3.0-3.5			38.25N, 27.07E**	2
1771	1.9.		Izmir	0	4.5-6.0			38.25N, 27.07E**	2
1771	15.12.		Izmir	Unknown	3.5-4.5			38.25N, 27.07E**	2
1772	25.10.	00:00	Chios	Unknown	3.0-3.5			38.10N, 26.10E**	2
1772	24.11.	07:45	Foça	Unknown	>6			38.41N, 26.49E**	2
1778	16.6.	18:00	Izmir	Unknown	4.5-6.0			38.25N, 27.07E**	2
1778	3.7.	02:30	Izmir	200+	>6	6776		38.25N, 27.07E**	2
1778	1.10.	13:00	Izmir	0	4.5-6.0			38.25N, 27.07E**	2
1778	november		Izmir	Unknown	3.5-4.5			38.25N, 27.07E**	2
1779	1.7.	16:00	Izmir	Unknown	3.0-3.5			38.25N, 27.07E**	2
1785	26.4.	17:00 and 21:00	Izmir	Unknown	3.0-3.5			38.25N, 27.07E**	2
1785	29.8.	03:00	Izmir	Unknown	3.5-4.5			38.25N, 27.07E**	2
1786	30.1.	20:00	Izmir	Unknown	3.0-3.5			38.25N, 27.07E**	2
1787	18.12.		Izmir	Unknown	3.0-3.5			38.25N, 27.07E**	2
1788	10-12.jul		Izmir	Unknown	3.5-4.5			38.25N, 27.07E**	2
1788	11.8.		Izmir	Unknown	3.0-3.5			38.25N, 27.07E**	2
1788	10.9.		Izmir	Unknown	3.0-3.5			38.25N, 27.07E**	2
1798	january		Izmir	Unknown	3.0-3.5			38.25N, 27.07E**	2
1798	10.7.	01:00	Izmir	Unknown	3.5-4.5			38.25N, 27.07E**	2
1798	28.8.	14:00	Izmir	Unknown	3.0-3.5			38.25N, 27.07E**	2
1845	12.10.		Midilli Island	Unknown			X	39.10N, 26.20E	1
1846	21.6.		Sisam Island, Soke	Unknown			IX	37.75N, 27.00E	1
1856	13.11.		Rhodos	Unknown			IX	38.25N, 26.25E	1
1862	3.11.	03:00	Turgutlu, Manisa	Unknown			IX	38.40N, 27.70E	1
1865	23.7.	21:30	Midilli, Canakkale, Gelibolu	Unknown			IX	39.40N, 26.20E	1
1867	7.3.		Midilli	500			IX	39.10N, 26.50E	1
1873	1.2.	01:00	Sisam Island, Izmir, Aydın	Unknown			IX	37.75N, 27.00E	1
1880	29.7.	04:40	Menemen, Emiralem, Izmir	Unknown			IX	38.60N, 27.10E	1
1881	3.4.	11:30	Chios	4000			X	38.25N, 26.10E	1
1883	15.10.	15:30	Cesme	1500			IX	38.30N, 26.30E	1
1885	29.2	18:30	Aegean Sea	Unknown			IX	37.20N, 27.20E	1
1889	25.10.	23:20	Midilli, Sakiz, Izmir	Unknown			IX	39.30N, 26.30E	1
1895	19.8.		Aydın	Unknown			IX	37.80N, 27.80E	1
1899	20.9.	10:30	Nazilli, Aydın, Denizli, Usak	Unknown			IX	37.90N, 28.10E	1

Source 1: (KOERI/UDIM, 2014)

Source 2: (Ambrayseys and Finkel, 1995)

*** Using the formula; $Log(M_W) = 47.34 - 10.81*log(A_{felt}) + (1.17*log(A_{felt}))^2$, to estimate the moment magnitude.**

Only events greater than 31624 km2 equal to log(A) = 4.5 is valid in this formula. Uncertainty = ± 0.5 (Johnston and Halchuk, 1993)

**** Geographical coordinates from Ambrayseys and Finkel, 1995 are found by locating the center of all places reported, which are affected.**

The data covers the period from 26 BC to 1899 and the events are listed chronological. There are several sources of uncertainties in the estimating process when deriving the moment magnitude for the various events. The data from Ambrayseys and Finkel (1995) is divided into four groups depending on the event information. M_W = 3.0 - 3.5 is for a felt earthquake. M_W = 3.5 - 4.5 is for a noticeably event with no damage reported. M_W = 4.5 - 6.0 is for events with little damage reported. $M_W > 6$ is for events causing total destruction, death, or collapsing of buildings. Since all of these earthquakes are measured before, the introduction of seismographs and the fact that all are based on subjective reports, gives uncertainties to the magnitude recordings. The geographical coordinates derived by Ambrayseys and Finkel (1995) are found

by locating the most reasonable place for the earthquake event, with respect to both reported affected places and intensity mapping.

4.1.3 The catalogues before merging

- USGS

Before merging, declustering and removing of dependent events (foreshocks, aftershocks and swarms) there was a total number of 8671 events collected from the USGS- database in the period from 1949-2014. Most of the events are reported in body-wave magnitude (M_b) or only magnitude (M), where M is the largest magnitude of any type. From fig, 4.1.1 is seen a noticeable change, with significant more earthquakes after 1989. In addition, the years 1993-94 and 2006 have significant more earthquakes because of resulting aftershock sequences from larger events. The coverage became better from 1973, because of the fact that monthly data became available from this year. From 2009, there is a significant drop in the number of events, probably due to some errors in the online USGS- database.

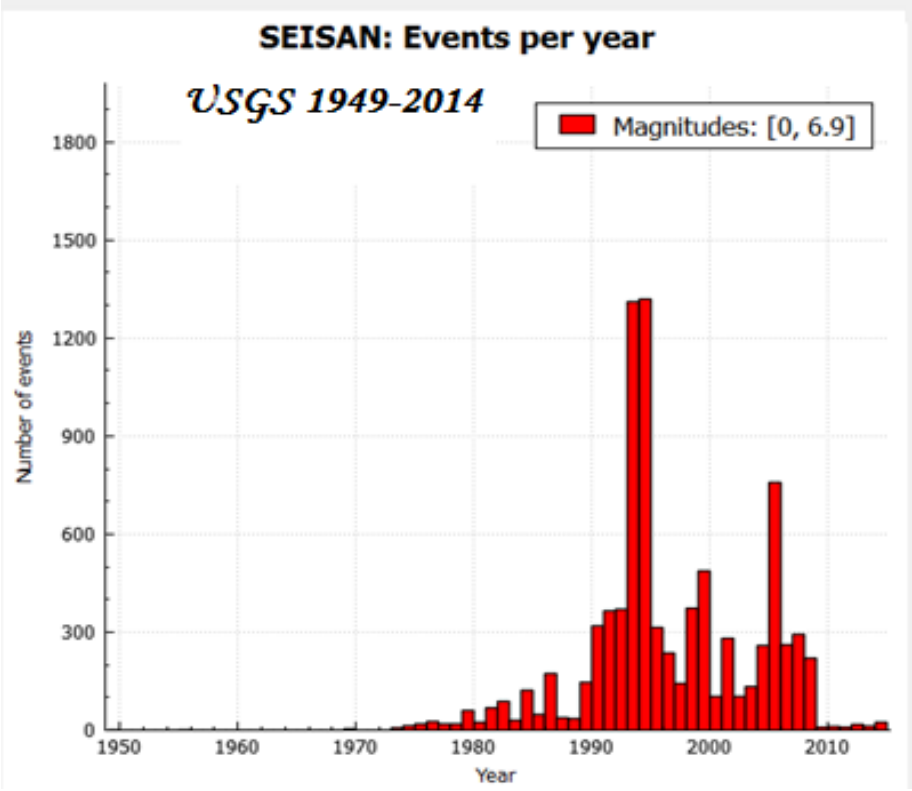

Fig. 4.1.1. Number of earthquakes before merging and magnitude homogenization with magnitude type M (largest magnitude of any type) in every year from 1949 to 2014 in the USGS- database.

- ISC

Before merging, declustering and removing of dependent events, there was a total number of 71309 events as seen in fig. 4.1.2, collected from the ISC-database in the period from 1928-2014. Most of the events are reported in local magnitude (M_L) and magnitude (M). From fig. 4.1.2, there are two significant jumps where the coverage becomes noticeable better, from 1969 and from 2008, respectively. In these years, there was an increase of seismic stations. Here, as well as at the USGS- database (fig. 4.1.1), the year of 2006 points out. This year have many aftershocks, due to larger events that happened in the Siğacık bay. It looks like the coverage from ISC is better than the coverage from USGS, because of a less difference in the amount of events during each year.

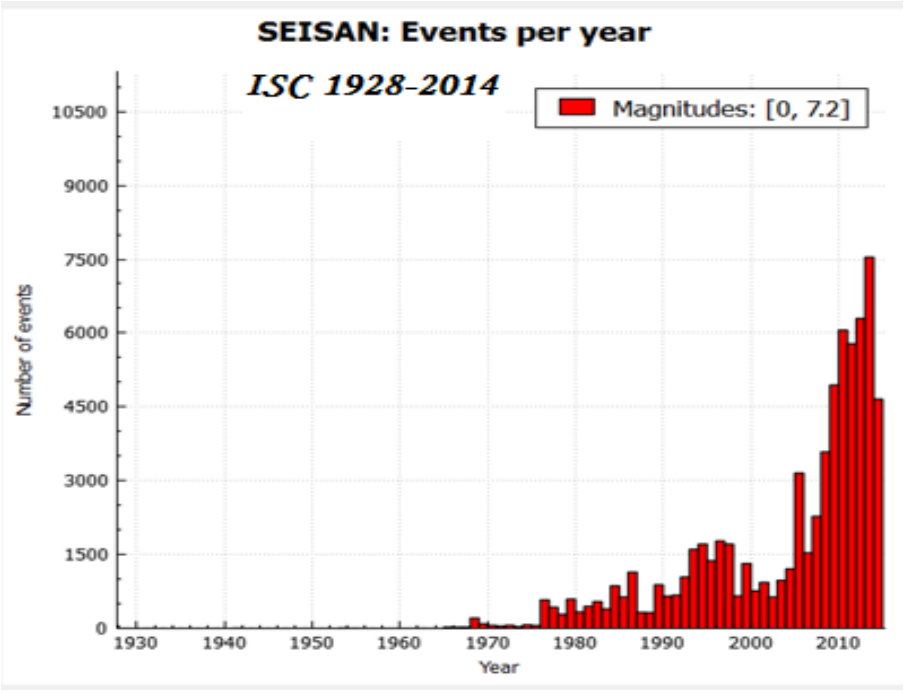

Fig. 4.1.2. Number of earthquakes before merging and magnitude homogenization in every year from 1928 to 2014 in the ISC-database.

- KOERI

Before merging, declustering and removing of dependent events, there was a total number of 51731 events collected from the KOERI- database in the period from 1901- 2014. Most of the events are reported in coda magnitude (M_c) and in local magnitude (M_L). From fig.4.1.3, it is possible to notice the peak of events in the year of 2006, which also were shown from the

USGS- and the ISC- catalogue. Otherwise, fig. 4.1.3 shows the same pattern as fig.4.1.2 with significant more earthquakes recorded after 1969.

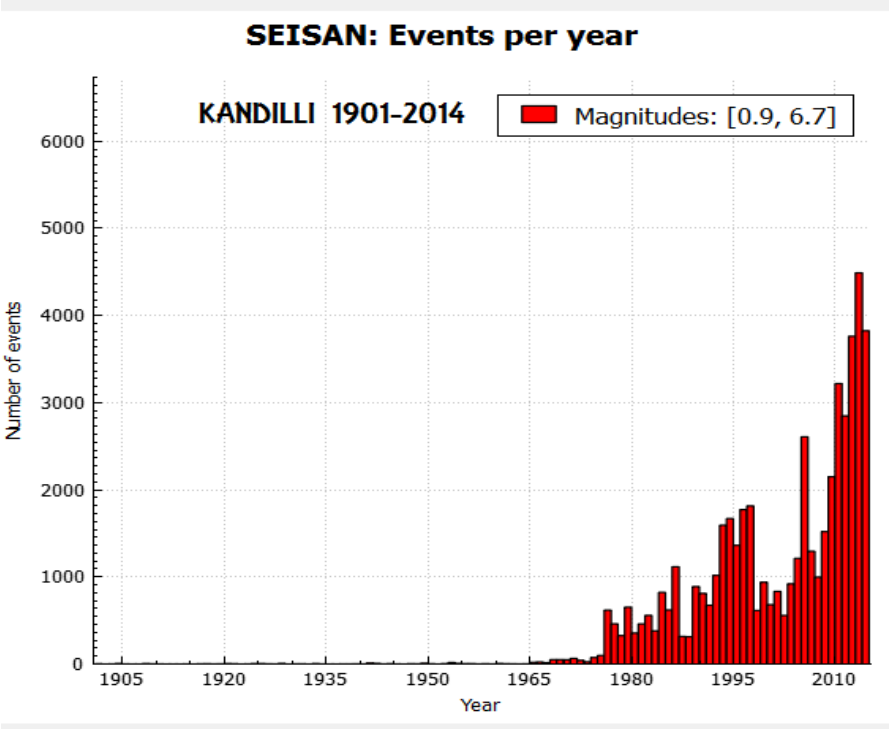

Fig. 4.1.3. Number of earthquakes before merging and magnitude homogenization with magnitude type M (largest magnitude of any type) in every year from 1901 to 2014 in the KOERI- database.

- AFAD

Before merging, declustering and removing of dependent events, there was a total number of 37168 events collected from the AFAD-database in the period from 2007-2014. Most of the events are reported in coda magnitude (Mc) and in local magnitude (M_L). From fig.4.1.4, it is shown more recordings every year from 2007 to 2010. From 2010, the coverage is quite stable with approximately 5000 events per year. The increasing events is presumable because of a better coverage of stations.

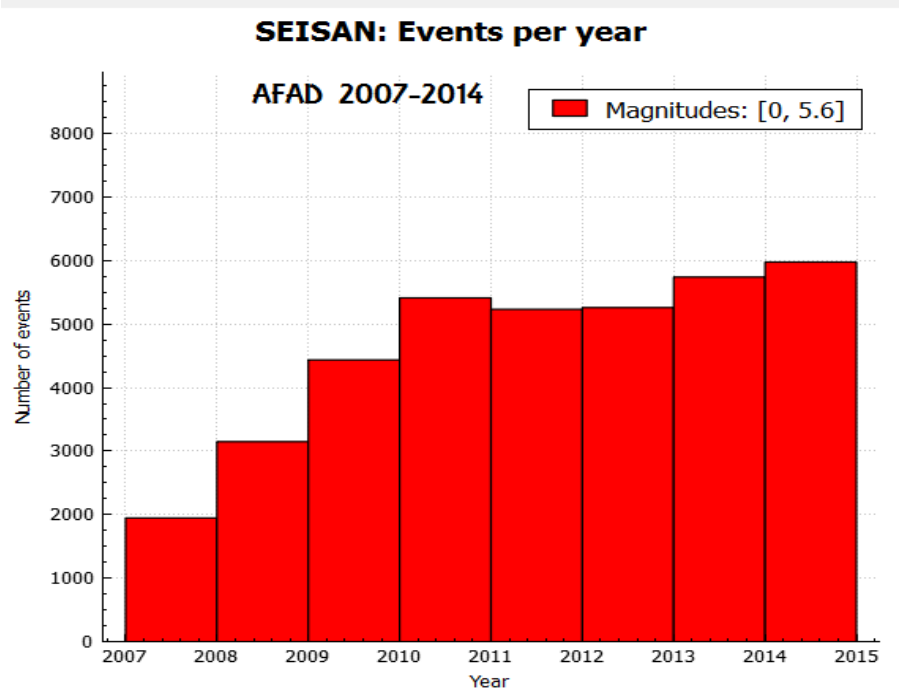

Fig. 4.1.4. Number of earthquakes before merging and magnitude homogenization with magnitude type M (largest magnitude of any type) in every year from 2007 to 2014 in the AFAD- database.

4.1.4 Merging of catalogues

The next step is to merge all the catalogues (USGS, ISC, KOERI and AFAD) into one final catalogue and improve the quality of the catalogue as much as possible. It is important (because of the merging process in Seisan) to start merging the two most reliable and complete catalogues first, then the two most reliable with the third most reliable, and at last include the least complete catalogue with the already merged catalogues.

First, the two most reliable and complete catalogues from AFAD and KOERI were merged together. These were chosen mainly based the events per year and the Poisson distribution. Then, the catalogue from ISC were merged with AFAD and KOERI, and at last, the catalogue from USGS were merged together with the other catalogues. ISC has generally better coverage of the seismicity than USGS/NEIC in global catalogues (Grünthal and Wahlström, 2009).

4.1.5 Improve the final earthquake catalogue

Several methods are used to improve the quality of the earthquake catalogue, such as to check and get rid of duplicates, fake events and dependent events. Duplicates are two or more events that in the reality is only one event. It is therefore important to look at many parameters (such as variation in time, location, depth and magnitude) at the same time in order to remove duplicates. However, it is not easy to get rid of all duplicates because there will always be some questionable events left after running all the filters.

Fake events are events caused by other factors than earthquakes, such as explosions, mining operations, traffic, construction work etc. Fake events are common features to the earthquake catalogue as seen in fig.4.1.5, and there are most of them during daytime. From fig. 4.1.5, it is easy to see that there are more events recorded from 7am in the morning, until 4pm in the afternoon. These are probably fake events and as many as possible are later removed from the final earthquake catalogue.

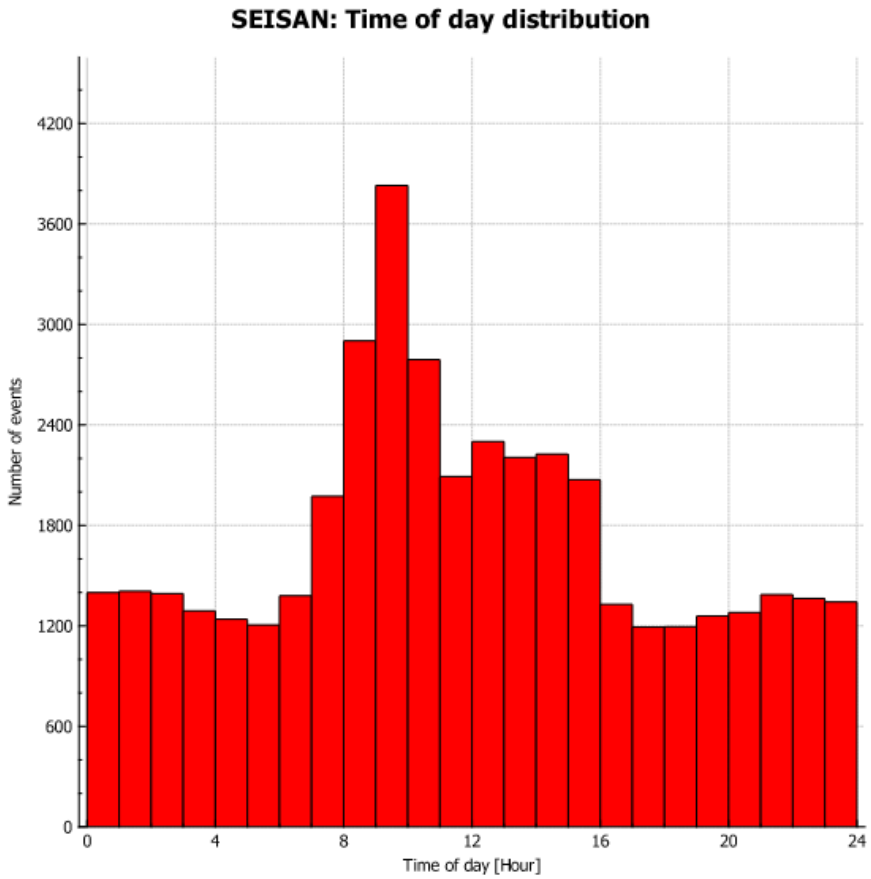

Fig. 4.1.5. Time of day distribution for all events before removing fake events, with number of events on the y-axis and time of the day on the x-axis.

Dependent events are either foreshocks, aftershocks or earthquake swarms and results from larger events. They are often small in magnitude and therefore the b- value becomes too high. The b- value is an indicator of the relative abundance of small earthquakes compared to large earthquakes, and will be constant for any period (Deniz, 2006). Therefore, it is important to clean the catalogue before estimating the b- value. It is possible to remove dependent events by marking all the main shocks, and delete all other smaller events within a minor window in either time or space.

4.1.6 Magnitude homogenization

It is important to be consistent and only use one type of magnitude in the final catalogue. In this chapter, the aim is to discuss the different magnitudes in the different catalogues from ISC, USGS, AFAD and KOERI, and finally decide which of them is the preferred magnitude scale. Regressions between different magnitude types are made in the homogenization process.

4.1.6.1 About the magnitudes in the catalogue

There are a lot of different magnitude scales used in the catalogues retrieved from ISC, USGS, AFAD and KOERI. All of these scales are explained and discussed with the aim to conclude which of them is the preferred magnitude to use in the final earthquake catalogue. There are many different methods to measure the strength of an earthquake, such as intensity (macroseismic scale), seismic moment, and the most common method called magnitude. Some of these methods are based on the surface effects, other on the rupture (Reiter, 1990).

The macroseismic scale is not the most common method used in probabilistic seismic hazard analysis, but it is important to estimate size of significant historical events. This method is based on the people's experience of the ground shaking and the observed damage. This subjective method is not based on instrumental recordings, but can be converted to magnitude scale, even though it is not a trivial thing to do. There are several such intensity scales, such as the "European Macroseismic Scale EMS-98" and the American scale, "Modified Mercalli Intensity Scale" (MMI) (Reiter, 1990).

Magnitudes (M): These scales are based on the amplitudes from waves generated from earthquakes, which again reflects the size of the earthquake. They are corrected due to the amplitude- decrease resulting from attenuation and geometric spreading. Magnitude scales are dependent on the distance from the source, and they are corrected with help from ground motion prediction equations.

Magnitudes are often used to quantify the earthquake size and there are both advantages and disadvantages using the magnitude scale. An advantage with this measurement is that the magnitudes are directly measured from seismograms without any complicated form for signal processing. There are also disadvantages, such as the fact that they all are empirical with little connection to the physics of the earthquakes, and the fact that the magnitude vary significant with different azimuth values (Stein and Wysession, 2003).

All magnitude scales have a general form;

$$M = \log (A/T) + F(h, \Delta) + C \qquad (4.1.1)$$

A is the amplitude of the signals, T is the period, F is a correction for the amplitude variation with both the earthquake depth (h) and the distance (Δ). C is a regional scale factor (Stein and Wysession, 2003).

Local magnitude (M_L): The earliest magnitude scale invented was the local magnitude scale, which often is referred to as the "Richter scale". It was introduced as early as 1935 for earthquakes in southern California. It measures the arrival times for P- and S-waves for the distance between the receiver and the source. Then the magnitude is given from a relation between the arrival time differences between the P- and the S-wave (Stein and Wysession, 2003). This magnitude scale has the form;

$$M_L = \log A + 2.76 \log \Delta - 2.48 \qquad (4.1.2)$$

A is the amplitude measured by the Wood-Anderson seismograph, and Δ is the distance from the seismometer. This scale is defined for earthquakes in southern California and is therefore not that common outside California. However, because many buildings have a resonant frequency close to 1 Hz, which again is close to the frequency used in the Wood-Anderson

seismograph (standard at that time) it is still in use worldwide. Other advantages are that the scale is easy to apply, and that the magnitude can be determined within only minutes after the event. However, this scale is not designed for larger earthquakes than M_L = 7 because of saturation, and not for epicentral distances greater than approximately 600 km since the data set from Richter only include seismograms recorded at distances less than this 600 km (Stein and Wysession, 2003).

Every magnitude scale except from the moment magnitude scale is determined with a particular wavelength and period, and this is the reason for a phenomenon, called "magnitude saturation" as seen in fig.4.1.6. If the wavelengths are smaller than the earthquake source, then the amplitude will not follow the increased size in earthquake source, energy release and moment. m_b saturates at about 6.5, while M_S saturates at about 8.0, and therefore these scales can give too low values for the largest earthquakes (Reiter, 1990).

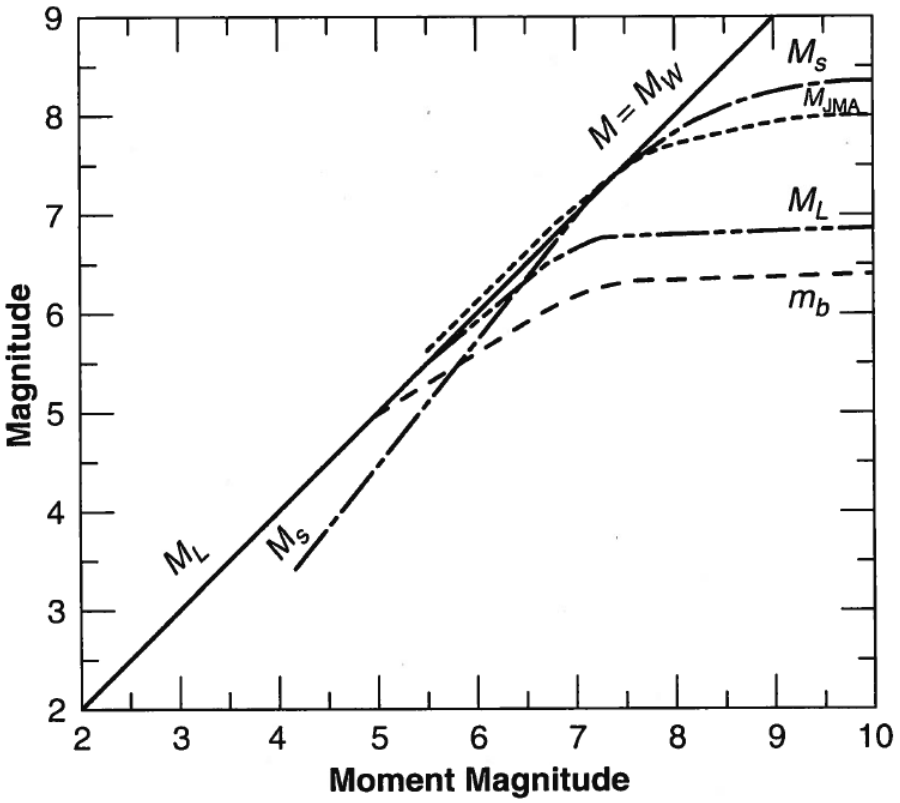

Fig. 4.1.6. Different magnitude scales and saturation points. The straight line is the moment magnitude, which not saturates (Reiter, 1990).

Later there have been used a great amount of both global and local magnitude scales, and the most common global magnitude scales are the body-wave magnitude (m_b) and the surface-wave magnitude (M_s) (Stein and Wysession, 2003).

Body-wave magnitude (m_b): This amplitude scale is measured at the first part of the body wave, which usually is the P-wave (Stein and Wysession, 2003). This part is observed on the vertical component of the seismogram and the wave- periods are about one second. It is best observed for epicentral distances greater than about 1000 kilometres because it rely on the P- wave, which propagate beneath the shallow crustal layer. Because m_b is determined from a short periodic wave, it cannot completely describe the strength of large earthquakes, which release more long period energy from a large fault rupture zone. This scale is therefore not supposed to be used on small regional/local earthquakes as well as on very large earthquakes (Reiter, 1990). The body wave magnitude is of the form;

$$m_b = \log (A/T) + Q (h, \Delta) \qquad (4.1.3)$$

A is the amplitude, T is the period, and Q is an empirical term depending on both the focal depth as well as on the distance (Stein and Wysession, 2003).

Body-wave magnitude (m_B): Another type of body-wave magnitude is the m_B. This scale is determined from various types of body waves, not only on P-waves as m_b does. The period is longer than m_b and it is in the order of one to ten seconds (Reiter, 1990).

Surface-wave magnitude (M_s): This scale measures the largest amplitude of the surface waves from zero to peak (Stein and Wysession, 2003). The scale is determined from Rayleigh wave-amplitudes with a period of approximately 20 seconds, and is a common scale for large earthquakes. These Rayleigh waves (surface waves) are only generated for shallow earthquakes, shallower than 70 km, and they are not easily observed for earthquakes smaller than $M_s = 5$, with distances less than about 1000 kilometres from the epicentre (Reiter, 1990). This scale is therefore not applicable for deep, very large (saturation), small, and regional/local and small earthquakes (Reiter, 1990). The general form is;

$$M_s = \log (A/T) + 1.66 \log \Delta + 3.3 \qquad (4.1.4)$$

A is the amplitude, T is the period, and Δ the distance in degrees (Stein and Wysession, 2003). Both the M_s and the m_b scale are in little use when describing small and regional earthquakes as well as the fact that they do not take allowance to the regional/local variation in the

attenuation. Because of these limitations in both the M_s and m_b scale, new regional/local magnitude scales have been developed for specific places when considering local attenuation functions and the short distances between the source and the receiver (Reiter, 1990).

Duration and coda magnitude (M_D and M_C): Many local and regional networks have magnitude scales based on the total duration of the wave train measured. The last part of this "train" is called the *coda* and is made up of scattered or reflected waves. The coda magnitude (M_C) is often just referred to as the duration magnitude (M_D) and it is good for detecting local earthquakes (Reiter, 1990).

Moment magnitude (M_W): A better and more applicable magnitude scale named the moment magnitude (M_W), is based on the seismic moment M_0. This scale is applicable to all earthquakes, no matter size, depth or location. The seismic moment is based on the size of the fault in the form (Reiter, 1990);

$$M_0 = \mu A D \qquad (4.1.5)$$

μ is the rigidity modulus, which is the resistance against shearing, A is the fault rupture area, and D is the relative slip movement between both sides of the fault. An advantage with using M_W instead of other magnitude scales is that it directly relates the size of an earthquake source to a magnitude. Another advantage is that it is determined from very long periodic waves for the largest events, and does therefore not saturate. However, a disadvantage is that it cannot be measured directly without additional analysis (Reiter, 1990). The general form is;

$$M_W = (\log M_0 / 1.5) - 10{,}73 \qquad (4.1.6)$$

M_0 is seismic moment in dyn-cm (Stein and Wysession, 2003).

4.1.6.2 Choosing one magnitude

If enough data is available, the best magnitude scale to use is in fact the moment magnitude scale. All the other scales have their disadvantages. The M_L scale is not designed for earthquakes larger than $M_L = 7$, and not for epicentral distances greater than approximately 600 km. The M_s scale is not applicable for smaller than $M_s = 5$, greater than $M_s = 8.0$, deeper than 70 km, and for regional/local earthquakes with an epicentral distance less than about 1000 km.

The m_b scale is not applicable for shallow, small, larger than m_b = 6.2, and regional/local earthquakes with an epicentral distance less than about 1000 km.

Every magnitude scale except from the moment magnitude scale is determined with a particular wavelength and period, and this causes all magnitude scales, except from M_W to saturate at some point, as seen in fig. 4.1.6. After considering all these facts, the preferred scale to use in this earthquake catalogue is the moment magnitude.

4.1.6.3 Magnitude regressions

All events in the final earthquake catalogue have to be measured in the same magnitude. This is important, because different magnitude scales measures the magnitude with different methods, and thus give different values for the same event. Before making the magnitude regressions, it is important to run some statistics about which magnitudes that are available and how many of each type that exists, in order to be sure that there is enough data to do the converting process. Statistics were carried out in "Seisan" and "Seisan Explorer" with the aim to decide which magnitude relations that should be made (Havskov and Ottemöller, 2014). However, it is important to keep in mind that an absolute harmonization hardly can be achieved (Grünthal and Wahlström, 2009).

Another important factor is the attenuation. In this study, two build in attenuation models from Boore and Atkinson (2008), and Campbell and Bozorgnia (2008) were applied to the probabilistic seismic hazard assessment. Both of them are based on the moment magnitude. Ground motion prediction equations (GMPEs) are important in magnitude homogenization, because magnitude scales such as body-wave magnitude and surface-wave magnitude are dependent on the distance. The distance can thus affect the attenuation, and there is therefore a need for an GMPE when comparing such scales with moment magnitude.

There are a total number of 42 059 events in the catalogue before going through the magnitude regressions. 7735 of them have coda magnitudes, and 10 770 have local magnitudes. The numbers from the moment magnitude, the body wave magnitude, and from the surface wave-magnitude are too small (less than 100) to make any regression relations. Therefore, some of the events are removed in the process. However, since the relation between WKAN and CKAN is a good relation as seen in fig.4.1.7, it is possible to use the moment magnitude from

KANDILLI as the main scale and compare all other magnitude types to this scale. CKAN is the coda magnitude from KANDILLI.

First, the relation between WKAN and CKAN was carried out, and a good relation between the coda and the moment magnitude was obtained as seen in fig.4.1.7. The best fitting regression curve between these scales give the relation: y = 1.038*x – 0.001. From this relation, it is easy to see that both scales are quite similar and comparable to each other.

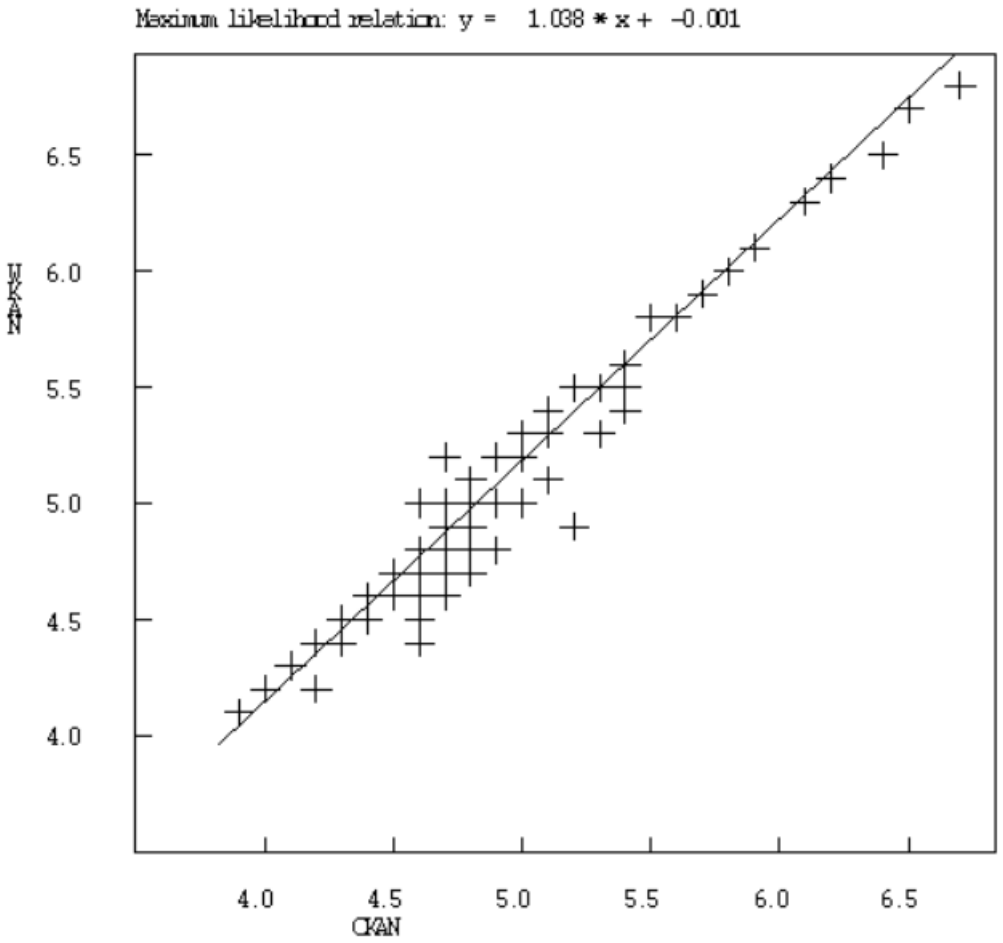

*Fig. 4.1.7. A relation between the moment and the coda magnitude. All recordings with both WKAN and CKAN is in the same event and are plotted to show the relationship between them. In this case, CKAN is based on WKAN. The best fitting regression curve gives the relation: y = 1.038*x – 0.001.*

Afterwards, both LDDA, L, D, and d were compared to CKAN to make regression values between them. At the end, the same process were done with comparing CKAN (same value as derived in fig. 4.1.7), LKAN, sKAN, and bKAN to WKAN. Finally, all events in the catalogue have been assigned a $M_{W,}$ based on the regressions. All regressions are listed in the table 4.1.3,

and plots are shown in appendix C.

Table 4.1.3. List off all the relations, including both the regression values and the quantity of all events involved in the regression process.

RELATION	**REGRESSION VALUES**	**QUANTITY**
LDDA - CKAN	y = 0.581 *X + 1.214	426
L - CKAN	y = 0.907 *X + 0.332	1180
D - CKAN	y = 0.951 *X + 0.119	7147
d - CKAN	y = 0.910 *X + 0.245	5683
CKAN - WKAN	y = 1.038 *X – 0.001	247
LKAN - WKAN	y = 1.101 *X – 0.329	294
sKAN - WKAN	y = 0.809 *X + 1.110	248
bKAN - WKAN	y = 1.107 *X – 0.337	248

4.1.7 Final earthquake catalogue

After removing duplicates, fake events, dependent events, and after merging all the catalogues, one final catalogue is remaining with approximately 42 000 events. Another important action was the homogenisation of the magnitudes, and making the regressions to convert all the magnitudes into the moment magnitude. All processes regarding finalizing the catalogue were done with a tool called Seisan (Havskov and Ottemöller, 2014) in order to control and make the completeness check, the weichert method, by plotting the Gutenberg Richer relation, the time of day distribution, the Poisson distribution, events per year, magnitude relations and by plotting all the hypocenter locations.

1. The completeness check

The purpose with estimating the completeness times, is to use these values in the weichert method in order to derive a- and b-values, that later will be used in the different source zones. The completeness time as seen in fig.4.1.8 for the different magnitudes in the catalogue varies with the annual seismicity rate. The completeness time for the largest events are often, but not always, longer than for the smallest events because of lacking recordings of small events in

earlier periods, and thus a resulting improvement in the coverage of seismic stations during the recent years. The completeness time must be determined for all the different magnitude classes and can be displayed using the Weichert method.

The completeness time is found by looking at the linear relation between the cumulative number of earthquakes and the years seen in fig. 4.1.8. The slope is proportional to the activity rate for every single magnitude class, and it is therefore important to choose the linear part of the slope before it start changing, because this is the complete part. In fig. 4.1.8, the completeness time for magnitudes 1-2 is from 2011 to present. For the magnitudes 2-3, 3-4, 4-5, 5-6, 6-7 as well as for 7-8, the completeness time is from the year 2009, 1978, 1968, 1901, 1901 and 1901 until 2014, respectively.

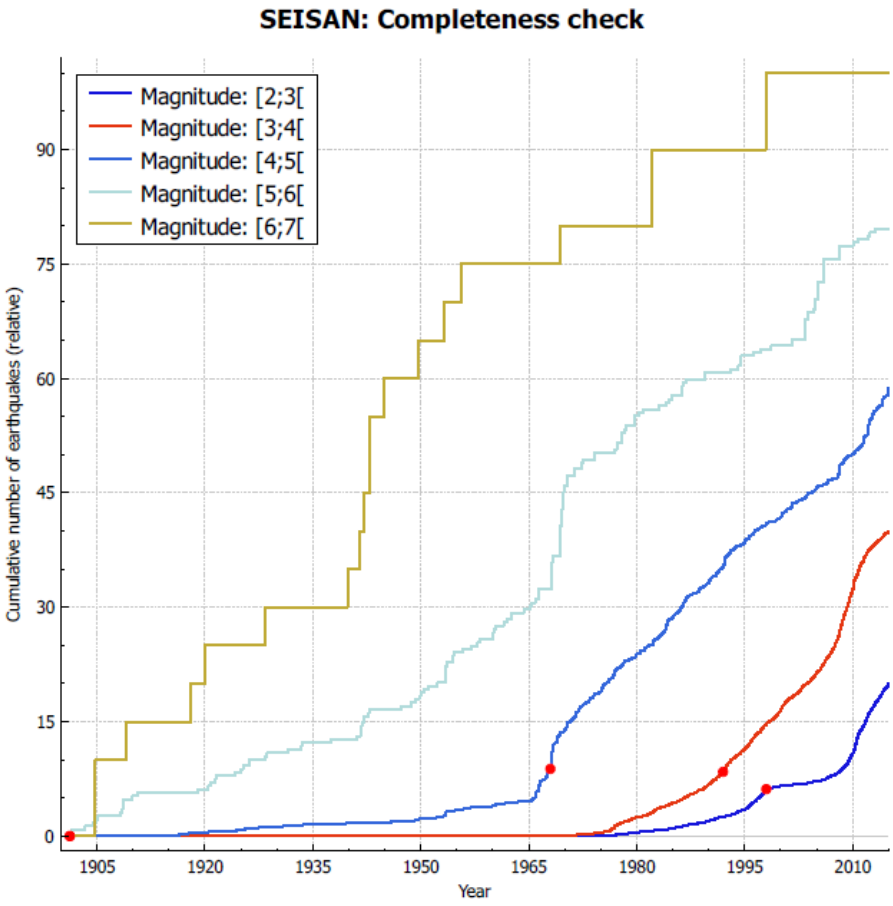

Fig. 4.1.8. The completeness time for all the magnitude classes. The cumulative number of events is on the y-axis, while the years are on the x-axis. The slope is proportional to the activity rate for each magnitude class.

1. The Gutenberg Richter relation and the weichert method

The Gutenberg Richter relation: “Log N = a – b*M” is used for describing the seismicity for probabilistic seismic hazard assessment studies, where both the “b- value” and “a” is derived empirically by a regression on the data from the catalogues. The a- value is the quantity of earthquakes expected at magnitude 0, and is a measurement for the seismic activity in the area. The b- value is the slope of the curve describing the relation between small and large earthquakes.

It is possible to get the a- and b- values only for the complete part of the earthquake catalogue by plotting the completeness time into the weichert method. The weichert method then calculates these values with respect to the completeness times. The weichert method derive as seen in fig. 4.1.9, a linear relation between the logarithmic number of earthquakes against the different magnitudes. The line is supposed to fit the different points, and the Weichert then uses these points to derive the b- value. It is possible to see that the cumulative estimated b- value in fig. 4.1.9 is close to one, which is expected in seismic active regions. Actually, almost all seismic hazard analysis rely on the idea of that the b- value are supposed to be constant (Jafari, 2008).

From fig.4.1.9, it is possible to see that the catalogue is complete only for earthquakes larger than about magnitude 3, and all events with smaller magnitudes are removed. The line is supposed to fit the points used to estimate the a- and b- value, and is in this case well fitting. As a conclusion, it is possible to argue that the earthquake catalogue is complete in some time-periods with magnitudes between 3 and 6, but there are always uncertainties.

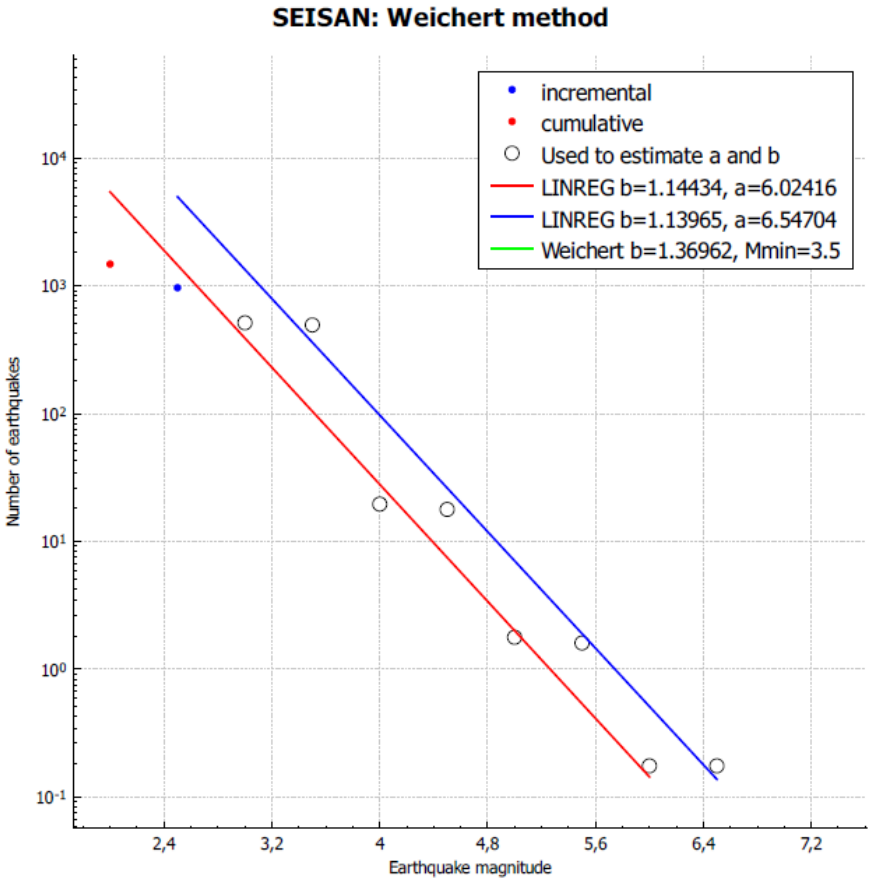

Fig. 4.1.9. Linear relation between the logarithmic number of the different earthquakes on the y-axis against the earthquake magnitude on the x-axis. The blue line is the incremental line, the red line is the cumulative line, and the circles are the points used to estimate the a- and b- value.

2. Time of day distribution

It is possible to check if most of the explosions are removed by checking the time of day distribution as seen in fig. 4.1.10. In the reality, there are supposed to be the same amount of events throughout the day.

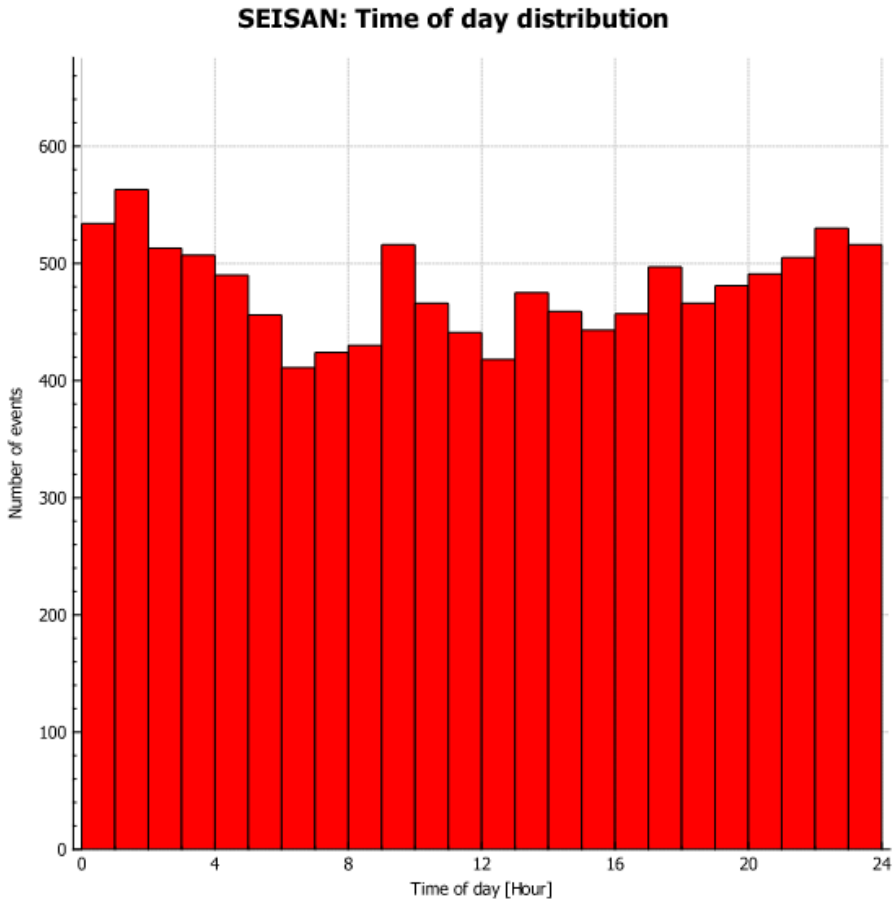

Fig. 4.1.10 Time of day distribution for all events in the final earthquake catalogue, with number of events on the y-axis and the time of the day on the x-axis.

3. The Poisson distribution

The purpose with looking at the Poisson distribution is to check if all dependent events are removed. The Poisson distribution is telling saying something about how many earthquakes that occurs in yearly intervals. In this catalogue there are different amount of events in every year and the most active year have more than 4200 events as seen in fig. 4.1.11. It is best to have as homogeneous distribution as possible, and if some years have large amount of events compared to the rest of the period, then there are probably too many dependent events left in the catalogue. In this earthquake catalogue, there are probably too many dependent events left, but being stricter in the process of removing dependent events will give too few events. The fact, that there probably still are some dependent events left in the catalogue, gives uncertainties in the final probabilistic seismic hazard assessmeny.

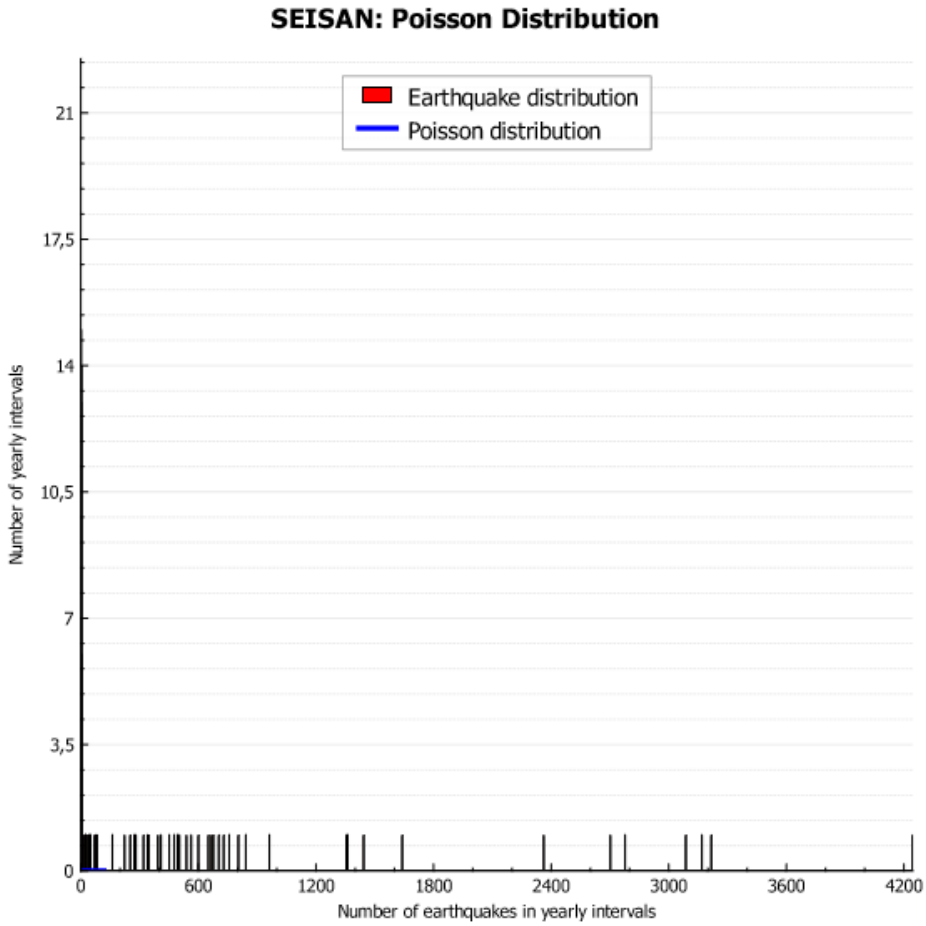

Fig. 4.1.11. The Poisson distribution is looking at the number of earthquakes in yearly intervals. The x- axis is the number of earthquakes in yearly intervals, while the y- axis is the number of yearly intervals.

4. Events per year

It is important to look at events per year for the same reason as for looking at the Poisson distribution, in order to look for years with more events than expected. From the final earthquake catalogue seen in fig. 4.1.12, it is possible to notice which years having most earthquake recordings. The year of 2011 as well as some years around 2006 have more earthquakes than expected, due to dependent events. The year of 2011 show large amount of events in both the events per year- figure and in the Poisson distribution. It is therefore still too many dependent events in the catalogue, but being stricter will cause fewer events in the catalogue. This was the deciding factor when considering being stricter or less strict in the removing of dependent events.

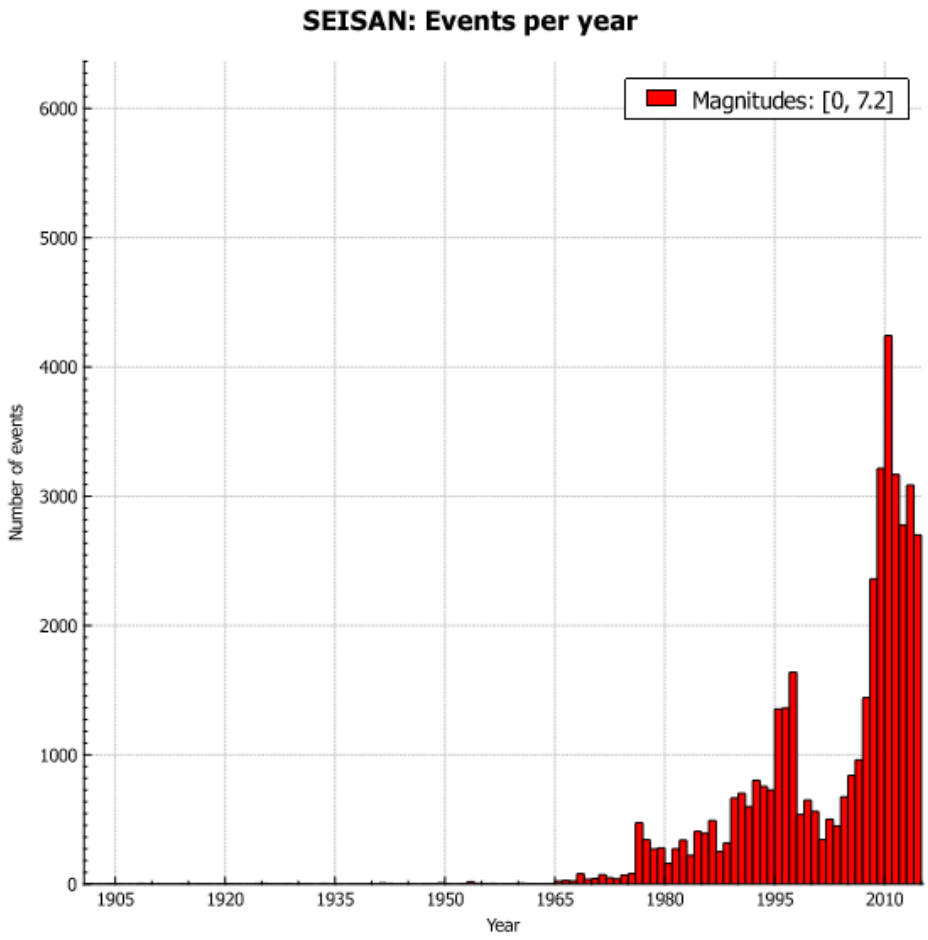

Fig. 4.1.12. The number of events per year in the earthquake catalogue. Number of earthquakes is on the y- axis, while the year is on the x- axis.

5. Distribution of hypocenters

It is also possible to look at the hypocenter distribution as seen in fig. 4.1.13 of all the earthquakes in the catalogue. Many of the events are located at +1000 km, and these probably reported with wrong depth in the catalogue. The main thing to retrieve from this distribution is that most of the earthquakes are shallow events, and thus located between 0 and 50 km depth.

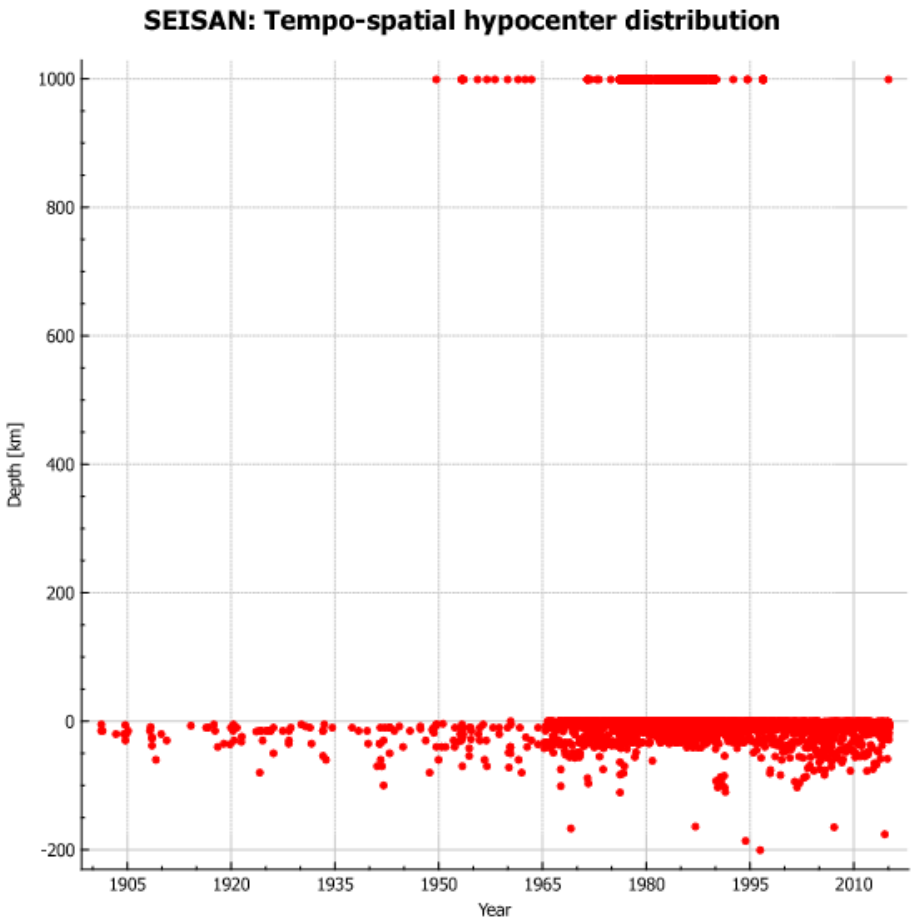

Fig. 4.1.13. The hypocenter distribution displayed with depth in kilometres on the y-axis and years on the x-axis.

4.1.8 Uncertainties and discussion

- Uncertainties

There is no purpose going through every single event looking for duplicates in the earthquake catalogue. Therefore, running the data through filters are the best way to filtrate out the most probable duplicates based on time, location, depth, and magnitude differences. If only one of these parameters are outside the limits, the event will not be considered as a duplicate and there is therefore a risk of having duplicates giving uncertainties to the catalogue.

Most of the fake events are already been removed by the different agencies, but errors from the agencies can still affect the catalogue. Dependent events are also capable of giving uncertainties to the earthquake catalogue. They are probably the biggest contributor of uncertainties because it is not always straightforward to separate a dependent event from a main event. Therefore, there will be a significant risk of having dependent events in the final catalogue. Other sources

capable of providing uncertainties to the catalogue can be location errors, especially for older events. There are also uncertainties in magnitudes, in depths and in incomplete datasequences, which is periods with bad coverage.

In the process of converting several magnitude scales into moment magnitude, the chance of having uncertainties is also present. Some of the events are removed in the process of converting all magnitudes into the final catalogue.

The converting process is based on everything from a few hundred to approximately 7000 events, which can give some uncertainties to the values, especially for the relations with only 200+ events. The main uncertainty here is regarding the low number of events considered in the converting process. These regressions are also based on the KANDILLI catalogue with chances of having errors from this agency. However, in overall, all the regression relations produced seems realistic.

- Discussion

In the process of making the final earthquake catalogue, there are as mentioned many factors capable of causing uncertainties to the catalogue. It is not possible to run through every single event looking for errors, but with all tools mentioned it is possible to rule out most of them. From the final catalogue, it seems like the number of events are large enough to make good analyses for the study area. From the Poisson distribution, it is seen a few years with too many dependent events.

However, a few years still stands out in fig. 4.1.12, compared to other years in the same period. There are too many events due to most likely dependent events, some duplicates and some fake events. A way of removing these events is to be stricter in the selection of the control limits (time and location of the dependent compared to the main event). However, when being stricter with the limits, the number of events will decrease significantly and thus cause trouble to the estimation of a- and b- values. Therefore, it is important to find a line between the number of events and the strictness in order to remove unwanted recordings.

The number of events with low magnitudes (M < 3) in the catalogue increases for almost each year, due to increasing number of seismic stations as well as improvement of the seismic stations in western Turkey.

4.2 Faults

4.2.1 Faults in the study area

One of the first tasks was to display the faults in the study area seen in fig. 4.2.1. Plotted 201 relevant faults compiled from mainly Bozkurt (2001) and Emre et al. (2005). These faults are coloured based on location and strike directions in order to differentiate between connected fault clusters.

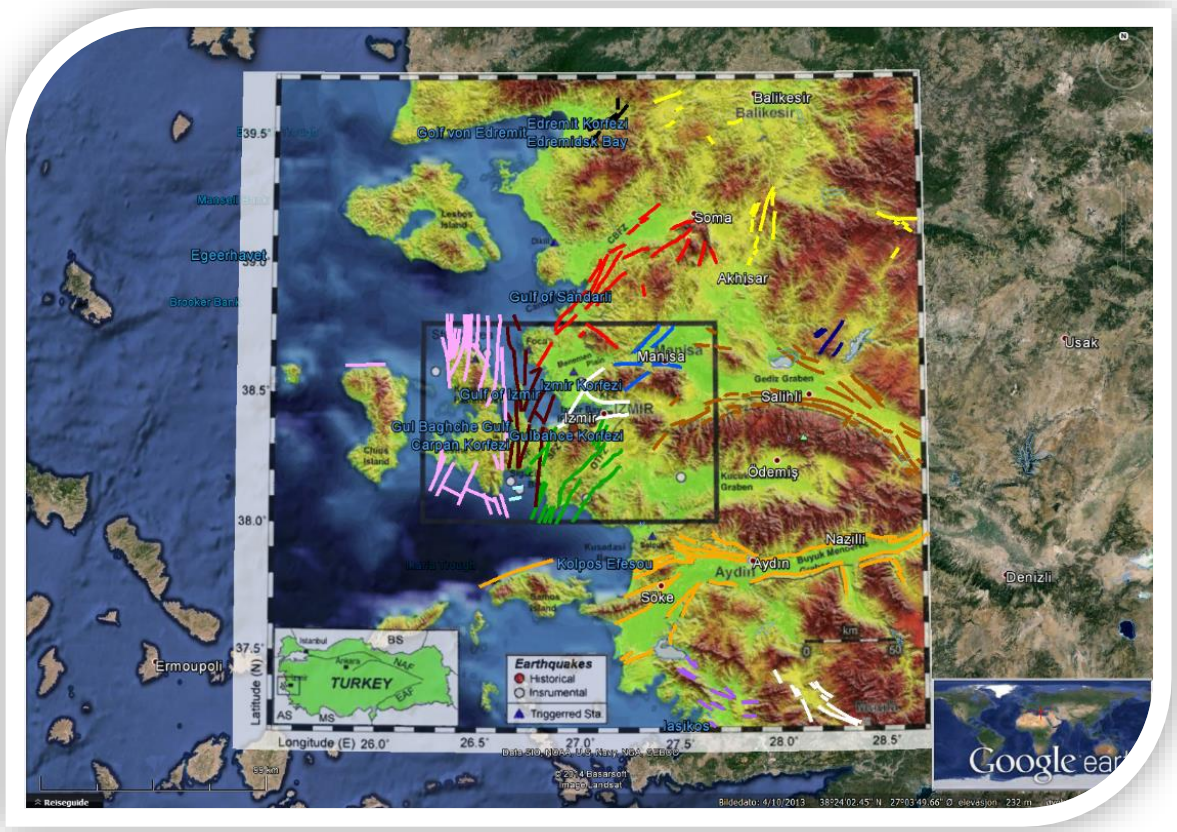

Fig. 4.2.1. Map of the main faults in the study area and surrounding region. All faults are compiled from Bozkurt (2001) and Emre et al., 2005, with minor modifications re-interpreted with respect to the local topography. The study area is located in western Turkey between the coordinates; 37-40˚N and 25-29˚E. The faults have different colours with intention to distinguish the different segments and tectonic trends. Base map is from Google Earth©.

The compiled maps from Bozkurt (2001) and Emre et al. (2005) are overlain on to the topographic map from Google Earth© in order to map all faults in the same map, as seen in fig. 4.2.1. The aim is to show all faults capable of causing earthquakes to the study area and make a list of all the faults. Later, some of these faults are used in stochastic ground motion simulations.

4.2.2 List of all faults

Table 4.2.1 presents a list of all faults found in the study area, and the region surrounding. They are divided into groups based on locality, how densely distributed they are, how connected they are to each other, and on the strike direction.

All of the faults were given different names, colours and numbers based on different parameters. The names were given based on the location. For instance, if they are located close to important places or cities. The colours are given in order to distinguish them based on how closely distributed they are, and on similarities in strike directions.

Table 4.2.1. List of all the faults. These are divided into groups based on location, strike and how they are connected. This table have columns based on group, quantity, colour, location, mean strike and strike of each fault. The strike directions are between 0˚ and 180˚ because of a lacking knowledge about the dip of the faults.

Group	Quantity	Colour	Location	Mean strike	Strike
Akhisar	09- nine	Yellow	Northeast in the study area. Close to the city of Gelenbe.	012.3˚ (N-S)	027,021,003,016,005,003,021,010,005
Balıkesir	05- five	Yellow	North in the study area. Southwest of the city Balıkesir.	078.1˚ (E-W)	068,061,058,145,072
Demirci	05- five	Yellow	Northeast in the study area.	102.5˚ (E-W)	098,123,120,123,035
Alaçatı	10- ten	Pink	Southern part of the Karaburun Peninsula, close to Izmir.	101.2˚ (E-W)	011,023,027,117,023,112,160,159,163,163
KaraburunPeninsula	13- thirteen	Pink	West of the Izmir-area on the north side of the peninsula.	028.3˚ (NE-SW)	178,172,178,001,007,013,009,003,008,003,
					010,003,144
Chios	1- one	Pink	North end of the Chios Island.	098.0˚ (E-W)	098
Büyük-Menderes-Graben-N	14- fourteen	Orange	North side of the Büyük-Menderes valley.	087.2˚ (E-W)	073,083,065,069,053,116,111,114,100,100,
					100,077,090,070
Büyük-Menderes-Graben-S	12- twelve	Orange	South side of the Büyük-Menderes valley.	080.1˚ (E-W)	052,045,066,017,027,095,080,171,073,079,
					149,150
Samos	01- one	Orange	North coast of the Samos Island, south in the study area.	069.0˚ (E-W)	069
Foça-Soma	22- twenty-two	Red	Between Foça and Soma, north in the study area.	053.3˚ (NE-SW)	031,044,032,024,065,051,056,052,032,067,
					071,048,049,055,047,045,127,031,174,031,
					015,157
Gediz-Alaşehir-Graben-N	12- twelve	Light brown	North side of the Gediz-graben, east in the study area.	118.1˚ (SE-NW)	117,094,097,128,108,122,133,134,130,117,
					120,116
Gediz-Alaşehir-Graben-S	29- twenty-nine	Light brown	South side of the Gediz-graben, east in the study area.	094.1˚ (E-W)	045,041,069,064,061,075,083,082,088,107,
					107,122,107,152,139,133,067,063,087,085,
					083,115,107,034,114,128,137,114,116
Gökeyüp	04- four	Dark blue	East in the study area, close to the city of Gökeyüp.	046.0˚ (NE-SW)	056,053,037,038
Havran	06- six	Black	North in the study area, close to the city of Havran.	043.6˚ (NE-SW)	000,062,052,062,040,042
Izmir	04- four	White	In the area sourrounding the city of Izmir.	065.6˚ (NE-SW)	081,052,032,097
Muğla+Yatağan	09- nine	White	Southeast in the study area.	138.0˚ (SE-NW)	153,152,149,158,115,138,127,122,128
Manisa	05- five	Blue	Right northeast of the city Izmir.	066.4˚ (NE-SW)	047,089,053,048,096
Milas	11- eleven	Purple	South in the study area, close to the city of Milas.	119.4˚ (SE-NW)	134,136,125,122,137,112,119,125,123,089,
					089
Seferihisar	08- eight	Green	Right south of the city Izmir.	025.7˚ (NE-SW)	016,041,034,024,025,025,025,016
Tuzla	06- six	Green	Right south of the city Izmir, right east of Seferihisar.	035.2˚ (NE-SW)	041,023,027,049,029,042
Sığacık	02- two	Light blue	In the Sığacık bat, right south of Izmir.	081.0˚ (E-W)	082,080
Urla	13- thirteen	Brown	Between Izmir and the Karaburun Peninsula.	059.6˚ (NE-SW)	016,153,008,172,179,156,001,066,024,029,
					135,020,005

In general, 31% of the mapped faults in table 4.2.1 have a NNE-SSW strike, which is comparable with the map in fig.2.1.2. The extension in the area are mainly perpendicular to this strike direction. The mean strike direction is calculated and included in the final list, in table 4.2.1 by taking the mean values from all faults in the same group. The different strike directions derived from the faults are calculated between 0˚ and 180˚, due to a lack information about the dip from these faults.

Some faults follows the topography, which is seen in fig.4.2.1, for instance in the southern part of the Gediz-Alaşehir graben. These faults are distributed along the border between the graben in north and the mountain range in south. Here the strike directions changes from a more SW-NE- to a more SE-NW direction from west towards east. All mean strike values are calculated based on the strike values from table 4.2.1.

Rose diagrams can be used in order to find the mean strike directions of faults in different regions in the mapping area. Here, all strike directions in the fault group are displayed in the same diagram. The length of the column reflects the number of faults with similar strike direction. There is a change in direction, from a more E-W strike in east, by the Gediz and the Büyük-Menderes graben, to a more NE-SW strike, closer to the Karaburun Peninsula. This also support the theory of having a small rotational point (Aktuğ and Kılıçoğlu, 2006) in the area surrounding Izmir.

It is interesting to observe the strike directions for other important areas, such as Izmir and in the Karaburun Peninsula. In Izmir, the mean strike direction from the four different faults is 65.6˚, NE-SW, which is seen in fig.4.2.2. From the rose diagram in fig.4.2.3 it is seen a main strike direction in an N-S direction for the Karaburun Peninsula. However, because of lacking knowledge about the dip of the faults, it is not possible to say if the strike direction is N-S or S-N, and therefore this particular mean strike value is uncertain.

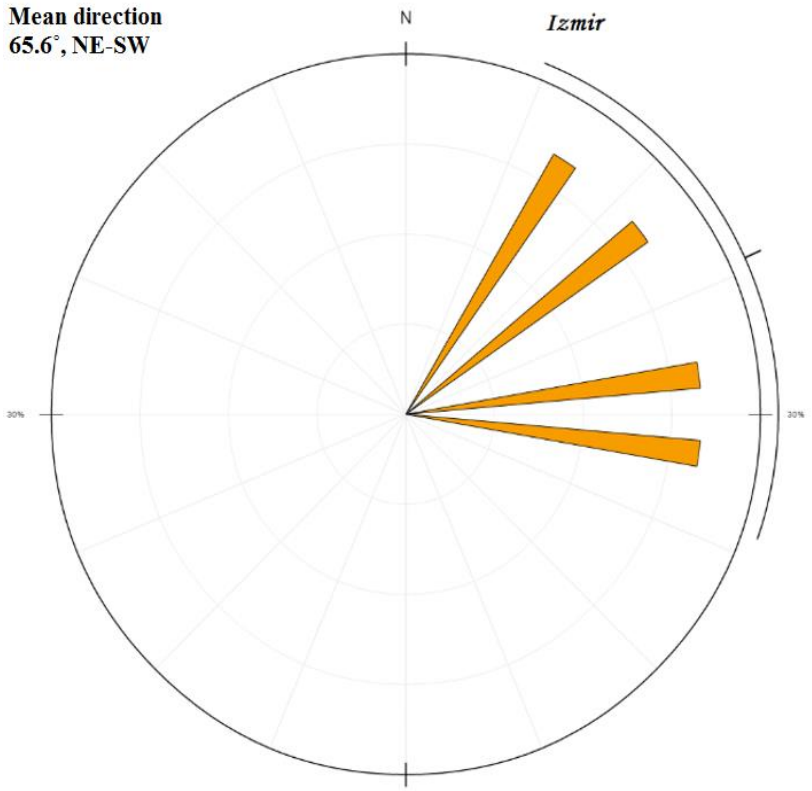

Fig. 4.2.2. A rose diagram showing the strike direction of the faults in Izmir. The length of the columns reflect the number of faults with the same strike direction.

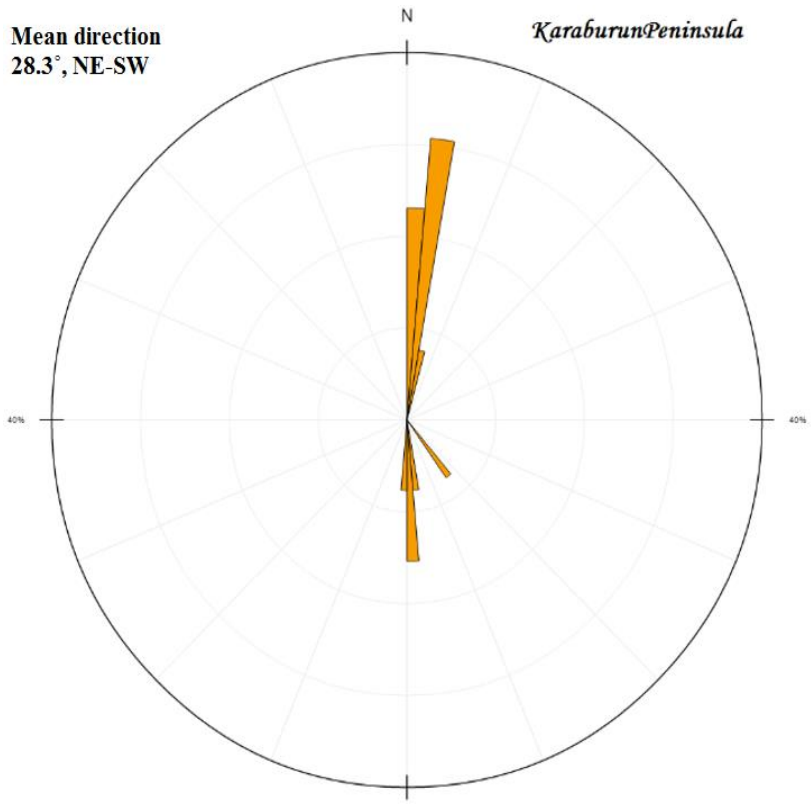

Fig. 4.2.3. A rose diagram showing the strike direction of the faults in the Karaburun Peninsula. The length of the columns reflect the number of faults with the same strike direction.

4.2.3 Fault parameters used in the stochastic ground motion simulations

In table 4.2.2, all fault parameters used in the stochastic ground motion simulations are listed. Relations from Wells and Coppersmith (1994) are used in order to derive fault source parameters such as the length, and width of the faults based on the chosen reference moment magnitude. In these simulations, random hypocenter locations is used. Important parameters that are capable of rapidly change the hazard is later discussed in the chapter 6.

Table. 4.2.2. List of fault parameters used in the stochastic ground motion simulation, included references.

Fault	**Izmir**	**Seferihisar**	**Tuzla**	**Manisa**	**Samos**	**Karaburun**
Mw	6.8	6.6	6.9	6.5	6.9	6.9
Reference	Bjerrum et al. (2013)	Bjerrum and Atakan (2008)	Bjerrum and Atakan (2008)	Bjerrum and Atakan (2008)	Wells and Coppersmith (1994)	Bjerrum and Atakan (2008)
Stress drop	30 bars	80 bars	79 bars	30 bars	30 bars	80 bars
Reference	Bjerrum and Atakan (2008)	Bjerrum and Atakan (2008)	Bjerrum and Atakan (2008)	Bjerrum and Atakan (2008)		Bjerrum and Atakan (2008)
Kappa	0.045	0.045	0.045	0.045	0.045	0.045
Reference	Akinci et al. (2013)					
Strike	259˚	194˚	43˚	270˚	249˚	179˚
Reference	Own	Own	Own	Own	Own	Own
Dip	60˚	80˚	80˚	48˚	80˚	80˚
Reference	Bjerrum et al. (2013)	Bjerrum et al. (2013)	Bjerrum et al. (2013)	Bjerrum et al. (2013)		Bjerrum et al. (2013)
Depth	2 km	2 km	2 km	2 km	2 km	2 km
Reference						
Fault type	Normal	Strike/slip	Strike/slip	Normal	Normal	Reverse
Reference	Bjerrum and Atakan (2008)	Benetatos et al. (2006)	Bjerrum and Atakan (2008)	Bjerrum and Atakan (2008)	Benetatos et al. (2006)	Benetatos et al. (2006)
Length/width	Wells and Coppersmith (1994)	Wells and Coppersmith (1994)	Wells and Coppersmith (1994)	Wells and Coppersmith (1994)	Wells and Coppersmith (1994)	Wells and Coppersmith (1994)
Subfaults	5x5 km	5x5 km	5x5 km	5x5 km	5x5 km	5x5 km
Reference						
Stress_ref	70 bars	70 bars	70 bars	70 bars	70 bars	70 bars
Reference						
V_rupture	2.5 km/s	3.0 km/s	3.0 km/s	2.5 km/s	2.5 km/s	2.5 km/s
Reference	Bjerrum and Atakan (2008)	Bjerrum and Atakan (2008)	Bjerrum and Atakan (2008)	Bjerrum and Atakan (2008)	Bjerrum and Atakan (2008)	
beta	3.2	3.2	3.2	3.2	3.2	3.2
Reference	Akinci et al. (2013)	Akinci et al. (2013)	Akinci et al. (2013)	Akinci et al. (2013)	Akinci et al. (2013)	Akinci et al. (2013)
Density/rho	2.8 g/cm^3	2.8 g/cm^3	2.8 g/cm^3	2.8 g/cm^3	2.8 g/cm^3	2.8 g/cm^3
Reference	Akinci et al. (2013)	Akinci et al. (2013)	Akinci et al. (2013)	Akinci et al. (2013)	Akinci et al. (2013)	Akinci et al. (2013)

Geometrical spreading function (km)	r^{-1} 1-20 $r^{-0.8}$ 20-40 $r^{-0.7}$ 40-100 $r^{-0.5}$ r>100	r^{-1} 1-20 $r^{-0.8}$ 20-40 $r^{-0.7}$ 40-100 $r^{-0.5}$ r>100	r^{-1} 1-20 $r^{-0.8}$ 20-40 $r^{-0.7}$ 40-100 $r^{-0.5}$ r>100	r^{-1} 1-20 $r^{-0.8}$ 20-40 $r^{-0.7}$ 40-100 $r^{-0.5}$ r>100	r^{-1} 1-20 $r^{-0.8}$ 20-40 $r^{-0.7}$ 40-100 $r^{-0.5}$ r>100	r^{-1} 1-20 $r^{-0.8}$ 20-40 $r^{-0.7}$ 40-100 $r^{-0.5}$ r>100
Reference	Akinci et al., 2013					
Qmin	60	60	60	60	60	60
Reference						
Q0	180	180	180	180	180	180
Reference	Akinci et al. (2013)					
eta	0.55	0.55	0.55	0.55	0.55	0.55
Reference	Akinci et al. (2013)					
Damping of response spectra	5%	5%	5%	5%	5%	5%
Reference	Bjerrum et al. (2013)					

4.2.4 Uncertainties

A few sources can potentially give uncertainties during the mapping of the faults in the study area and in the surrounding region. The compiled maps from Bozkurt (2001) and Emre et al. (2005) are overlain on to the topographic map from Google Earth© to make sure that the uncertainties in the fault coordinates are as small as possible.

Differences in the map projections can give small uncertainties in this process. Visual inspection of both the coordinates and the shape of the shoreline were done to improve mismatches, but this process also bring uncertainties. It is not possible to perfectly match the overlain maps with the Google Earth map without uncertainties, because both of these maps have been stretched and squeezed to best fit the Google Earth map. Both the stretching, the squeezing and miss judging of the topography can give uncertainties to the drawing process of the faults.

All of the interpretations are based on previous studies by Emre et al. (2005), Bozkurt (2001) and by the topography as mentioned. There is always a chance that these interpretations are somehow uncertain and thus not entirely correct. It is not easy to differentiate the true from the fake faults in the Google Earth map and in the overlain maps. In some of the loctions, there is a small deviation between the interpreted faults and the original interpreted faults, due to bad imaging, poor resolution, vegetation, infrastructure, the Aegean Sea etc.

All faults in table 4.2.1 have strike directions between 0˚ and 180˚, which gives a great error to some of the mean values, especially with those striking close to 0˚ or 180˚. This because there is a lack of information about the dip from these faults, and when doing the mean calculations it is of importance if the strike is N-S or S-N.

Areas close to Izmir as well as areas as the Büyük-Menderes graben and the Gediz graben are well covered, but other areas are not as well covered. The fact that some areas are not so well studied, and the fact that most of the offshore faults are incomplete, gives a significant uncertainty to the mapping process.

4.3 Source zones

The zonation is carried out by determining source areas having a similar frequency of earthquakes of different magnitudes. Many factors influence the choice of source zones. They are decided based on differences in the morphology, the seismicity and by the amount and the size of faults.

4.3.1 Zonation process

The zonation in this study is based on both the morphology, faults, and the seismicity.

- The morphology

The morphology is a factor worth considering, because earthquakes occur at faults, and faults tend to occur in areas where the morphology changes. Such areas can for instance be transition zones between flat and high areas, which often are created by an offset (movement of the earth). It is also worth mentioning that flat areas in the valleys often have a higher seismicity than the mountain regions, due to the rifting process. In addition, the graben areas often consists of softer rock materials than the mountain regions, and the attenuation models used in the probabilistic hazard analyses often use different parameters on different rock densities. Therefore, some source zones are cut in the transition between high and low areas, especially if also the seismicity is different.

An important observation is the fact that the western parts of Turkey still goes through reactivation of earlier faults, due to the collision between the Eurasian plate, the African plate and the Arabian plate. The Anatolian microplate then move westwards in the same time as the Anatolian microplate move towards the Hellenic arc in south.

This causes the Anatolian plate to crack up and produce normal faulting, especially in the area close to Izmir. The reactivation of faults have earlier created this system of grabens bordered and followed by mountain ridges all along the west coast from north to south. These structures are asymmetric and visible on the morphology as seen in fig.4.2.1.

- The seismicity

The seismicity is important in the zonation process because it differentiates areas based on the seismic activity. It is important to have source zones with similar seismicity, where also the events are homogeneous distributed. The seismicity is the first factor considered when making the zonation for the area, because of the lacking knowledge about faults, and because the seismicity is well mapped for the study area.

- The faults

The faults are also important in the zonation process. It is important to have clusters of faults with similar strike in the same source area. Often these faults follows the morphology and increase the seismicity in that area. All these three parameters are well connected to each other and have to be considered together in the zonation.

4.3.2 List of source zones

All source zones are listed in table 4.2.2, and plotted in fig. 4.2.4, below. They are differentiated based on the morphology, the seismicity and the faults. These arguments are described together with additional information about the zones. In the PSHA analysis, all these source zones will be used in order to find the a- value, the b- value and the maximum expected magnitude earthquake, and use this to compute the probabilistic seismic hazard map.

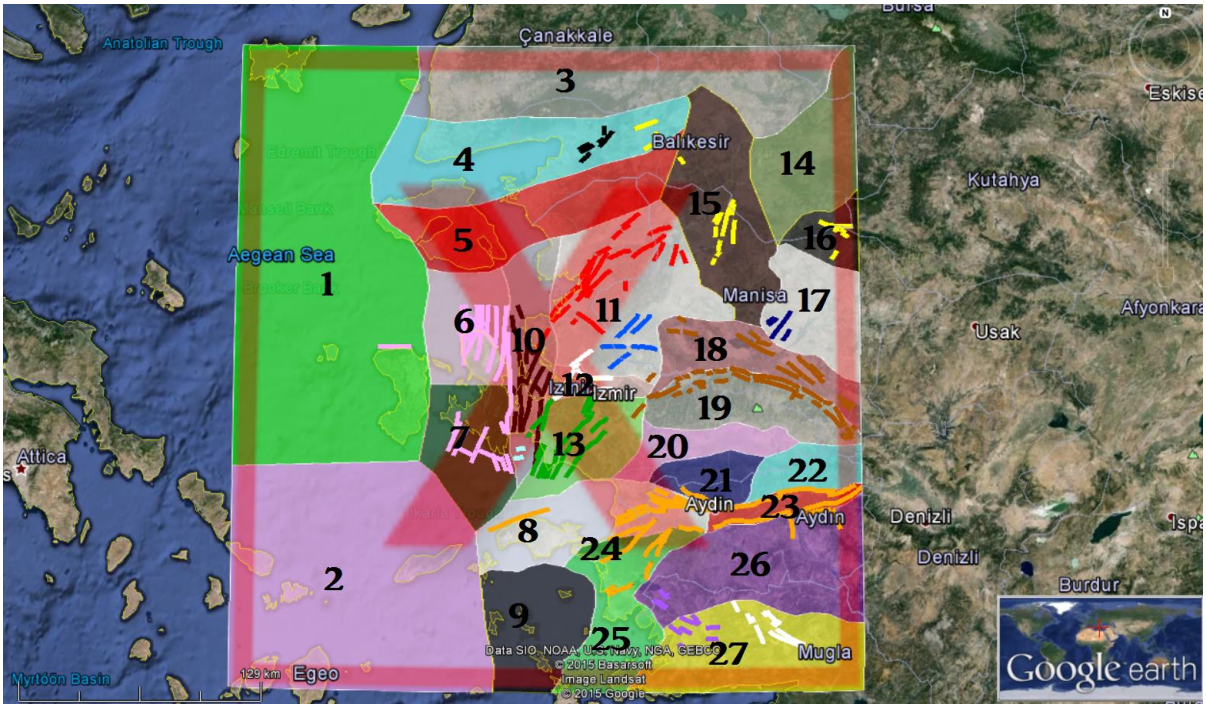

Fig 4.2.4. Map from GoogleEarth© with all source zones numbered together with all mapped faults in the study area.

Table 4.2.2. A complete list of all source zones with both source zone number and a description of the zonation decision.

Source zone	**Description**
1	This zone has a homogeneous seismicity throughout the zone and is based on the seismicity. There are only one E-W trending fault, and no bathymetry to follow.
2	The seismicity in this zone is considerably lower than in all surrounding zones. This is the main factor considered in why choosing this zone. The zone is located in the Aegean Sea, and there is no visible bathymetry.
3	This zone is located in a mountain region with approximately the same seismicity as in zone1, and is divided based on the fact that this zone is on land, while zone1 is located in the ocean. The seismicity in surrounding zones except from zone1 is also different from this zone. There are no mapped faults. Originally, a part of this zone had too few recordings and it was not possible to get good a-, and b- values from the Gutenberg-Richter relation. It was possible to merge them together, because of a similar seismicity in both areas. For earthquakes greater than M_W = 4, it was a slight difference, but in overall the best option was to merge them together.
4	The seismicity follows the same trend as the morphology with strike in a SW-NE direction. This trend is seen at the Çanakkale Peninsula in fig. 4.2.4. The mapped faults

	follows the same trend. This zone is located in a graben area, and is divided from surrounding zones mainly based on differences in the seismicity.
5	This zone has a hilly topography, but have the same strike trend in the seismicity and in the morphology as in zone4. However, this zone is less active than all surrounding zones and is mainly based on the relatively low seismicity.
6	This zone is mainly based on the faults, which distinctly trends N-S. The seismicity is also quite high compared to the surrounding zones, except for the zone lying right east of this zone.
7	This zone is divided through the middle of the peninsula based on differences in the seismicity. This zone has less seismicity than the surrounding zones, except from the quite zone in southwest (zone2). The faults also have a strike in a SW-NE direction, which is different from the surrounding zones.
8	This zone is divided in two at the city of Aydın, because of a less seismicity east of this city. The seismicity is in fact lower in all surrounding areas, except from the bordering zone in south. This zone is therefore based on the seismicity, the morphology (it is located in a graben area), and because of some E-W trending faults.
9	This zone is mainly based on the seismicity and maintain a higher seismicity than all surrounding zones. This is an offshore zone and there is no visible topography or detected faults, and the only factor considered is the seismicity.
10	This area has quite high seismicity but has not experienced very destructive earthquakes during the last 100 years. The faults are more than 30 km long in an N-S direction, is located just 30 km from Izmir, and has the potential to cause large earthquakes. Therefore, this zone is mainly based on the seismicity level, which is higher than in the surrounding areas.
11	This zone has a quite homogeneous seismicity and have experienced some large earthquakes in the past. The area is dominated by mountain regions divided by valleys. Most of the faults have a strike in SW-NE direction, but they are not as long as the faults closer to the Karaburun Peninsula. All these three factors are considered in the process of differentiating this zone from the surrounding zones.
12	This zone consists of three large faults, including the main Izmir fault. Two of the faults have a strike direction in E-W, while the third one have a strike in a SW-NE direction. The seismicity is also relatively high, but this zone is mainly based on the fact that these faults have other strike directions than surrounding faults, as well as the differences in the morphology.
13	This zone follows the structures, the morphology, and the faults in a SW-NE direction. This zone is chosen mainly based on the faults, because this area maintains more faults,

	including the large Seferihisar fault than the surrounding zones. The seismicity is similar to other zones nearby, and the morphology is quite complex with no distinct grabens or mountain regions. However, the seismicity is lower in the Menderes graben and in the mountain regions east of this zone.
14	There are no visible structures or detected faults in this mountain region, and therefore the only factor considered is the seismicity. The seismicity is higher here than in the zone bordering in north, but lower than in the other surrounding zones.
15	The faults are in a SW-NE direction and follows the valleys. This zone is mainly based on the seismicity, which is higher than in the surrounding areas.
16	This zone is located in a mountain region with some minor valleys. The faults follows the valleys in a SE-NW trend. The seismicity is homogeneous and higher than in the surrounding areas. This zone is mainly based on the seismicity level and on the distinct SE-NW trending faults, which differentiate this zone from the surrounding zones.
17	It is a mountain region with some SW-NE trending faults that follows the structures. This zone is also based on the fact that the seismicity is significantly lower here than in the surrounding zones.
18	This zone is mainly based on the topography. It is located in a graben area, while the surrounding areas are located in more mountain dominated environments. It is also divided from the southern part of the Gediz graben based on a higher seismicity in this zone than in the mountain region in south. There are also faults that mainly strikes SE-NW and follows the topography.
19	This zone is located in a mountain region with less seismicity than in the Gediz graben. It is mainly based on the morphology, because this zone is bordered by lower graben areas. There are faults following the structures and the topography from east towards west.
20	This is a graben zone based mainly on the morphology, because it is trapped in between two mountain regions. The seismicity is quite low in this zone, lower than in all surrounding zones, except from the mountain region bordering to the north. There are no faults detected, and the zone is therefore based on only the seismicity and the topography.
21	In addition, this zone is mainly based on the morphology and the seismicity. This zone is trapped between graben areas surrounding this mountain region, and the seismicity is different from the surrounding regions. One fault strikes in a SE-NW direction.
22	This mountain region is based on the seismicity, which is significant lower than in all surrounding areas. There are no detected faults in this zone.

23	This zone is based on all three factors. The faults are in this zone located in an E-W direction and the zone is located in a graben area. All other areas are mountain regions except from the zone west of Aydın, but this zone maintains a higher seismicity.
24	It is a small source zone that follows the topography with a small mountain ridge trending NE-SW. The zone is mainly based on a relatively low seismicity level compared to the surrounding zones.
25	This graben area stretches out in the Aegean Sea and is based mainly on the seismicity, which is quite low compared to nearby zones. The faults detected are striking in a SW-NE direction and follows the same trend as the structures do. Originally a part of this zone had too few recordings and it was not possible to get good a-, and b- values from the Gutenberg-Richter relation. It was possible to merge them together, because of a similar seismicity in both areas.
26	This zone is located in a mountain region with distinct lower seismicity than the source zone bordering to the south. This zone is based on the seismicity, the topography as well as on the faults. Most of the faults are trending in a SE-NW direction, and they are not large. The main factor considered is therefore the seismicity level.
27	This zone is a hilly region with valleys in between. This area is mainly based on the seismicity level, which is higher than in the surrounding areas. There are also some SE-NW striking faults following the same trend as the valleys.

4.3.3 Seismicity values for PSHA

Seismicity values for the various source zones in the study area are derived, in order to use them in the probabilistic seismic hazard assessment. Table 4.2.3 is made up by the seismicity values derived from the Gutenberg Richter relation in each of the source zones in fig. 4.2.5.

*Table 4.2.3. For each zone, a- value, alpha, b- value, beta, standard deviation, max observed magnitude and number of events as input. *Historical event.*

ZONE	a-value	alpha	b-value	beta	Standard deviation	Max observed /expected M_W	Number of events
1	4.69384	1.01069	1.042050	2.39940	0.15	6.6/7.1	2458
2	4.03641	0.13225	1.092220	2.51492	0.17	5.9/6.5	401
3	3.85188	0.25902	0.986344	2.27114	0.43	6.8/7.3	1512
4	4.35697	0.34355	1.071330	2.46682	0.26	6.6/7.1	1572
5	5.70329	0.05560	1.546270	3.56041	0.46	6.7/7.2	1371
6	3.93115	0.34992	0.974930	2.24485	0.23	6.4/6.9	706
7	4.31504	0.07638	1.207120	2.77947	0.44	6.2/6.7	601
8	4.66886	0.32589	1.145730	2.63814	0.13	6.1/6.6	1739
9	5.04358	0.14092	1.309910	3.01617	0.19	5.0/6.5	696
10	5.26648	0.17721	1.337330	3.07931	0.14	5.4/6.5	1331
11	5.02350	0.40201	1.204280	2.77295	0.20	6.4/6.9	6410
12	3.34738	0.07012	1.000340	2.30336	0.40	8.0*/8.5	208
13	3.76571	0.20337	0.990536	2.28079	0.39	6.3/6.8	717
14	4.59508	0.23195	1.162150	2.67594	0.16	6.0/6.5	1972
15	5.26867	0.41441	1.255830	2.89165	0.07	6.0/6.5	5010
16	2.82442	0.21871	0.774343	1.78299	0.42	5.9/6.5	325
17	4.88622	0.00940	1.536210	3.53725	0.24	4.9/6.5	402
18	3.62367	0.23854	0.943579	2.17267	0.51	6.9/7.4	723
19	4.37392	0.04394	1.273560	2.93248	0.16	4.9/6.5	470
20	3.01278	0.06366	0.935307	2.15362	0.35	5.6/6.5	143
21	3.56902	0.05444	1.074020	2.47302	0.12	5.1/6.5	186
22	3.18352	0.01620	1.105290	2.54502	0.33	4.0/6.5	87
23	2.32934	0.04433	0.818366	1.88435	0.44	6.0*/6.5	64
24	2.86498	0.00891	1.092230	2.51495	0.19	4.4/6.5	42
25	4.17620	0.04139	1.235400	2.84461	0.43	6.5/7.0	323
26	4.56773	0.08579	1.252060	2.88297	0.20	6.0*/6.5	880
27	5.53260	0.49980	1.296400	2.98507	0.14	6.3/6.8	6793

CRISIS, the program used to derive the probabilistic seismic hazard is using alpha and beta values as input. These values are derived from the a-, and b- value with the formulas (4.3.1) and (4.3.2). These formulas originate from the Gutenberg Richter relation; log N = a – b*M.

$$beta = b*ln(10) \quad (4.3.1)$$

$$alpha = 10\hat{}(a-b*M_0) \quad (4.3.2)$$

alpha is reflecting the seismicity rate, but has to be considered together with the area of the various zones because larger zones normally gives a higher seismicity. beta, which looks at the relation of small versus large events has an uncertainty, measured in standard deviation of about 0.1 - 0.5. The max observed M_W in the source zone also has an uncertainty of about 0.5, which are used in the probabilistic seismic hazard assessment to derive the maximum expected magnitude.

4.3.4 Uncertainties

There are possible uncertainties connected to the zonation process. A zonation is a subjective process where decisions of source zones are based on a few factors regarding the morphology, the seismicity and on the faults.

A problem is that not all of the faults are discovered and many of the offshore faults are not mapped completely. Lacking knowledge about the faults provides a possibility of having faults cut either by two-source zones or because of lacking information about the subsea faults. This can be the case in some zones, if it is not possible to do the zonation based on the seismicity.

The morphology is often quite complex and there is therefore a possibility of having uncertainties in the process of dividing areas with respect to changes in the morphology. Another possible problem with the seismicity is areas with low seismicity, because these areas actually can build up large amount of stresses, which later eventually can be released in form of very destructive events.

5. Results

In this chapter, all results are given from both the probabilistic seismic hazard analysis and from the stochastic ground motion simulations.

5.1 Probabilistic seismic hazard analysis

The probabilistic seismic hazard analysis for the study area is done by using 10% and 2% probabilities combined, with 50 and 100 year time intervals, by using two ground motion prediction equations (GMPE's) from Boore and Atkinson (2008) and from Campbell and Bozorgnia (2008). The 10% probability for 50 years is equal to a return period of 475 years, while the 2% probability in 50 years is equal to a return period of 2475 years. These return periods are the most common return periods used in seismic hazard analyses. The 10% probability in 100 years equals to a return period of 949 years, while a 2% probability in 100 years equals to a return period of 4950 years.

Periods of 50 and 100 years refers to the expected lifetime of solid buildings, e.g., governmental buildings and structures, and are chosen for this study. There are no large infrastructures except from a larger oil refinery at the north side of Izmir, and therefore longer time periods are not considered in this thesis.

The ground motion is calculated and expressed in peak ground acceleration (PGA), and with spectral acceleration (SA), both measured in acceleration of gravity, g. The peak ground acceleration is the measurement for what a particle on the ground experiences, while spectral acceleration is the measurement for what is experienced by a building. In this study, 5% damping is used together with two different periods of 0.3s and 1.0s in order to calculate the seismic hazard.

The seismic hazard is calculated for the whole area as shown in fig. 5.1.1, including values from the cities of Izmir, Çeşme, Aydin, Nazilli, Salihli, Dikili, Kuşadası, Manisa and Akhisar. All cities are marked in fig. 5.1.1. The study area inside the yellow box is the area that will be used to show the final hazard map. The corner areas outside the study area will give lower hazard

because of side effects, due to lacking information about the seismicity and are therefore not considered in the final hazard map.

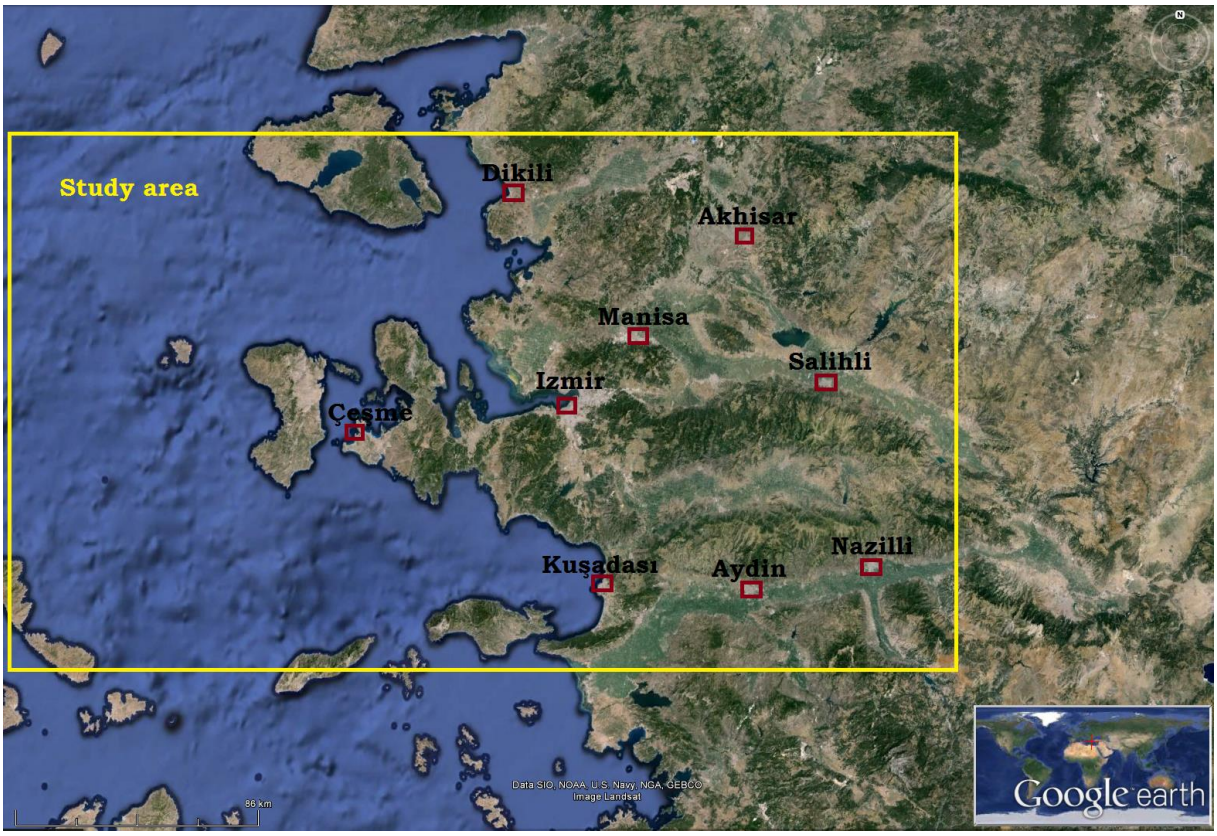

Fig. 5.1.1. Map showing the cities included in the probabilistic seismic hazard assessment. The yellow box show the study area.

All ground motion values from these nine cities, including both PGA and SA values are listed in table 5.1.1. All other ground motion values are shown in figures either in chapter 5.1 or in appendix A. The reason for giving the seismic hazard in form of PGA and SA values is that these are the most common values used to display the seismic hazard in other scientific studies, and thus make it easier to compare results.

PGA, and SA values based on a period of 0.3s and 1.0s will be described separately for the return period of 475 years, by using both the GMPE from Boore and Atkinson (2008) and Campbell and Bozorgnia (2008). Using other return periods for the same GMPE's does not change the differences between the different regions in the study area as seen in the table 5.1.1. Table 5.1.1 is shown in chapter 5.1.5. The only thing changed is the level of ground motion. To save space, the results using return periods of 2475, 949, and 4950 years are briefly commented. All values are listed in table 5.1.1, and maps showing the hazard are listed in appendix A. For practical reasons, all results are plotted separately for Turkey and Greece.

Results using a return period of 475 years are found in chapter 5.1.1, while PGA results using return periods of 2475, 949, and 4950 years are listed in chapter 5.1.2, 5.1.3, and 5.1.4 respectively. The SA results using return periods of 2475, 949, and 4950 years are found in appendix A.

5.1.1 Results by using a return period of 475 years

The PGA values calculated by using a return period of 475 years are shown in fig. 5.1.2, giving the ground motion values in selected Turkish cities. The calculations are based on the GMPE's from Boore and Atkinson (BA08) and Campbell and Bozorgnia (CB08), and gives the highest values for Izmir with 0.27g and 0.16g, respectively.

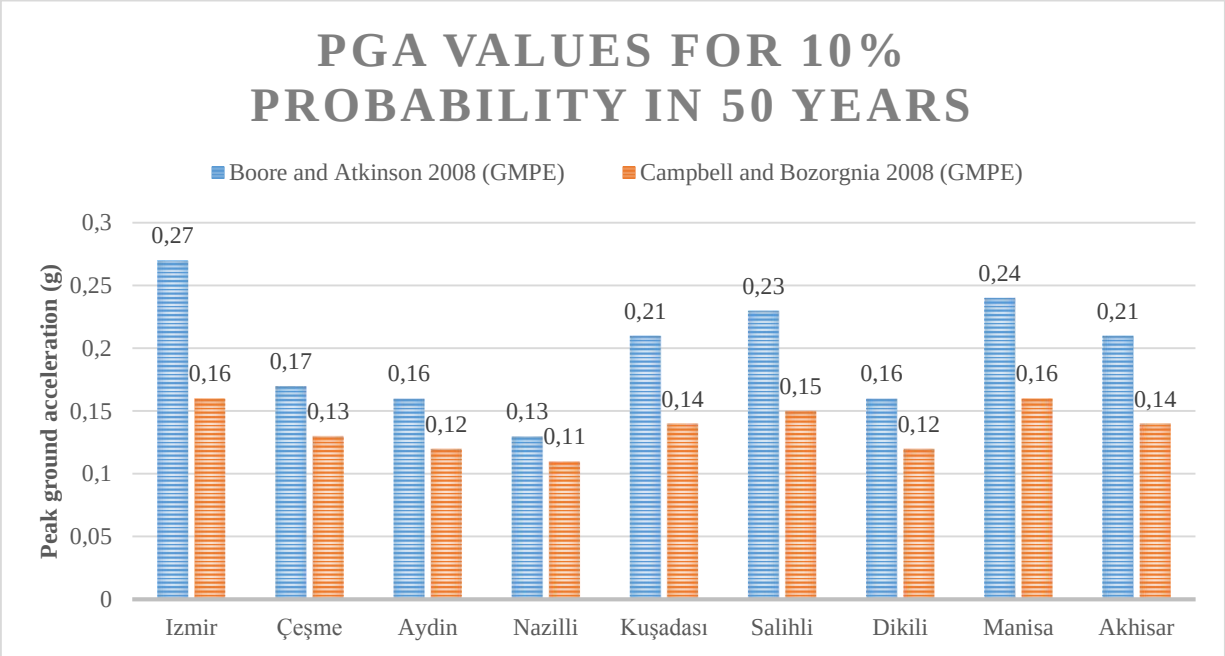

Fig. 5.1.2. The PGA values in different Turkish cities for a return period of 475 years. The results in the blue column are calculated based on the GMPE from Boore and Atkinson (2008), while the results in the orange column are calculated based on the GMPE from Campbell and Bozorgnia (2008).

In general, all PGA values based on the BA08 relation give higher values than calculated from the CB08 relation. The cities with the lowest PGA values have the smallest differences between the BA08 and CB08 results.

By using the BA08 relation, except from Izmir, the cities of Kuşadası, Salihli, Manisa and Akhisar have the highest PGA values with around 0.22g, while Çeşme, Aydin and Dikili have

PGA values of about 0.16g. The city of Nazilli have the lowest value of 0.13g. The same pattern is found for the CB08 relation, with Izmir and Manisa having the highest PGA values of 0.16g. All the other cities, except from Aydin, Nazilli and Dikili have PGA values above 0.12g. Nazilli have the lowest value of 0.11g. All data is shown in table 5.1.1.

Results using the GMPE from Boore and Atkinson (2008)

1) PGA results

The seismic hazard on the Turkish side of the study area, by using a return period of 475 years, and GMPE from Boore and Atkinson (2008) is shown in fig. 5.1.3, by using PGA values, measured in g.

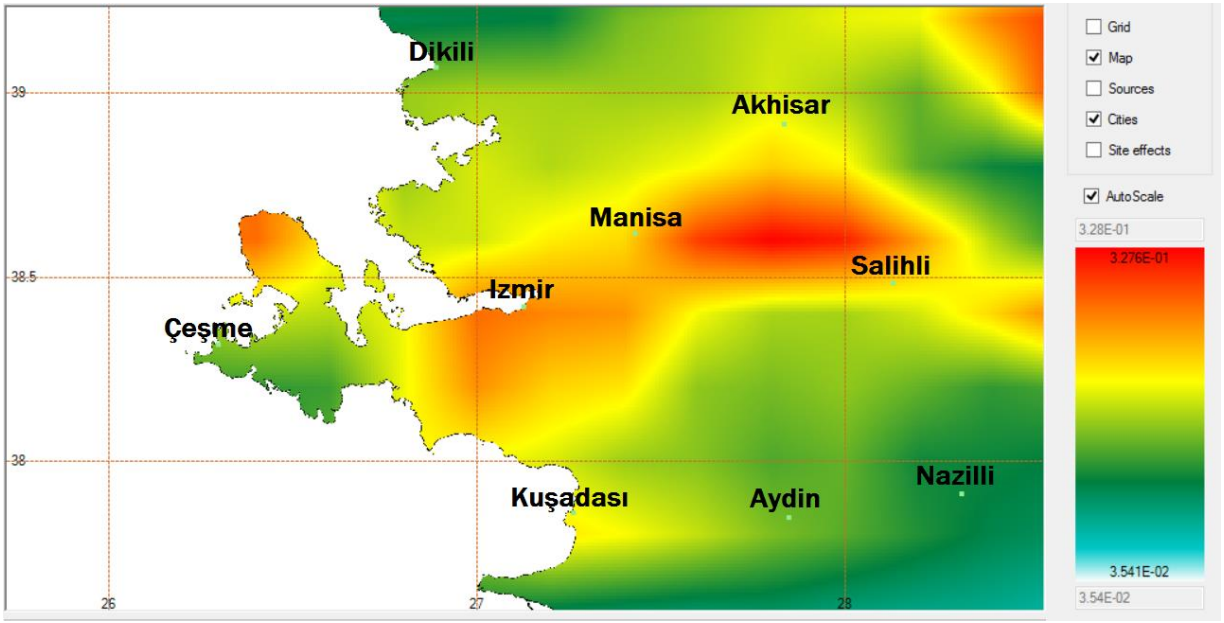

Fig. 5.1.3. Seismic hazard map showing PGA values on the Turkish side of the study area for a return period of 475 years. The colours represent the different PGA values measured in g. These results are based on the GMPE from Boore and Atkinson (2008).

The area in fig.5.1.3, extending from approximately 50 km southwest of Izmir and northeast towards the cities of Akhisar and Salihli, have high PGA values ranging from 0.18g to 0.33g. The highest PGA values are found in the triangle between the cities of Manisa, Akhisar and Salihli. This area is located in a low lying area in the Gediz graben were the PGA values varies from around 0.20g and up to peak values of 0.33g. Izmir have PGA values of about 0.27g in the city centre, but there are even higher values a few kilometres southwest of the city located at the southern side of Izmir bay with peaks up to 0.28g.

Another area worth considering is the Karaburun Peninsula, seen in fig.5.1.3. This peninsula is located west of Izmir. This region have considerably higher PGA values for the northern part than for the southern part. The northern part have values above 0.28g, while the southern part have values around 0.17g. A PGA value of 0.17g was found in the seaside resort of the town Çeşme. The PGA values are even lower further south on the peninsula, which are down to around 0.14g.

There are relatively high PGA values northeast of Akhisar. This area is located in a graben area bordering to a mountain region in the south. There are identified PGA values ranging from about 0.25g to 0.29g in the area. In addition, a small region close to the city of Kuşadası, southwest in the study area have values of about 0.21g, slightly higher than in the surrounding region.

The areas with lowest PGA values are the hilly areas north of Dikili as well as the areas southeast of the cities Aydin and Nazilli, south in the study area. The area stretching from Dikili and northwards along the coast have lower PGA values than surrounding areas. This area have PGA values ranging from about 0.16g in Dikili and down to about 0.13g further north. The mountain region south of the Büyük Menderes graben, south of Aydin and Nazilli also have lower PGA values than the surrounding areas. This area have PGA values estimated to be between 0.09g and 0.13g. The mountain region located northeast of Salihli have lower PGA values than the surrounding graben areas with values ranging from about 0.12g to about 0.15g.

The seismic hazard on the Greek side of the study area, by using a return period of 475 years, and the GMPE from Boore and Atkinson (2008) is shown in fig. 5.1.4, by using PGA values.

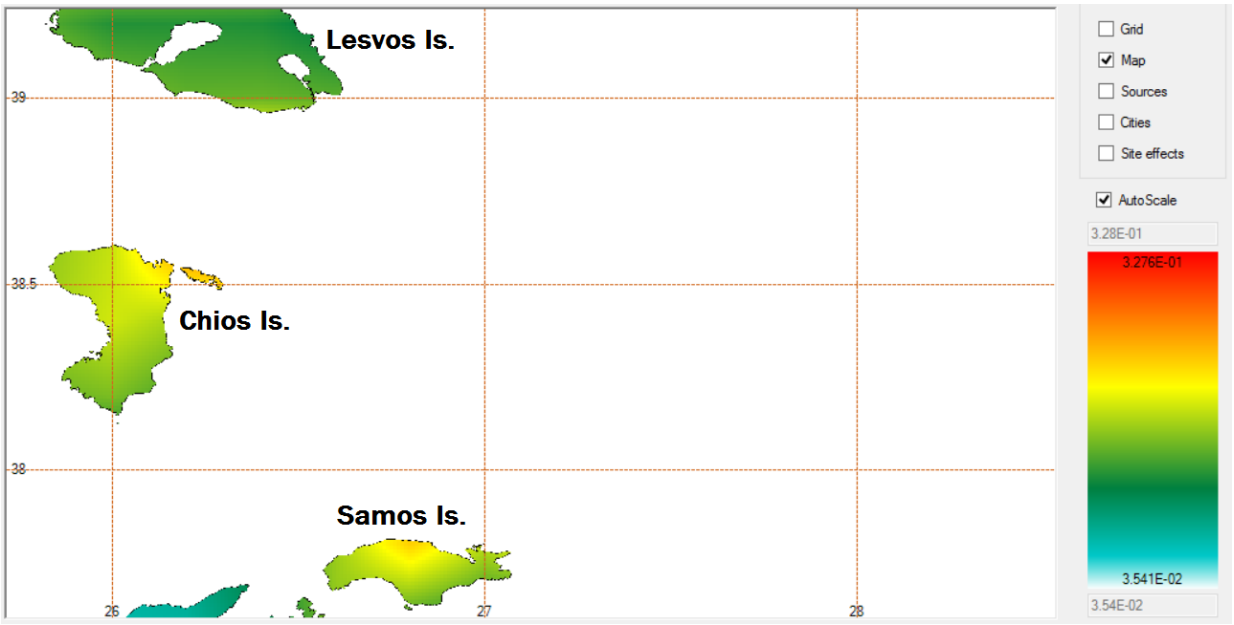

Fig. 5.1.4. Seismic hazard map showing PGA values on the Greek side of the study area for a return period of 475 years. The colours represent the different PGA values measured in g. These results are based on the GMPE from Boore and Atkinson (2008).

On the Greek side of the study area as seen in fig.5.1.4, three islands have been considered. The PGA values are highest on the Chios Island, a bit lower on Samos Island, and lowest on Lesvos Island. The PGA values on Lesvos are ranging from about 0.13g to about 0.17g, with the highest values south on the island. On the Chios Island, which is located west of the Karaburun Peninsula, the PGA values are higher, ranging from about 0.15g in the southern part to the peak value of 0.24g in northeast. On Samos Island, the highest values are found north on the island with PGA values reaching up to 0.23g.

2) SA results with a period of 0.3s

The seismic hazard on the Turkish side of the study area, by using a return period of 475 years, and the GMPE from Boore and Atkinson (2008) is shown in fig. 5.1.5, by using SA values for the period of 0.3s.

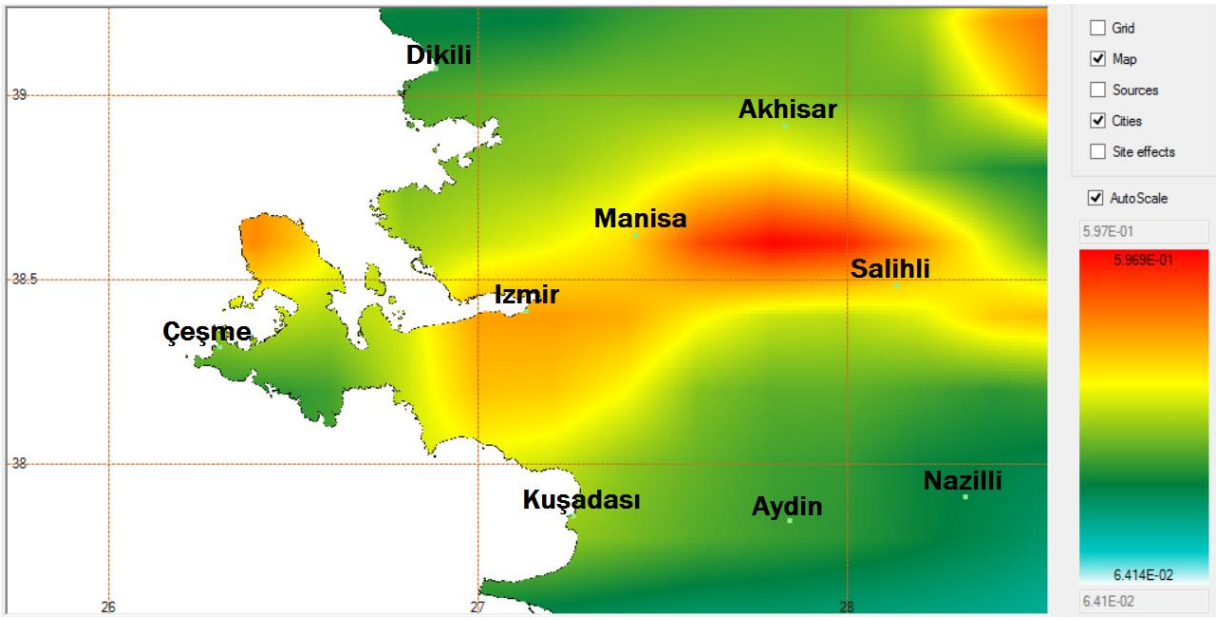

Fig. 5.1.5. Seismic hazard map showing SA values for the period T = 0.3s on the Turkish side of the study area for a return period of 475 years. The colours represent the different SA values measured in g. These results are based on the GMPE from Boore and Atkinson (2008).

The SA values found in the study area show the same pattern of values as the results derived in fig. 5.1.3, by using PGA values, but with the same GMPE and return period. This is shown by looking at the results in table 5.1.1.

The area in fig.5.1.5, extending from approximately 50 km southwest of Izmir and northeast towards the cities of Akhisar and Salihli have high SA values, ranging from 0.45g to 0.50g. The highest SA values are located in the triangle between the cities of Manisa, Akhisar and Salihli with SA values ranges from around 0.47g to peak values of 0.50g. Izmir have SA values of 0.46g in the city centre.

The Karaburun Peninsula have higher SA values for the northern part than the southern part of the peninsula. The northern part have values above 0.48g, while the southern part have values around 0.30g, similar to the values found in the seaside resort town of Çeşme. The SA values are even lower further south on the peninsula, down to about 0.26g.

There are relatively high SA values in an area northeast of Akhisar. This graben area maintain values ranging from 0.45g to 0.47g. The small region close to the city of Kuşadası, have values of about 0.32g, slightly higher than in the surrounding region.

The areas with lowest SA values are the same as for the PGA data with the same return period and GMPE. The hilly areas north of Dikili have lower SA values than the surrounding areas with values ranging from about 0.26g in Dikili and down to about 0.20g further north. The mountain region south of the Büyük Menderes graben also have lower SA values than the areas surrounding, with the lowest SA values estimated to be between 0.16g and 0.20g. The mountain region northeast in the study area, still have lower SA values than the surrounding graben areas with values ranging from about 0.20g to about 0.25g.

The seismic hazard on the Greek side of the study area, by using a return period of 475 years, and the GMPE from Boore and Atkinson (2008) is shown in fig. 5.1.6, by using SA values for the period of 0.3s.

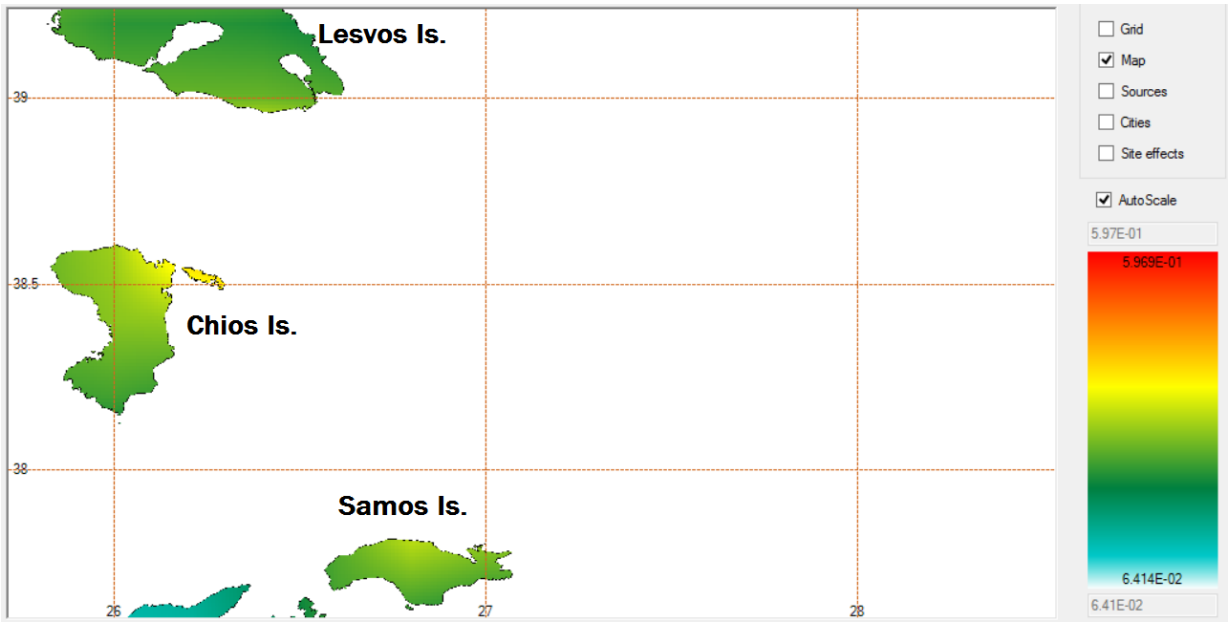

Fig. 5.1.6. Seismic hazard map showing SA values for the period T = 0.3s on the Greek side of the study area for a return period of 475 years. The colours represent the different SA values measured in g. These results are based on the GMPE from Boore and Atkinson (2008).

The SA values found in the study area on the Greek side as seen in fig. 5.1.6 show the same pattern of values as the results derived in fig. 5.1.4 by using PGA values, but with the same GMPE and return period.

The SA values are still highest on Chios Island, and lowest on Lesvos Island. The SA values on Lesvos are ranging from about 0.24g to about 0.32g, with the highest values south on the Island. On Chios Island, the SA values ranges from about 0.25g in the southern part to the peak value of 0.40g in northeast. On Samos Island, the highest values are found north on the Island

with SA values reaching 0.34g.

3) SA results with a period of 1.0s

The seismic hazard on the Turkish side of the study area, by using a return period of 475 years, and the GMPE from Boore and Atkinson (2008) is shown in fig. 5.1.7, by using SA values for the period of 1.0s.

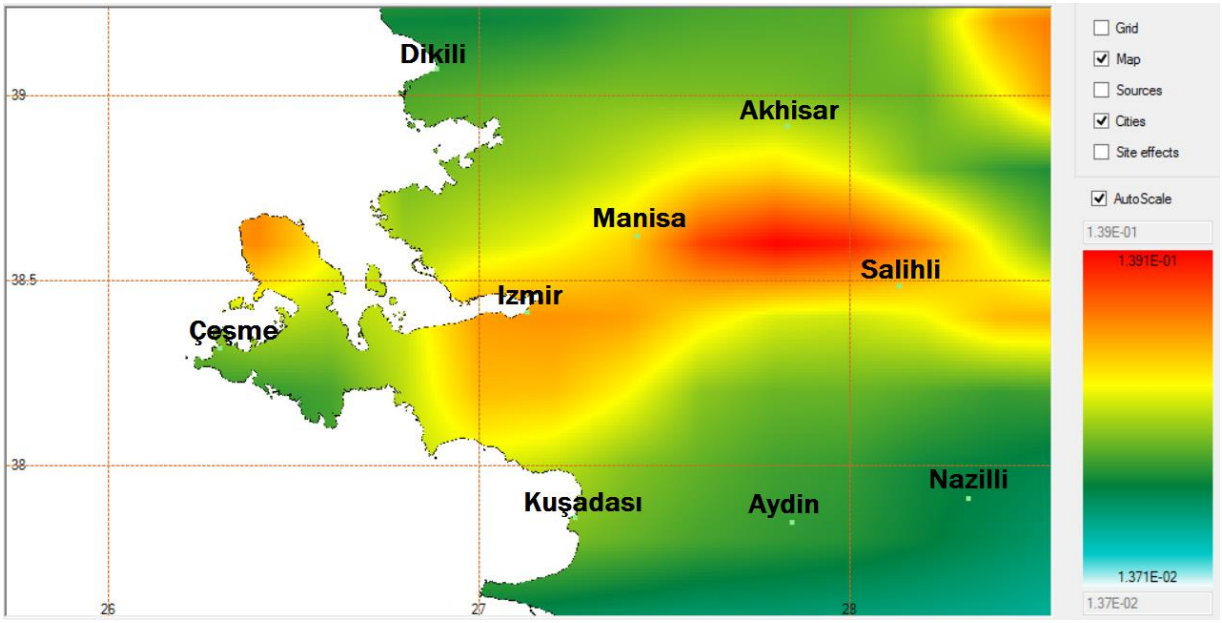

Fig. 5.1.7. Seismic hazard map showing SA values for the period T = 1.0s on the Turkish side of the study area for a return period of 475 years. The colours represent the different SA values measured in g. These results are based on the GMPE from Boore and Atkinson (2008).

The SA values found in the study area using a period of 1.0s show the same pattern of values as the results derived in fig. 5.1.5 using SA values with a period of 0.3s, but with the same GMPE and return period. The only clear difference is the fact that the values using a 1.0s period instead of a 0.3s period are significant lower.

The highest SA values are still found in the triangle between the cities of Manisa, Akhisar and Salihli as seen in fig. 5.1.7, and the SA values ranges from around 0.10g up to peak values of 0.14g. Izmir have SA values of 0.11g in the city centre.

The Karaburun Peninsula also have higher SA values for the northern part than the southern part of the peninsula, but as for all other values using a period of 1.0s, these values are significant lower. The northern part have values above 0.11g, while the southern part have

values around 0.07g such as the value found in the seaside resort town of Çeşme. The SA values are even lower further south on the peninsula down to around 0.06g.

The highest SA values in the area northeast of Akhisar, ranges from 0.10g to 0.12g. The small region close to the city of Kuşadası, have values of about 0.07g, slightly higher than in the surrounding region. The areas with lowest SA values are the same as for the SA data using a period of 0.3s as well as the PGA values with the same return period and GMPE. The hilly areas north of Dikili have lower SA values than the surrounding areas with values ranging from about 0.06g in Dikili and down to about 0.05g further north. The mountain region south of the Büyük Menderes graben also have lower SA values than the areas surrounding, with the lowest SA values estimated to be between 0.04g and 0.05g. The mountain region northeast in the study area also have lower SA values than the surrounding graben areas with values ranging from about 0.05g to about 0.07g.

The seismic hazard on the Greek side of the study area, by using a return period of 475 years, and the GMPE from Boore and Atkinson (2008) is shown in fig. 5.1.8, by using SA values for the period of 1.0s.

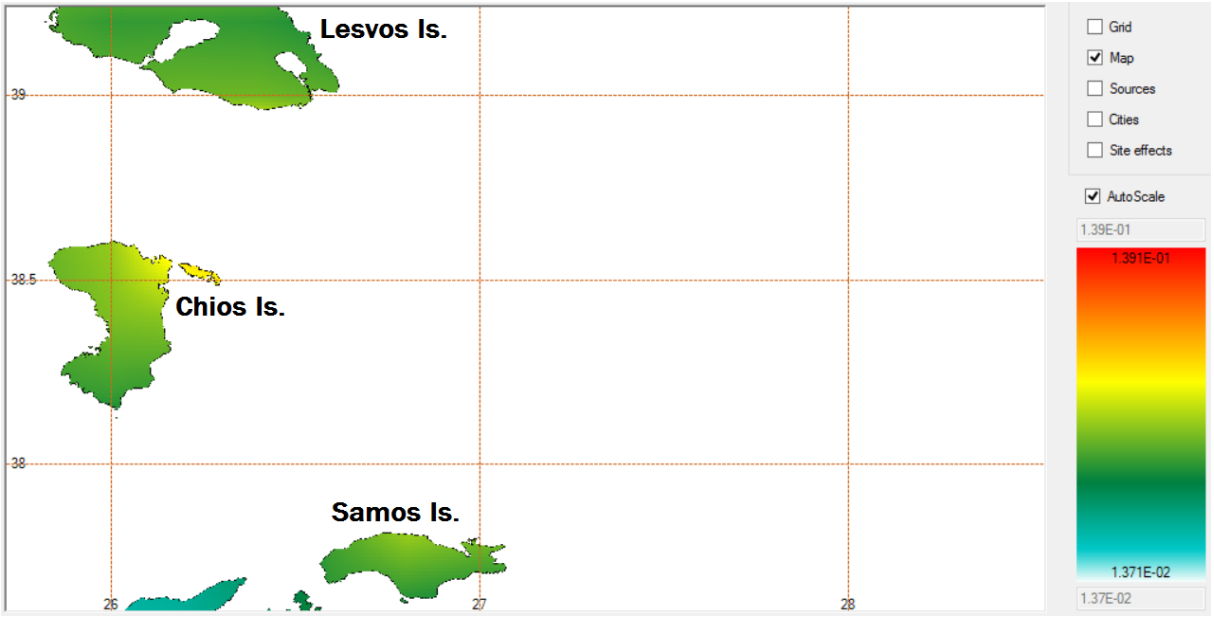

Fig. 5.1.8. Seismic hazard map showing SA values for the period T = 1.0s on the Turkish side of the study area for a return period of 475 years. The colours represent the different SA values measured in g. These results are based on the GMPE from Boore and Atkinson (2008).

The SA values for a 1.0s period found in the study area on the Greek side as seen in fig. 5.1.8, show the same pattern of values as the results derived in fig. 5.1.6 using SA values with a period

of 0.3s, both with the same GMPE and return period. The only clear difference is the fact that the values using a 1.0s period instead of a 0.3s period are significant lower. The SA values are still highest on Chios Island, and lowest on Lesvos Island. The SA values on Lesvos are ranging from about 0.06g to about 0.07g, with the highest values south on the Island. On Chios Island, the SA values ranges from about 0.06g in the southern part to the peak value of 0.09g in northeast. On Samos Island, the highest values are found north on the Island with SA values reaching 0.07g.

Results using the GMPE from Campbell and Bozorgnia (2008)

1) Results in PGA

The seismic hazard on the Turkish side of the study area, by using a return period of 475 years, and GMPE from Campbell and Bozorgnia (2008) is shown in fig. 5.1.9, by using PGA values, in g. The colour bars in the figures from CB08 differs from BA08, using an auto scale. This for easier observe differences in the seismic hazard throughout the study area in CB08, which has a more homogenous distributed hazard.

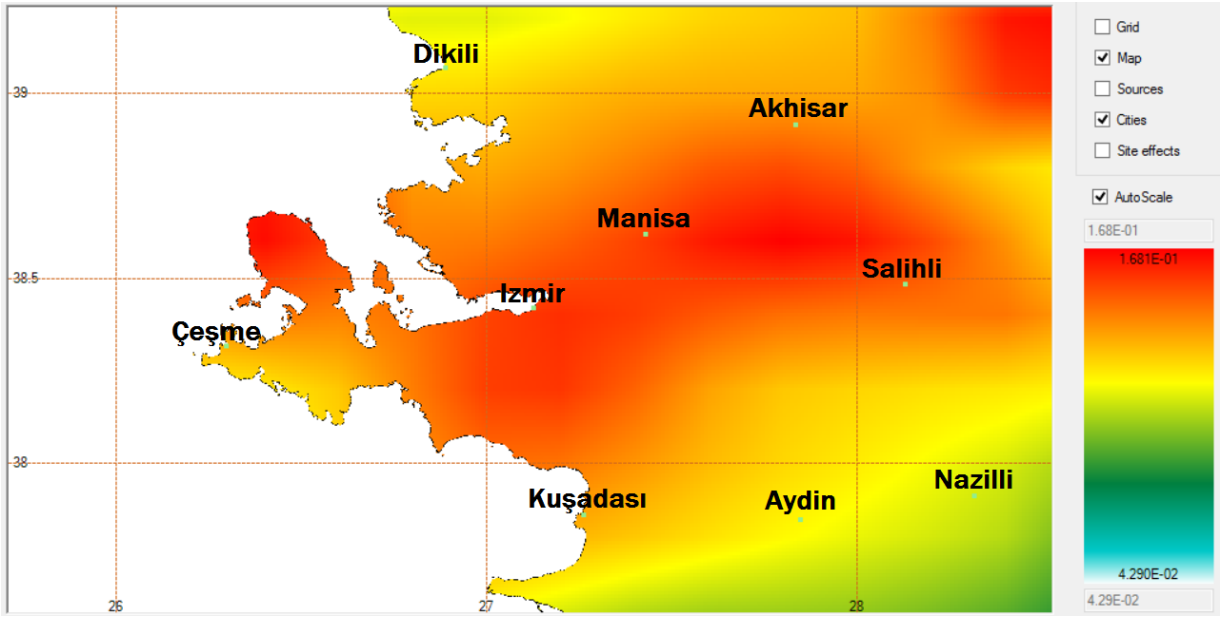

Fig. 5.1.9. Seismic hazard map showing PGA values on the Turkish side of the study area for a return period of 475 years. The colours represent the different PGA values measured in g. These results are based on the GMPE from Campbell and Bozorgnia (2008).

The PGA values seen in fig.5.1.9 are similar but not identical to the one using the GMPE from Boore and Atkinson (2008). The distribution of ground motions are systematically smaller, and there are less differences between the highest and lowest values by using the GMPE from Campbell and Bozorgnia (2008) than by using the GMPE from Boore and Atkinson (2008) as seen in fig. 5.1.2.

High PGA values are found in three places in the study area with values peaking at 0.17g. One of the areas is still the low-lying graben area extending from approximately 50 km south of Izmir and northeast towards the cities of Akhisar and Salihli. This area have PGA values of about 0.16g to 017g, including Izmir with a value of 0.16g. Northern parts of the Karaburun Peninsula still have PGA values higher than on the southern part, with values of about 0.17g in north and 0.12g in south. Also, the area northeast in the study area have considerably high values of about 0.17g.

The area with lowest PGA values is the hilly region just south of the Büyük Menderes graben as seen in fig. 5.1.9. The PGA values in this mountain region vary between 0.09g and 0.11g. Also the area stretching from Dikili and north along the coast have lower PGA values than surrounding areas, ranging from 0.12g in Dikili and down to about 0.11g further north.

The seismic hazard on the Greek side of the study area, by using a return period of 475 years, and GMPE from Campbell and Bozorgnia (2008) is shown in fig. 5.1.10, by using PGA values.

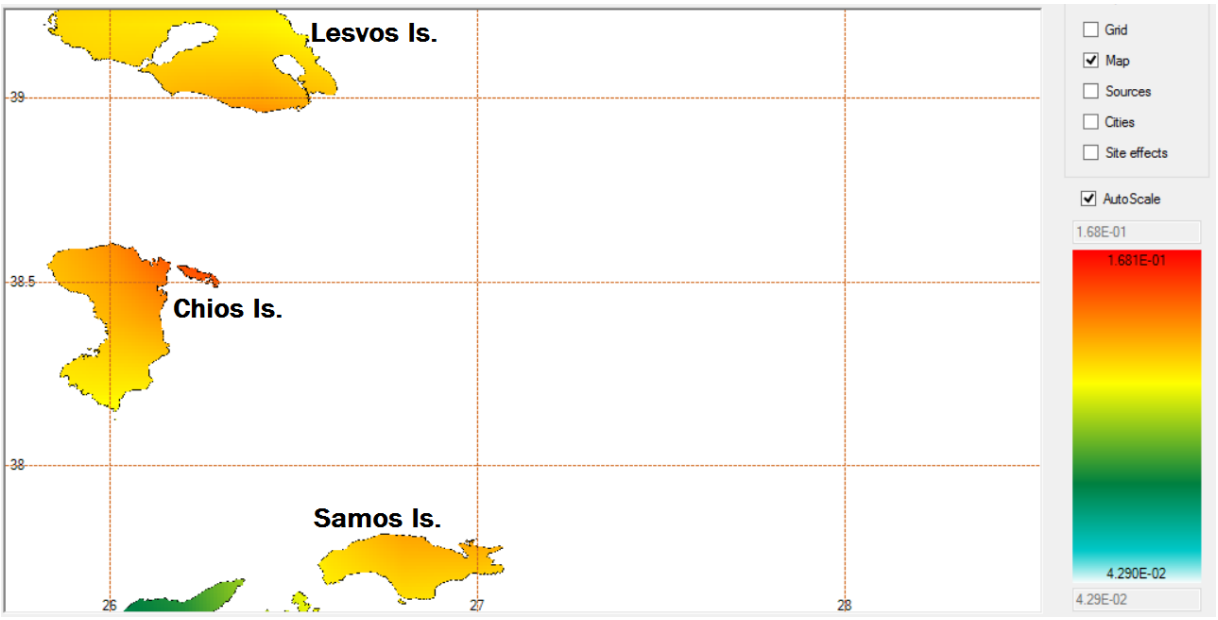

Fig. 5.1.10. Seismic hazard map showing PGA values on the Greek side of the study area for a return period of 475 years. The colours represent the different PGA values measured in g. These results are based on the GMPE from Campbell and Bozorgnia (2008).

The PGA values on the Greek side of the study area are generally lower than on the Turkish side. The PGA values at Lesvos Island are highest at the southern part of the island with values up to 0.14g, while the values decreases further northeast to around 0.12g. The PGA values are even higher on the Chios Island, with values ranging from about 0.12g in south to 0.15g in northeast. The highest values found on Samos Island are found on the north coast with PGA values reaching 0.14g.

2) SA results with a period of 0.3s

The seismic hazard on the Turkish side of the study area, by using a return period of 475 years, and the GMPE from Campbell and Bozorgnia (2008) is shown in fig. 5.1.11, by using SA values for the period of 0.3s.

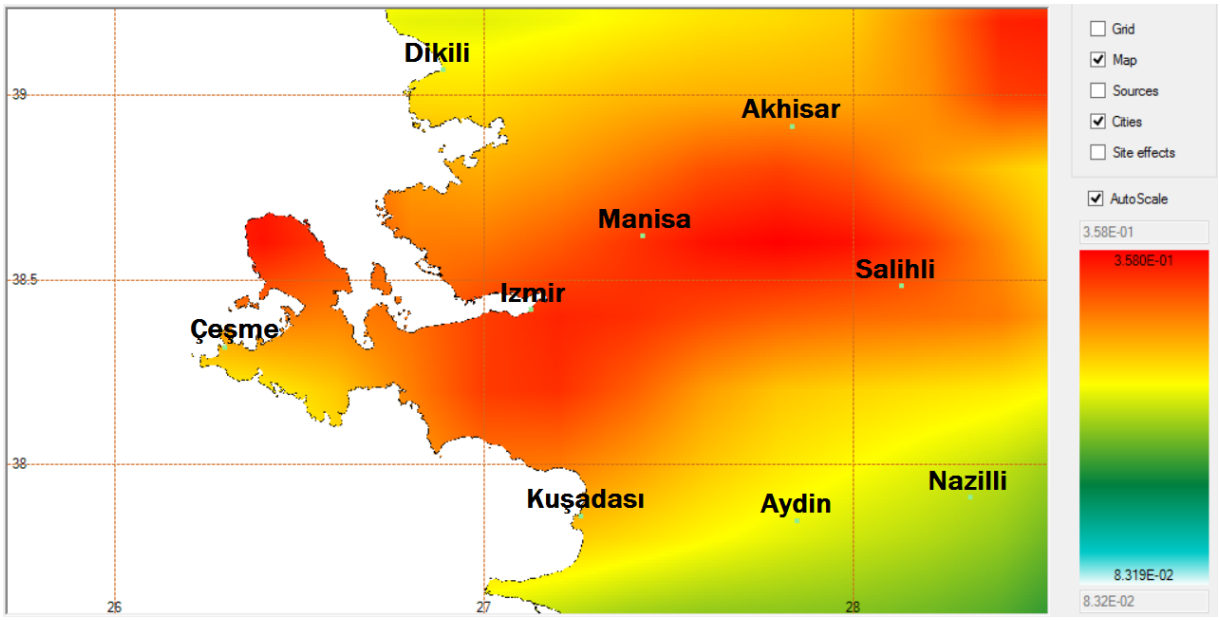

Fig. 5.1.11. Seismic hazard map showing SA values for the period T = 0.3s on the Turkish side of the study area for a return period of 475 years. The colours represent the different SA values measured in g. These results are based on the GMPE from Campbell and Bozorgnia (2008).

The SA values found in the study area with a period of 0.3s show the same pattern of values as the results derived in fig. 5.1.9 using PGA values, but with the same GMPE and return period.

The area in fig.5.1.11, extending from approximately 50 km southwest of Izmir and northeast towards the cities of Akhisar and Salihli have high SA values ranging from 0.32g to 0.36g. The highest SA values are found in the triangle between the cities of Manisa, Akhisar and Salihli, and the SA values ranges from around 0.34g up to peak values of 0.36g. Izmir have SA values of 0.34g in the city centre.

The Karaburun Peninsula also have higher SA values in the northern part, than in the southern part. The northern part have values above 0.35g, while the southern part have values around 0.28g, such as the value found in the seaside resort town of Çeşme. The SA values are even lower further south on the peninsula down to around 0.26g.

There are relatively high SA values in the area northeast of Akhisar. This graben area maintain values ranging from 0.32g to 0.34g. The small region close to the city of Kuşadası, have values of about 0.28g, slightly higher than in the surrounding region.

The areas with lowest SA values are the same areas as found by using PGA values with the

same return period and GMPE. The hilly areas north of Dikili have lower SA values than the surrounding areas with values ranging from about 0.26g in Dikili and down to about 0.24g further north. The mountain region south of the Büyük Menderes graben also have lower SA values than the areas surrounding, with the lowest SA values estimated to be between 0.18g and 0.21g.

The seismic hazard on the Greek side of the study area, by using a return period of 475 years, and the GMPE from Campbell and Bozorgnia (2008) is shown in fig. 5.1.12, by using SA values for the period of 0.3s.

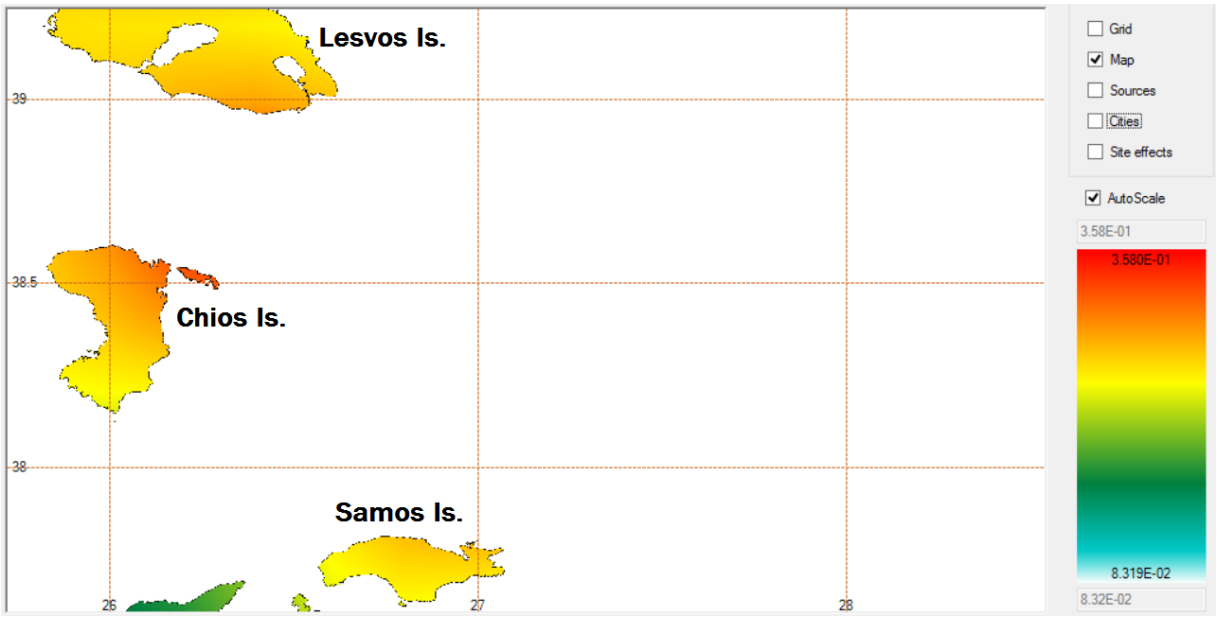

Fig. 5.1.12. Seismic hazard map showing SA values for the period T = 0.3s on the Greek side of the study area for a return period of 475 years. The colours represent the different SA values measured in g. These results are based on the GMPE from Campbell and Bozorgnia (2008).

The SA values are still highest on Chios Island, and lowest on Lesvos Island. The SA values on Lesvos are ranging from about 0.26g to 0.29g, with the highest values south on the Island. On Chios Island, the SA values ranges from about 0.24g in the southern part to the peak value of 0.32g in northeast. On Samos Island, the highest values are found on the north of the Island with SA values reaching 0.28g.

3) SA results with a period of 1.0s

The seismic hazard on the Turkish side of the study area, by using a return period of 475 years, and the GMPE from Campbell and Bozorgnia (2008) is shown in fig. 5.1.13, by using SA values for the period of 1.0s.

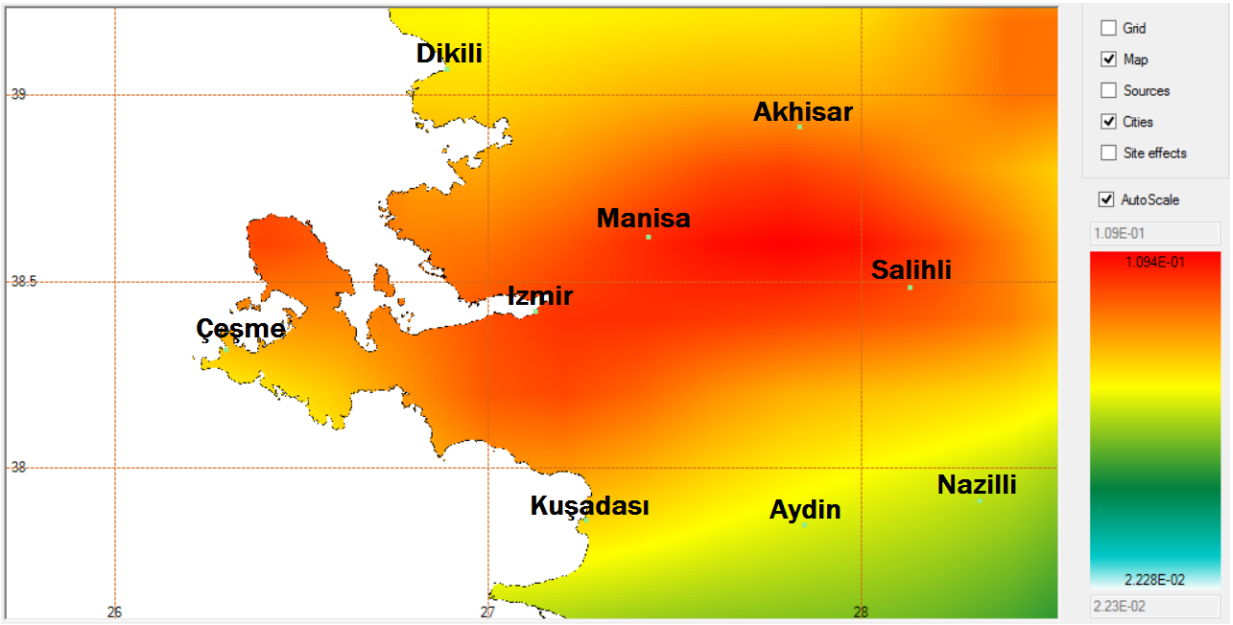

Fig. 5.1.13. Seismic hazard map showing SA values for the period T = 1.0s on the Turkish side of the study area for a return period of 475 years. The colours represent the different SA values measured in g. These results are based on the GMPE from Campbell and Bozorgnia (2008).

The SA values found in the study area for a period of 1.0s is shown in fig. 5.1.13, and show the same pattern of values as the results found in fig. 5.1.11, by using SA values with a period of 0.3s, but with the same GMPE and return period. The only clear difference is the fact that the values, by using a 1.0s period instead of a 0.3s period are significant lower. These values are quite comparable to the values derived by using the GMPE from Boore and Atkinson (2008) as seen in table 5.1.1.

The highest SA values are still found in the triangle between the cities of Manisa, Akhisar and Salihli as seen in fig. 5.1.13, and the SA values ranges from around 0.10g up to peak values of 0.11g. Izmir have SA values of 0.10g in the city centre.

The Karaburun Peninsula also have higher SA values for the northern part than the southern part of the peninsula, but as for all other values using a period of 1.0s, these values are significant lower than using a period of 0.3s. The northern part have values above 0.10g, while

the southern part have values around 0.08g, e.g. the value found in the seaside resort town of Çeşme. The highest SA values in the area northeast of Akhisar, ranges from 0.08g to 0.09g. The hilly areas north of Dikili have lower SA values than the surrounding areas with values of about 0.08g in Dikili. The mountain region south of the Büyük Menderes graben also have lower SA values than the areas surrounding, with the lowest SA values estimated to be between 0.05g and 0.06g.

The seismic hazard on the Greek side of the study area, by using a return period of 475 years, and the GMPE from Campbell and Bozorgnia (2008) is shown in fig. 5.1.14, by using SA values for the period of 1.0s.

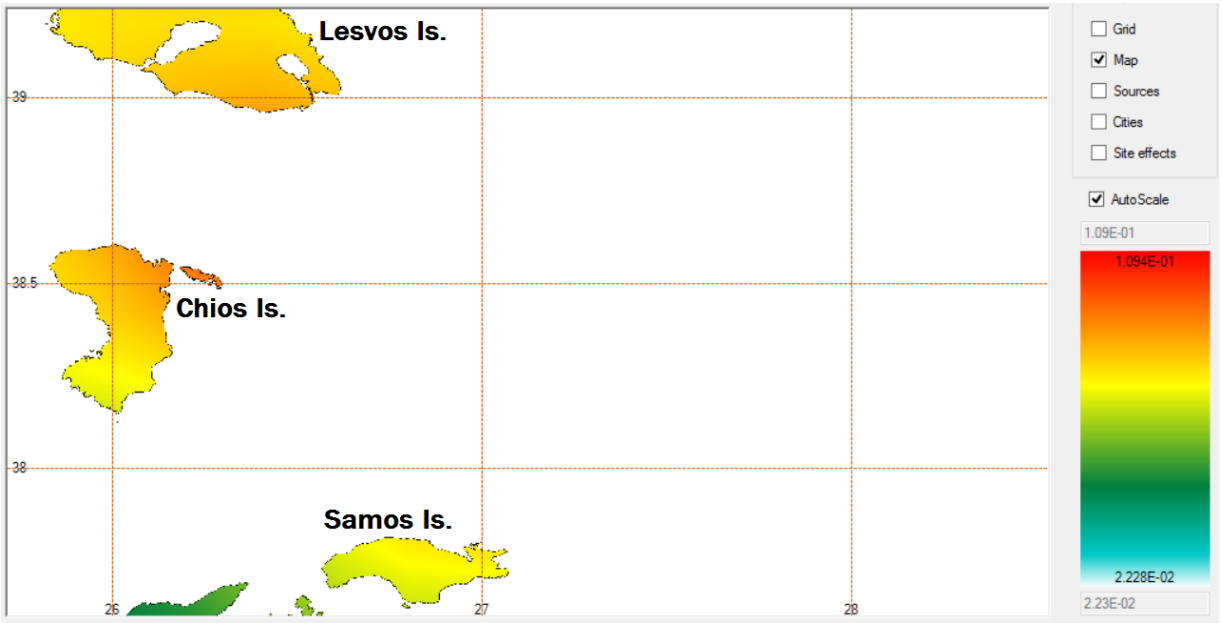

Fig. 5.1.14. Seismic hazard map showing SA values for the period T = 1.0s on the Greek side of the study area for a return period of 475 years. The colours represent the different SA values measured in g. These results are based on the GMPE from Campbell and Bozorgnia (2008).

The SA values for a period of 1.0s on the Greek side of the study area are shown in fig. 5.1.14. This figure show the same pattern of values as the results derived in fig. 5.1.12, by using SA values with a period of 0.3s, with both the same GMPE and return period. The only clear difference is also here the fact that the values using a 1.0s period instead of a 0.3s period are significant lower.

The SA values on Lesvos are ranging from about 0.08g to about 0.09g, with the highest values south on the Island. On Chios Island, the SA values ranges from about 0.07g in the southern

part to the peak value of 0.09g in northeast. On Samos Island, the highest values are found north on the Island with SA values reaching up to 0.08g.

5.1.2 Results by using a return period of 2475 years

For a return period of 2475 years as shown in fig. 5.1.15, selected cities are shown with corresponding PGA values. The highest values calculated for Izmir is 0.49g and 0.24g, by using the GMPE from Boore and Atkinson (BA08) and the GMPE from Campbell and Bozorgnia (CB08), respectively.

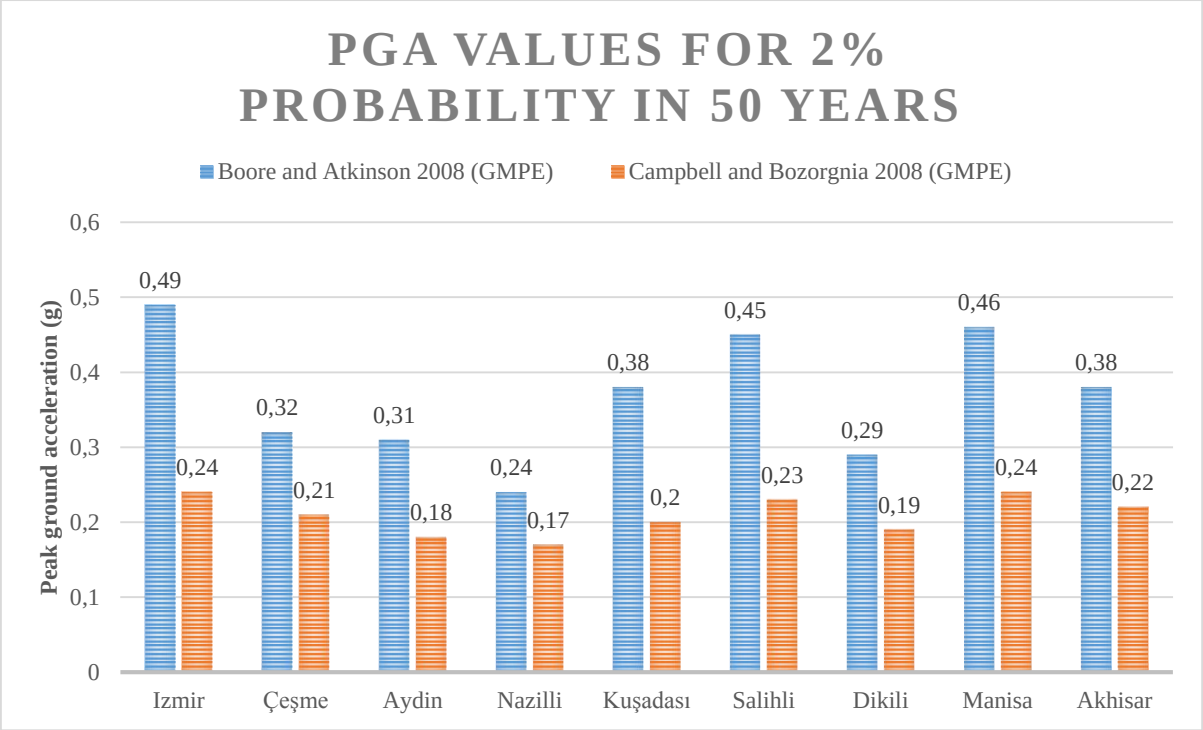

Fig. 5.1.15. The PGA values in different Turkish cities for a return period of 2475 years. The results in the blue column are calculated based on the GMPE from Boore and Atkinson (2008), while the results in the orange column are calculated based on the GMPE from Campbell and Bozorgnia (2008).

The PGA values from the GMPE by using BA08 are in general higher than the values calculated from the GMPE using CB08. Least differences between the two GMPE's are found in the cities with lowest PGA values, and thus higher differences in cities with high PGA values. By using the BA08 relation, except from Izmir, the cities of Salihli and Manisa have the highest PGA values with 0.45g, while Kuşadası and Akhisar have high PGA values reaching 0.38g. The same

pattern is found for the GMPE from CB08, with Izmir, Salihli and Manisa standing for the highest PGA values of about 0.24g.

All results using 2% probability in 50 years follows the same trend as using 10% probability in 50 years for both the GMPE's. This is the case for results in PGA, SA with a period of 0.3s, and for SA with a period of 1.0s. All the results using a 2% probability in 50 years are listed in table 5.1.1. The maps showing all the ground motion values in the study area, by using a return period of 2475 years are shown in Appendix A.1, by using the GMPE from BA08 and in Appendix A.2 by using the GMPE from CB08.

5.1.3 Results by using a return period of 949 years

For a return period of 949 years as seen in fig. 5.1.16, selected cities are shown with corresponding PGA values. The highest values calculated for Izmir is 0.36g and 0.16g, by using the GMPE from Boore and Atkinson (BA08) and the GMPE from Campbell and Bozorgnia (CB08), respectively.

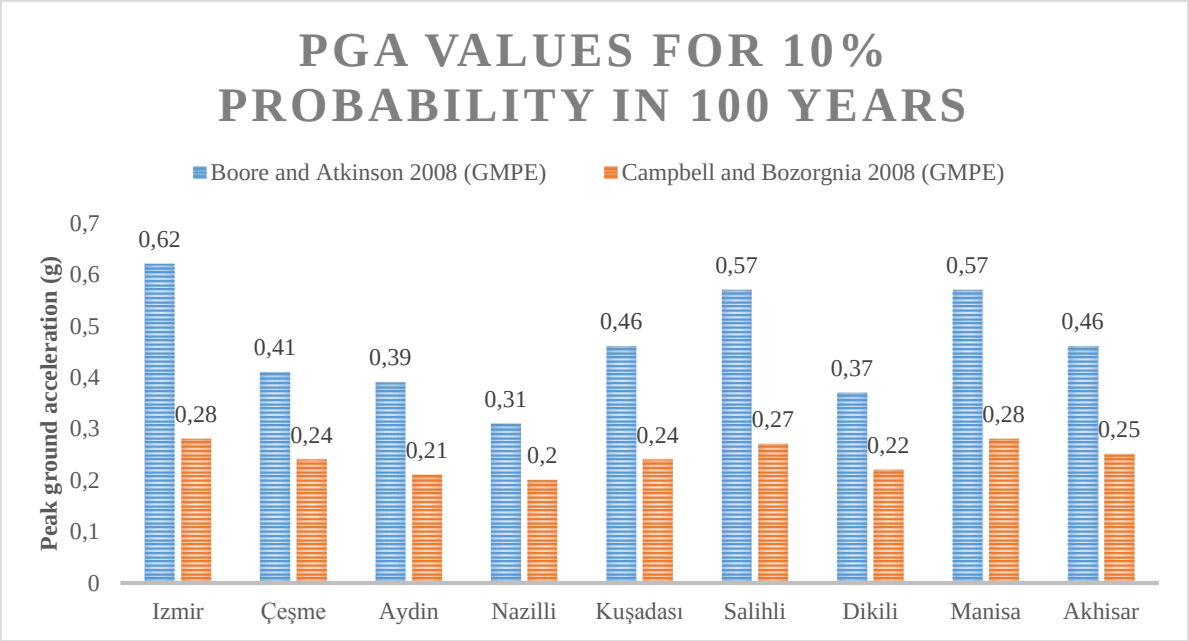

Fig. 5.1.16. The PGA values in different Turkish cities for a return period of 949 years. The results in the blue column are calculated based on the GMPE from Boore and Atkinson (2008), while the results in the orange column are calculated based on the GMPE from Campbell and Bozorgnia (2008).

The PGA values from the GMPE by using BA08 are in general higher than the values calculated from the GMPE using CB08. Least differences between the two GMPE's are found in the cities

with lowest PGA values, and higher differences are thus found in cities with high PGA values. Except from Izmir, the cities of Salihli and Manisa have the highest PGA values using the GMPE from BA08 with 0.32g. The same pattern is shown for the GMPE from CB08, with Izmir, Salihli and Manisa standing for the highest PGA values of about 0.15g to 0.19g.

All results using 10% probability in 100 years follows the same trend as using 10% probability in 50 years in fig. 5.1.2 for both the GMPE's. The only difference is that the ground motion values with a period of 100 years are slightly higher. This is the case for results in PGA, SA with a period of 0.3s, and for SA with a period of 1.0s. There are in general higher values in SA with a period of 0.3s than with a period of 1.0s. All results using a 10% probability in 100 years are listed in table 5.1.1. The maps showing all the ground motion values in the study area, by using a return period of 949 years are shown in Appendix A.3, by using the GMPE from BA08 and in Appendix A.4 by using the GMPE from CB08.

5.1.4 Results by using a return period of 4950 years

For a return period of 4950 years as seen in fig. 5.1.17, selected cities are shown with corresponding PGA values. The highest values calculated for Izmir is 0.62g and 0.28g, by using the GMPE from Boore and Atkinson (BA08) and the GMPE from Campbell and Bozorgnia (CB08), respectively.

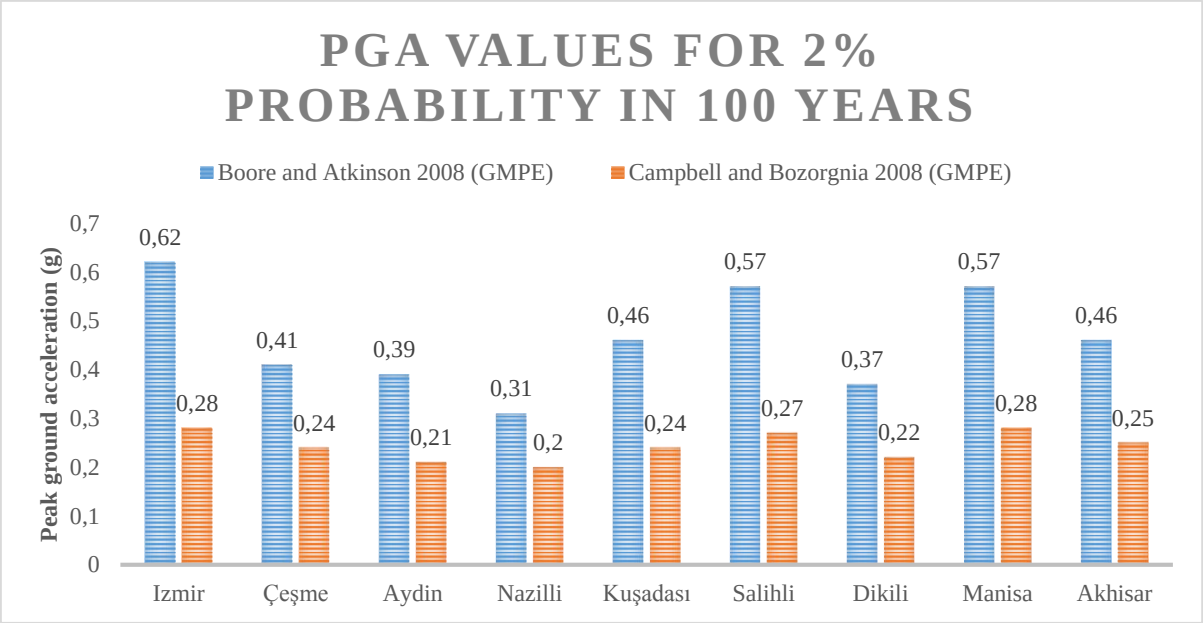

Fig. 5.1.17. The PGA values in different Turkish cities for a return period of 4950 years. The results in the blue column are calculated based on the GMPE from Boore and Atkinson (2008), while the results in the orange column are calculated based on the GMPE from Campbell and Bozorgnia (2008).

The PGA values from the GMPE, by using BA08 are in general higher than the values calculated from the GMPE using CB08, and using a return period of 4950 years. Least differences between the two GMPE's are found in the cities with lowest PGA values, and thus higher differences in cities with high PGA values. There are in overall less difference in the PGA values by using the GMPE from CB08 than the GMPE from BA08.

Except from Izmir the cities of Salihli and Manisa have the highest PGA values, by using the GMPE from BA08 with 0.57g. The same pattern is shown for the GMPE from CB08, with Izmir, Salihli and Manisa standing for the highest PGA values of about 0.27g to 0.28g.

With reference to fig. 5.1.2, the results using 2% probability in 100 years follows the same trend as the results using 2% probability in 50 years for both the GMPE's. The only difference is that the ground motion values with a period of 100 years are slightly higher. This is the case for both results in PGA, SA with a period of 0.3s, and for SA with a period of 1.0s. The same pattern also appear, with higher values in SA with a period of 0.3s than with a period of 1.0s. All results using 2% probability in 100 years are listed in table 5.1.1. The maps showing all the ground motion values in the study area, by using a return period of 4950 years are shown in

Appendix A.5, by using the GMPE from BA08 and in Appendix A.6 by using the GMPE from CB08.

5.1.5 Summary

All results using the different GMPE's as well as different return periods show the same pattern of both PGA values and SA values. The differences is that the results using the GMPE from Boore and Atkinson (2008), in general are higher than by using the GMPE from Campbell and Bozorgnia (2008). There are also smaller differences (more homogeneous distributed values) between the values inside the study area using the GMPE from CB08 than the GMPE from BA08. Using a longer period, such as 1.0s instead of 0.3s gives lower spectral acceleration values. A longer period is equivalent with a lower frequency, and having lower frequency gives lower values in form of spectral acceleration.

Three locations distinguishes from the other locations were they have higher possible ground motion values. These areas are the zone stretching from approximately 50 km south of Izmir and northeast towards the cities of Manisa, Akhisar and Salihli, which are located at the northern part of the Karaburun Peninsula, and a small area northeast of Akhisar.

Table 5.1.1. All peak ground accelerations measured from Izmir, Çeşme, Dikili, Kuşadası, Manisa, Akhisar, Salihli, Aydin, and Nazilli, using different return periods and GMPE's. The GMPE's are Boore and Atkinson (2008), and Campbell and Bozorgnia (2008), and the different return periods are 475, 2475, 949, and 4950 years.

USING A 50 YEAR- PERIOD									
City	**Izmir**	**Çeşme**	**Dikili**	**Kuşadası**	**Manisa**	**Akhisar**	**Salihli**	**Aydin**	**Nazilli**
PGA 10%pr. BA08	0.27g	0.17g	0.16g	0.21g	0.24g	0.21g	0.23g	0.16g	0.13g
PGA 10%pr. CB08	0.16g	0.13g	0.12g	0.14g	0.16g	0.14g	0.15g	0.12g	0.11g
PGA 2%pr. BA08	0.49g	0.32g	0.29g	0.38g	0.46g	0.38g	0.45g	0.31g	0.24g
PGA 2%pr. CB08	0.24g	0.21g	0.19g	0.20g	0.24g	0.22g	0.23g	0.18g	0.17g
SA 0.3s 10%pr. BA08	0.46g	0.30g	0.26g	0.32g	0.42g	0.34g	0.42g	0.26g	0.22g
SA 0.3s 10%pr. CB08	0.34g	0.28g	0.26g	0.28g	0.34g	0.30g	0.32g	0.24g	0.23g
SA 0.3s 2%pr. BA08	0.95g	0.60g	0.49g	0.61g	0.90g	0.68g	0.90g	0.51g	0.43g
SA 0.3s 2%pr. CB08	0.53g	0.45g	0.40g	0.44g	0.53g	0.48g	0.52g	0.39g	0.37g
SA 1.0s 10%pr. BA08	0.11g	0.07g	0.06g	0.07g	0.10g	0.08g	0.10g	0.06g	0.05g
SA 1.0s 10%pr. CB08	0.10g	0.08g	0.08g	0.08g	0.10g	0.09g	0.10g	0.07g	0.07g
SA 1.0s 2%pr. BA08	0.23g	0.15g	0.12g	0.14g	0.23g	0.17g	0.23g	0.18g	0.10g
SA 1.0s 2%pr. CB08	0.18g	0.14g	0.14g	0.14g	0.19g	0.16g	0.18g	0.12g	0.12g
USING A 100 YEAR- PERIOD									
City	**Izmir**	**Çeşme**	**Dikili**	**Kuşadası**	**Manisa**	**Akhisar**	**Salihli**	**Aydin**	**Nazilli**
PGA 10%pr.	0.36g	0.22g	0.21g	0.27g	0.33g	0.27g	0.31g	0.21g	0.17g

BA08									
PGA 10%pr. CB08	0.19g	0.16g	0.15g	0.16g	0.19g	0.17g	0.19g	0.14g	0.13g
PGA 2%pr. BA08	0.62g	0.41g	0.37g	0.46g	0.57g	0.46g	0.57g	0.39g	0.31g
PGA 2%pr. CB08	0.28g	0.24g	0.22g	0.24g	0.28g	0.25g	0.27g	0.21g	0.20g
SA 0.3s 10%pr. BA08	0.65g	0.40g	0.34g	0.42g	0.61g	0.46g	0.61g	0.35g	0.29g
SA 0.3s 10%pr. CB08	0.41g	0.35g	0.31g	0.35g	0.41g	0.37g	0.40g	0.30g	0.28g
SA 0.3s 2%pr. BA08	1.22g	0.78g	0.62g	0.77g	1.17g	0.86g	1.17g	0.66g	0.56g
SA 0.3s 2%pr. CB08	0.63g	0.53g	0.48g	0.52g	0.64g	0.57g	0.63g	0.46g	0.44g
SA 1.0s 10%pr. BA08	0.15g	0.10g	0.08g	0.10g	0.15g	0.11g	0.15g	0.08g	0.07g
SA 1.0s 10%pr. CB08	0.13g	0.11g	0.10g	0.10g	0.13g	0.12g	0.13g	0.09g	0.09g
SA 1.0s 2%pr. BA08	0.31g	0.20g	0.15g	0.19g	0.29g	0.22g	0.30g	0.16g	0.13g
SA 1.0s 2%pr. CB08	0.22g	0.18g	0.17g	0.17g	0.23g	0.20g	0.22g	0.15g	0.15g

5.2 Stochastic ground motion simulations

Multiple stochastic ground motion simulations are carried out for important faults in the study area. These faults are the Izmir fault, the Manisa fault, the Karaburun fault, the Seferihisar fault, the Tuzla fault, and the Samos fault. The simulations for the Seferihisar fault is carried out by using two different stress drops and two different dip's, which will be discussed in the chapter 6.

These ground motion simulations gives the maximal possible ground motion values for the various faults. The fault parameters are carried out, by using the relations by Wells and Coppersmith (1994). All simulations are measured in peak ground acceleration, g.

The Izmir fault is a normal fault and has the possibility to produce a M_W = 6.8 earthquake and is located near the city of Izmir, while the Manisa fault is a normal fault and has the possibility to produce a M_W = 6.5 earthquake and is located near the city of Manisa as shown in fig. 5.2.1.

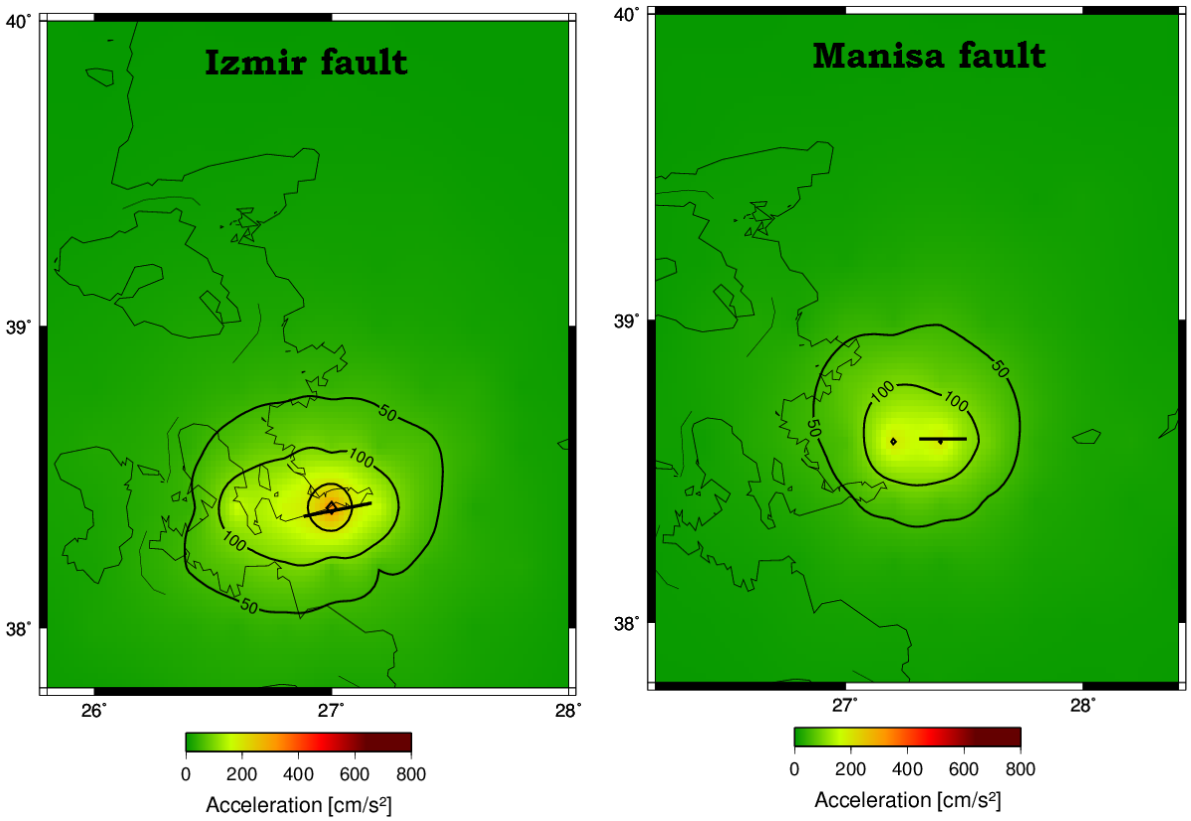

Fig. 5.2.1. At left the Izmir fault, and at right, the Manisa fault, with PGA levels indicated by the isolines, measured in cm/s^2.

The maximum possible PGA levels from the Izmir fault are between 0.2g to 0.3g, while they are just above 0.1g at the Manisa fault, by using the selected parameters used in table 4.2.2.

The Karaburun fault is a reverse fault and has the possibility to produce a M_W = 6.9 earthquake and is located on the east coast of the Karaburun Peninsula, while the Seferihisar fault (original) is a strike-slip fault and has the possibility to produce a M_W = 6.9 earthquake and is located on southwest of Izmir, as shown in fig. 5.2.2.

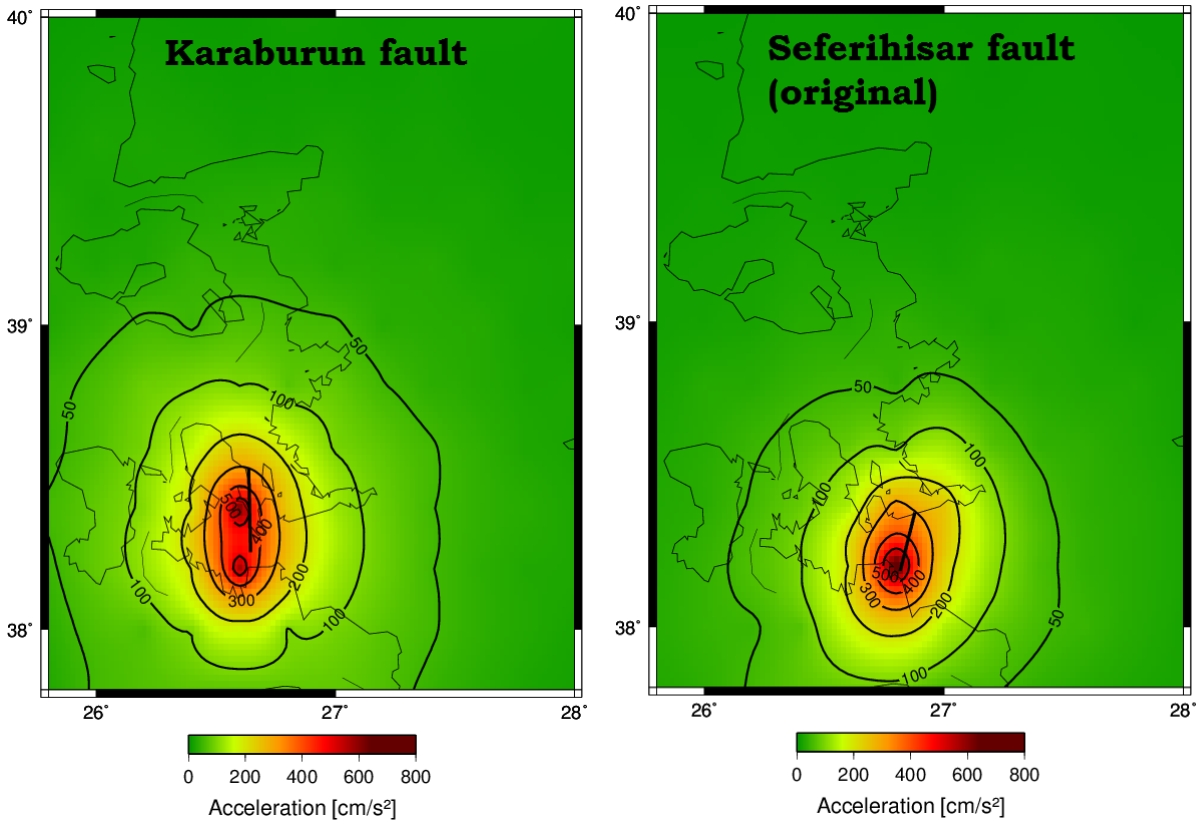

Fig. 5.2.2. At left the Karaburun fault, and at right the Seferihisar fault (original), with PGA levels indicated by the isolines, measured in cm/s².

The maximum possible PGA levels from the Karaburun fault are just above 0.5g, while they are just above 0.5g from the Seferihisar fault (original), by using the selected parameters used in table 4.2.2.

The Seferihisar fault (other dip) using a dip of 60° instead of 80°, and the same fault Seferihisar fault (other stress drop) using a stress drop of 30 bars instead of 80 bars are shown in fig. 5.2.3.

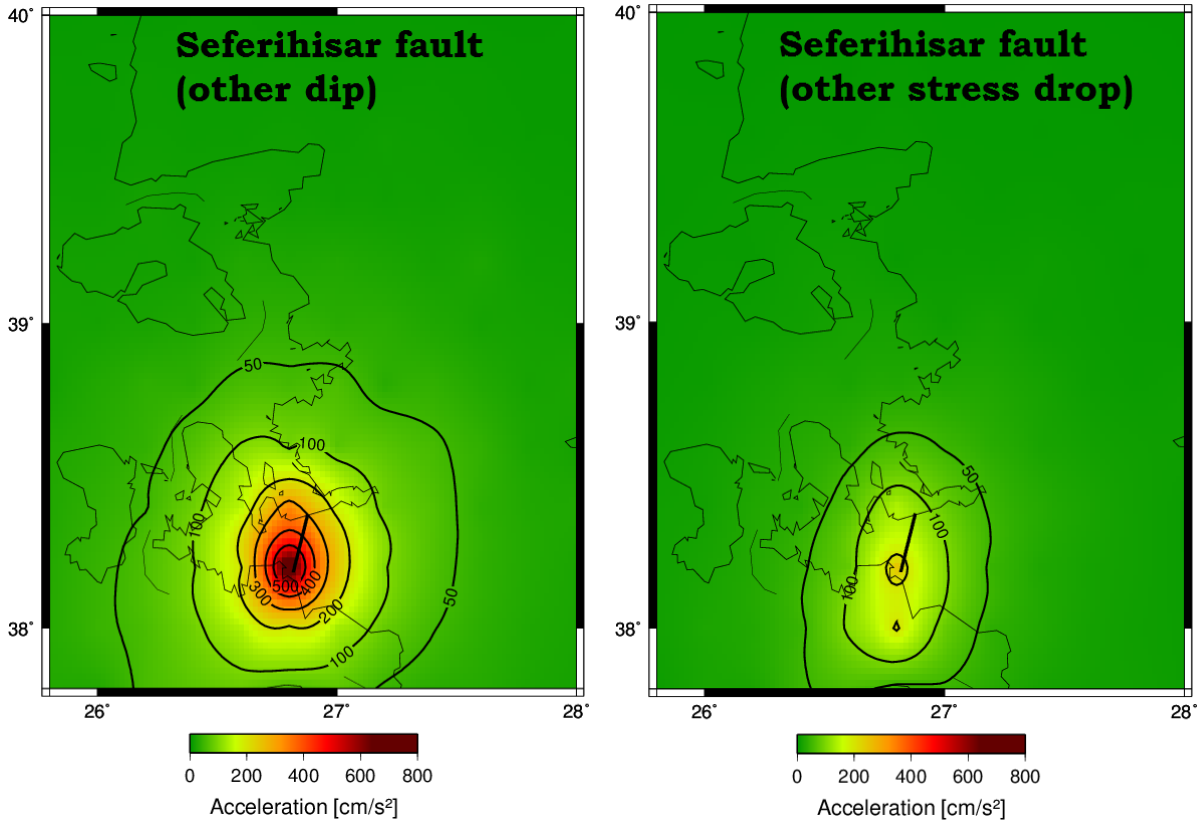

Fig. 5.2.3. At left the Seferihisar fault (other dip), and at right the Seferihisar fault (other stress drop), with PGA levels indicated by the isolines, measured in cm/s^2.

The maximum possible PGA levels from the Seferihisar fault are just above 0.5g, by using the selected parameters used in table 4.2.2, but by using a dip of 60˚ instead of 80˚. These ground motion values are slightly higher, using a smaller dip for the same fault. The maximum possible PGA levels from the Seferihisar fault are just above 0.2g, by using the selected parameters used in table 4.2.2, only changed by using a stress drop of 30 bars instead of 80 bars. The ground motion values are much lower, using a smaller stress drop for the same fault.

The Tuzla fault is a strike-slip fault and has the possibility to produce a M_W = 6.9 earthquake and is located northeast of the Sığacık Bay, while the Samos fault is a normal fault and has the possibility to produce a M_W = 6.9 earthquake and is located right north of Samos Island, as shown in fig. 5.2.4.

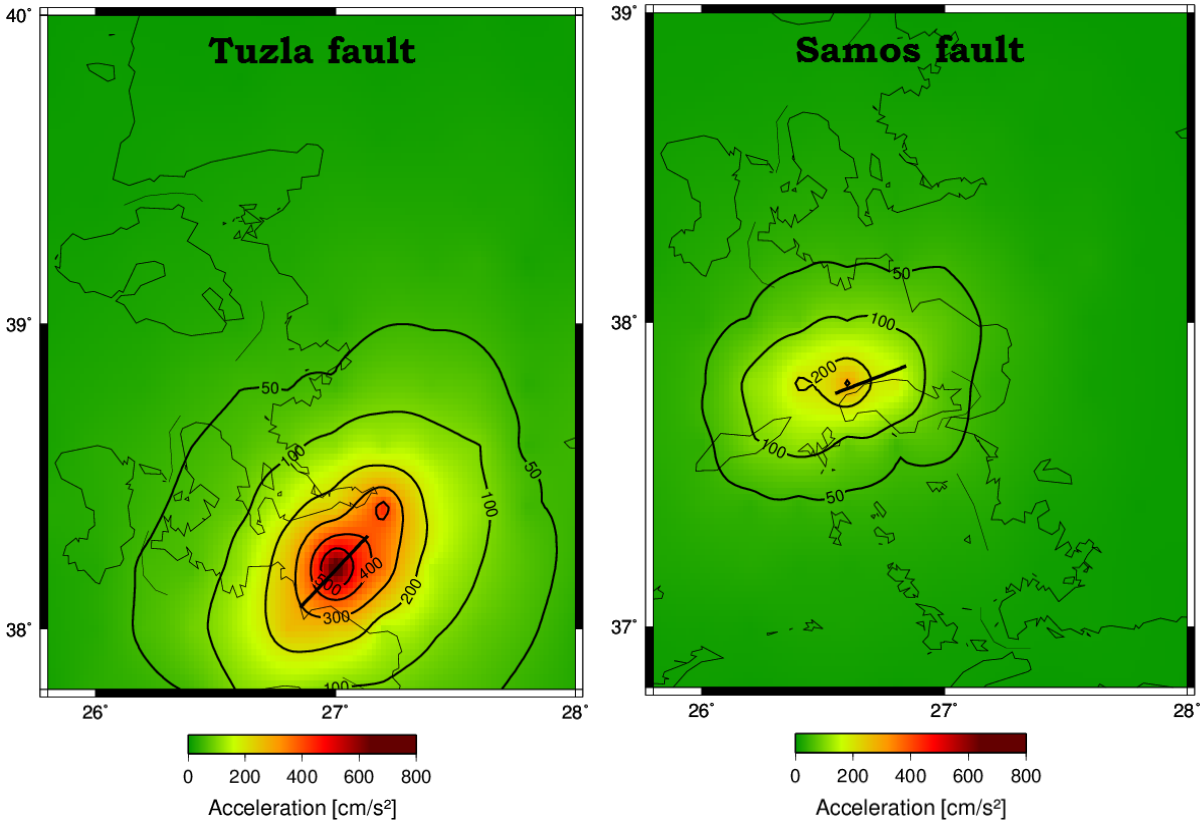

Fig. 5.2.4. At left the Tuzla fault, and at right, the Samos fault, with PGA levels indicated by the isolines, measured in cm/s^2.

The maximum possible PGA levels from the Tuzla fault is somewhere just above 0.5g, while they are above 0.3g from the Samos fault, by using the selected parameters used in table 4.2.2.

6 Discussion

Based on the seismic hazard assessment carried out in this thesis, there are several places, which deserves further discussing. Of all cities considered, Izmir is the city with highest PGA-, and SA values and have a considerably high seismic hazard.

The discussion will consider different aspects from the results. These aspects will consider;

- Distribution of hazard
- Comparison of ground motion measures and attenuation models
- Comparison of previous PSHA studies
- Stochastic ground motion results and comparison with similar studies

6.1 Distribution of hazard

There are several areas with significant high seismic hazard, such as the metropolitan of Izmir, and an area extending from approximately 50 km southwest of Izmir and northeast towards the cities of Akhisar and Salihli. The area with the highest hazard is found in a "triangle" between the cities of Manisa, Akhisar and Salihli. This area have significant high PGA and SA values. It is also identified that the north side of the Karaburun Peninsula have high seismic hazard. The northern part of the peninsula have higher hazard than the southern part. An area northeast of Akhisar also have a high seismic hazard compared to the surrounding areas.

Why some areas in the study area have a considerably lower seismic hazard compared to surrounding areas is also interesting. The area stretching from Dikili and northwards along the west coast, as well as an area south of the Menderes graben have relatively low seismic hazard values compared to the rest of the study area. It is identified that the Menderes graben have significant lower seismic hazard values compared to what is found at the Gediz graben.

On the Greek side, the identified seismic hazard values on Chios Island and on Samos Island will be discussed. The seismic hazard is highest on the northeast coast at Chios Island and on the north coast on Samos Island.

When discussing the hazard in Izmir and on Samos Island, the seismic hazard from the PSHA are compared to the seismic hazard found from stochastic simulations, and the aim is to understand why these areas possess such large seismic hazard values.

The seismic hazard will be discussed based on different factors, such as the seismicity (a-, and b- values), the morphology, the faults, and by maximum magnitude in that region. The program used in order to derive the seismic hazard is based on the a- value, the b- value, and the maximum magnitude. The explanation for higher hazard values in some areas than in others is because of higher seismicity, resulting from more earthquakes.

- Izmir metropolitan

Of all cities considered, Izmir is the city with highest PGA and SA values in the study area. It was found PGA values of 0.27g using the GMPE from BA08, and 0.16g using the GMPE from CB08 with a return period of 475 years as shown in fig. 5.1.2. The stochastic simulation of the Izmir fault is shown in fig. 5.2.1. This simulation shows a maximum PGA value between 0.2g and 0.3g, which seems credible compared to the PSHA results.

Izmir is located in source zone 12 as shown in fig. 4.2.4, and borders to zone 11 in north, zone 13 in south and zone 10 in west. Considering the size of zone 12, this zone maintain a high seismicity when looking at the a-, and b- values seen in table 4.2.3. Zone 10 have a very high seismicity and affects Izmir with a greater hazard. In addition, the maximum magnitude chosen is as high as $M_W = 8.0$, giving a high hazard to Izmir.

There is extension in the area around Izmir resulting in normal faulting, and this have in the past reactivated many faults. Izmir is located in an area with large faults capable of causing significant earthquakes, such as the Izmir fault. There have also been several destructive events in the past. All these faults, gives thus a higher hazard to Izmir.

In overall, it seems like the high hazard in Izmir is a result of a considerably high seismicity, and a large maximal magnitude chosen. These seems reasonable based on the large faults in the area.

- Area between Manisa, Akhisar, and Salihli

The highest seismic hazard is found in an area between the cities of Manisa, Akhisar and Salihli for both PGA, and SA values using all the different GMPE's and return periods. The PGA values using a return period of 475 years and the GMPE from BA08 is up to 0.33g, and up to 0.17g using the GMPE from CB08 as shown in fig. 5.1.3.

This area is located in zone 18, and partly in zone 11 as seen in fig. 4.2.4, and borders to zone 15, 17, and 19. All bordering zones, including zone 11 have a large seismicity. The seismicity level in zone 18 is moderate taking the size of the area into consideration, but have in return a considerably high maximum magnitude of $M_W = 6.9$.

This high hazard area is located in a low- lying area called the Gediz graben. From the distributed seismicity in the study area, it seems like there in general are higher seismicity in lower- graben areas than in mountain regions. One explanation for this pattern can be that the extension is more widespread here. There are several larger faults located in this graben as seen in fig. 4.2.4, especially south in the Gediz graben close to the city of Salihli, which are capable of giving high seismic hazard to this area.

In overall, the high hazard in this area is a result of a high seismicity, and a large possible maximum magnitude. However, the seismicity here is not as high as I would have expected with these high PGA values. Altogether, this high seismic hazard seems reasonable based on the relatively high seismicity in this area, reflected by several large faults in this graben.

- Karaburun Peninsula

The Karaburun Peninsula show a considerably higher hazard in the northern part than in the southern part of the peninsula for both the GMPE's from BA08 and CB08, using all return periods for both PGA and SA values. The PGA values using a return period of 475 years are around 0.14g in south and 0.28 in north using the GMPE from BA08, and analogous 0.12g in south and 0.17g in north using the GMPE from CB08 as shown in fig. 5.1.3.

From the stochastic simulation on the Karaburun fault as shown in fig. 5.2.2, a maximum PGA value of about 0.5g was found, which is much higher than the PSHA values. This variation has

nothing to do with the maximum magnitude chosen, because they were both set to be M_W = 6.4, but rather because the PGA value found in the stochastic simulation does not consider any return period as the PSHA does. Therefore, it is expected larger ground motions from the PSHA using a relatively short return period than ground motions from the stochastic simulations. One other aspect is the relatively high stress drop of 80 bars. It is shown in fig. 5.2.2 and fig. 5.2.3, by switching the stress drop from 80 to 30 bars for the Seferihisar fault that the maximal PGA value dropped from above 0.5g to just above 0.2g.

In table 4.2.4, zone 6 represents the northern part of the Karaburun Peninsula, while zone 7 represents the southern part. The seismicity is slightly higher in zone 6, by considering the size of both zones. This is reflected by a higher a- values in zone 6, looking at the level of earthquakes in a given zone and time- period. In the northern part, there are more large events compare to small events, reflected by a lower b- value. The fact that the northern part of the peninsula has a higher seismic hazard than the southern part is supported by a higher seismicity in north, shown in fig. 2.2.1 and fig. 2.2.2.

The high seismic hazard is a result of a large chosen maximum magnitude and a high seismicity. The seismicity is higher on the north part of the peninsula, which is reasonable based on the fact that this part have more recorded earthquakes. This area also have more faults capable of producing destructive earthquakes.

- Area northeast of Akhisar

The area northeast of Akhisar also have a significant high seismic hazard. This based on PGA and SA values using all the different return periods and GMPE's in this thesis. The PGA values using a return period of 475 years are ranging from 0.25g to 0.29g using the GMPE from BA08, and from 0.15g to 0.17g using the GMPE from CB08 as shown in fig. 5.1.3.

It is therefore reasonably to conclude that this area have a significant high hazard. It is used a maximum magnitude of M_W = 6.0, which is low compared to other areas with high hazard in the study area. This maximum magnitude value could had been set higher in this thesis, because it from historical data look like it is possible of larger events to occur throughout the whole study area. This would in fact increase the seismic hazard for some areas. However, there are

not that many large faults, and not many larger events above $M_W = 5$, as seen in fig.2.2.1, and therefore it is possible to support the decision of setting maximum magnitude to $M_W = 6.0$.

The controlling factor regarding the seismic hazard is the seismicity. This area is located in a hilly region, mainly in zone 16 as seen in fig. 4.2.4. It borders to zone 14 in north, zone 15 in west, and zone 17 in south. By looking at fig.2.2.1 and fig. 2.2.2, it seems like the seismicity in this area is much higher than in the bordering regions in south and west. This high seismic hazard seems reasonable based on the high seismicity in the area alone, and since the maximum magnitude is not very large.

- West coast north of Dikili

The west coast stretching from Dikili and north along the coast have lower seismic hazard values than surrounding areas. This is shown using PGA and SA values for both the GMPE's from BA08 and CB08, with all return periods used in the thesis. The PGA values as seen in fig. 5.1.3, by using a return period of 475 years are ranging from 0.16g in Dikili and down to about 0.13g further north using the GMPE from BA08. For the GMPE from CB08 the PGA values are ranging from 0.12g in Dikili and down to about 0.11g further north.

From fig. 2.2.1 and 2.2.2, it seems like the seismicity around Dikili is lower than in the surrounding region. The maximum magnitude chosen for these zones are not higher than $M_W = 6.6$, indicating a lower seismic hazard compared to surrounding areas. There are no large structures or faults in this area capable of causing larger earthquake, and thus this relatively low seismic hazard is found reasonable.

- Mountain region in south

The area with lowest seismic hazard is a mountain region south of the Büyük Menderes graben. This is found for both PGA and SA values using different GMPE's and return periods. The PGA values found by using a return period of 475 years and the GMPE from BA08 is between 0.09g and 0.13g, and between 0.09g and 0.11g using the GMPE from CB08 as shown in fig. 5.1.3.

This area is located in a mountain region with a relatively low seismicity compared to other bordering regions as seen in fig. 2.2.1 and in fig. 2.2.2. There are not many faults in the region, except from the bordering Büyük Menderes graben to the north. The maximum magnitude is chosen to M_W = 6.0 based on the earthquake catalogue. This is a relatively low maximum magnitude applied, and together with the seismicity rate, it can explain the relatively low seismic hazard in this area compared to surrounding areas.

- Büyük Menderes graben

The Büyük Menderes graben is located in a low- lying valley, which trends east- west. This graben, include the cities of Aydin and Nazilli as seen in fig. 5.1.1. From the PGA, and SA results it is shown that the hazard values are significant lower here than in the Gediz graben. Both of these grabens are similar in size and both have several large faults.

In Aydin and Nazilli, the PGA values using the GMPE from BA08 and the return period of 475 years are 0.16g and 0.13g, respectively. Using the same return period but the GMPE from CB08, the same cities have PGA values of 0.12g and 0.11g, respectively. This is significant lower than the PGA values of 0.33g and 0.17g found in the Gediz graben using BA08 and CB08, respectively.

As seen in fig. 2.2.1 and fig. 2.2.2, it shown that the seismicity is significant lower in Büyük Menderes graben than in the Gediz graben. Büyük Menderes graben is located in zone 23 as seen in table 4.2.3, and it is interesting to see the low a- value.

The maximum magnitude is set to M_W = 6.0, which is lower than what was used for the Gediz graben. It can be argued that this value in fact could had been set higher based on the large faults in the area. In historical times, few people lived in this area, and lacking knowledge about previous destructive earthquakes could in fact lowering the chosen maximum magnitude. Both the chosen maximum magnitude and the relatively low seismicity contributes in lowering the hazard. However, the PGA results are mainly based on the low chosen maximum magnitude, and the seismicity, which is significant lower in this graben than in the Gediz graben.

- Chios Island

Chios Island is located in the Aegean Sea, west for the Karaburun Peninsula as shown in fig. 2.1.5. The seismic hazard is higher in the northeast corner of the island than in south, both by using the GMPE's from BA08 and CB08, using all return periods. However, in overall it seems like the seismic hazard is relatively moderate. The PGA values by using a return period of 475 years are around 0.15g in south and 0.24g in northeast using the GMPE from BA08, and analogous 0.12g in south and 0.15g in northeast by using the GMPE from CB08 as shown in fig. 5.1.3.

Chios Island is located in zone 1, and the northeast side borders to zone 6 as seen in fig. 2.4.2. Regarding the size of the zones, zone 6 has in fact significant higher a- values than zone 1, and a similar maximum magnitude is chosen for both zones. Form fig. 2.2.1 and fig. 2.2.2, it is seen a significant higher seismicity at the northeast part of the island, and the deciding factor is in this case the seismicity. Zone 1 and zone 2, located in the Aegean Sea has a relatively low seismicity, and is the main reason for the relatively moderate seismic hazard values found in the Aegean Sea.

- Samos Island

Samos Island is located south of Izmir in the Aegean Sea as shown in fig. 2.1.5. The seismic hazard is higher at the north coast of the island than in southern parts, by using both the GMPE's from BA08 and CB08, by using all return periods. Al in all, the seismic hazard is relatively moderate. The PGA values by using a return period of 475 years are around 0.15g in south and 0.23g in north using the GMPE from BA08, and analogous 0.12g in south and 0.14g in north using the GMPE from CB08 as shown in fig. 5.1.3.

There is one large fault discovered in the ocean just north of Samos Island. In fig. 2.2.2, it is seen a significant distribution of previous earthquakes just north of the Samos Island. The stochastic simulation of the Samos fault is shown in fig. 5.2.4. This simulation shows a maximum PGA value 0.3g, which are slightly higher than the values from the PSHA results, due to differences regarding the expected return period in both methods. There are in overall a significant high seismic hazard from this large fault.

6.2 Comparison of ground motion measures and attenuation models

In this thesis, results are measured both in peak ground acceleration (PGA), and in spectral acceleration (SA), using periods of 0.3s and 1.0s. Both relations gives hazard results within the same pattern, using all return periods (475, 2475, 940, and 4950 years), and both attenuation models from Boore and Atkinson (2008) and Campbell and Bozorgnia (2008). The SA values using a long period of 1.0s (1 Hz) is generally lower than the values using a short period of 0.3s (3.3 Hz), as seen in table 5.1.1.

The main difference between the two GMPE's used in this thesis is that the hazard values, by using the GMPE from BA08 are higher than by using the GMPE from CB08 as seen in fig 5.1.2. The largest difference is found in the areas with highest PGA, and SA values, while the smallest difference is found in the areas with lowest values as seen in table 5.1.1.

6.3 Comparison of previous PSHA studies

There have been several studies carried out regarding seismic hazard mapping in the area surrounding Izmir. Some of the most important probabilistic seismic hazard studies are carried out by Deniz et al. (2010), Jimenez et al. (2001), and EFEHR (2015). Jimenez et al. (2001) estimated PGA values between 0.20g and 0.40g in the whole study area using a return period of 475 years.

The ground motion values by using the GMPE from BA08 is closer to the values found in other studies, such as Deniz et al., (2010), EFEHR, (2015), and Jimenez et al., (2001) then by using the GMPE from CB08 as shown in table 6.1.1. In Izmir, the PGA value using a return period of 475 years and the GMPE from BA08 is 0.27g, while it is 0,16g by using the GMPE from CB08. Analogues, Deniz et al., (2010) estimated a PGA value of 0.34g, Jimenez et al., (2011) a PGA value between 0.20g and 0.40g, and EFEHR., (2015) estimated a PGA value of 0.35g. It therefore seems like the PGA values using the GMPE from BA08 is more realistic.

Table 6.1.1. Comparison of previous studies, using a return period of 475 years in Izmir.

Study	GMPE from BA08	GMPE from CB08	Deniz et al. (2010)	EFEHR (2015)	Jimenez et al. (2001)	Return period
PGA Izmir	0.27g	0.16g	0.34g	0.35g	0.2g – 0.4g	475 years

The PGA values and the SA values using a period of 0.3s as seen in fig. 6.1.1 and in fig. 6.1.2 from EFEHR (2015) are in general higher than the values found in my thesis.

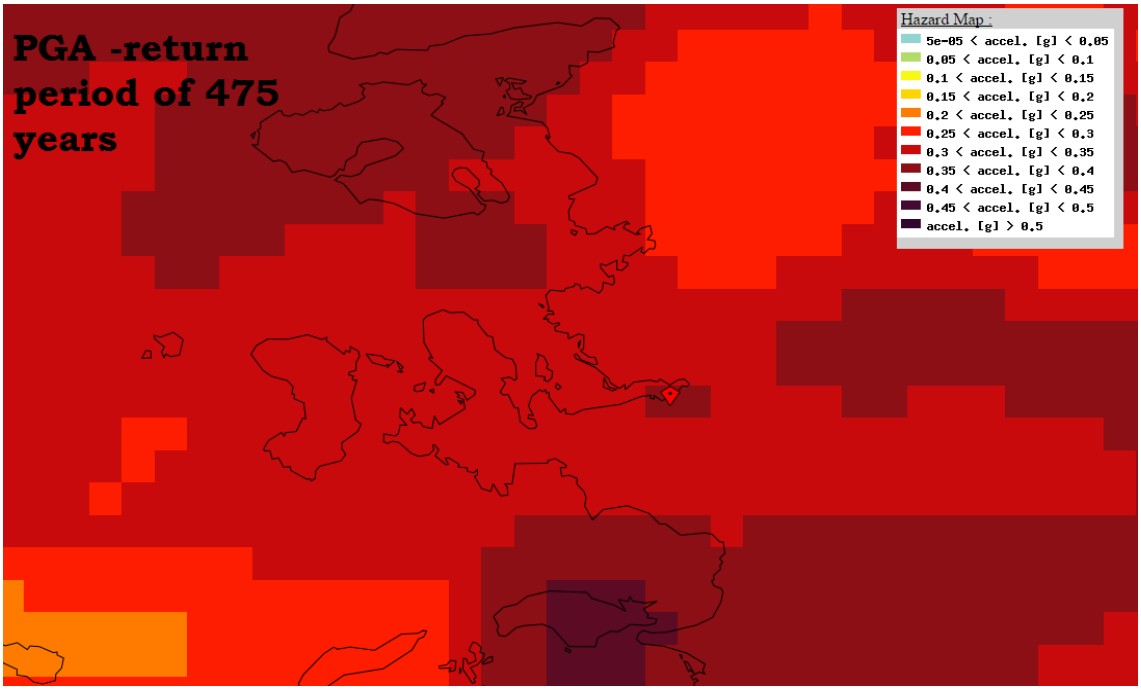

Fig. 6.1.1. PGA values using a return period of 475 years from EFEHR (2015).

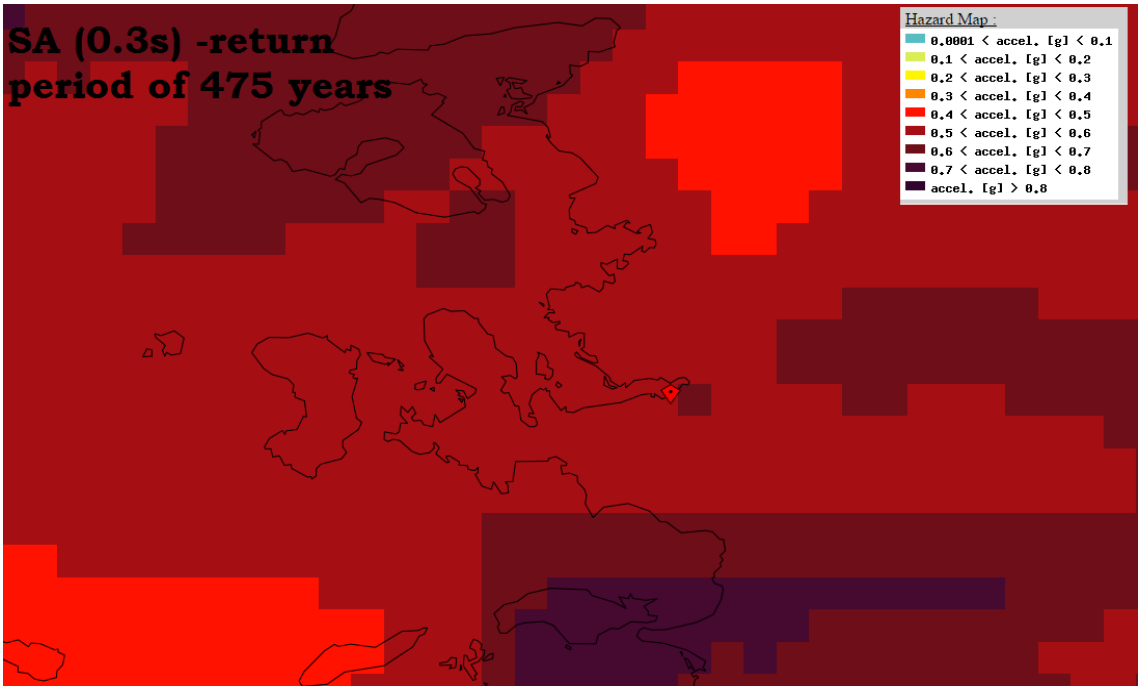

Fig. 6.1.2. SA values using a period of 0.3s and a return period of 475 years from EFEHR (2015).

SA values using a period of 1.0s from EFEHR (2015) are on the other hand similar to the values found in the thesis. For the city of Çeşme, the SA value using a return period of 475 years is 0.07g, by using the GMPE from BA08, and 0.08g by using the GMPE from CB08 as seen in fig. 5.1.3. EFEHR (2015) estimated a SA value of about 0.10g as seen in fig. 6.1.3.

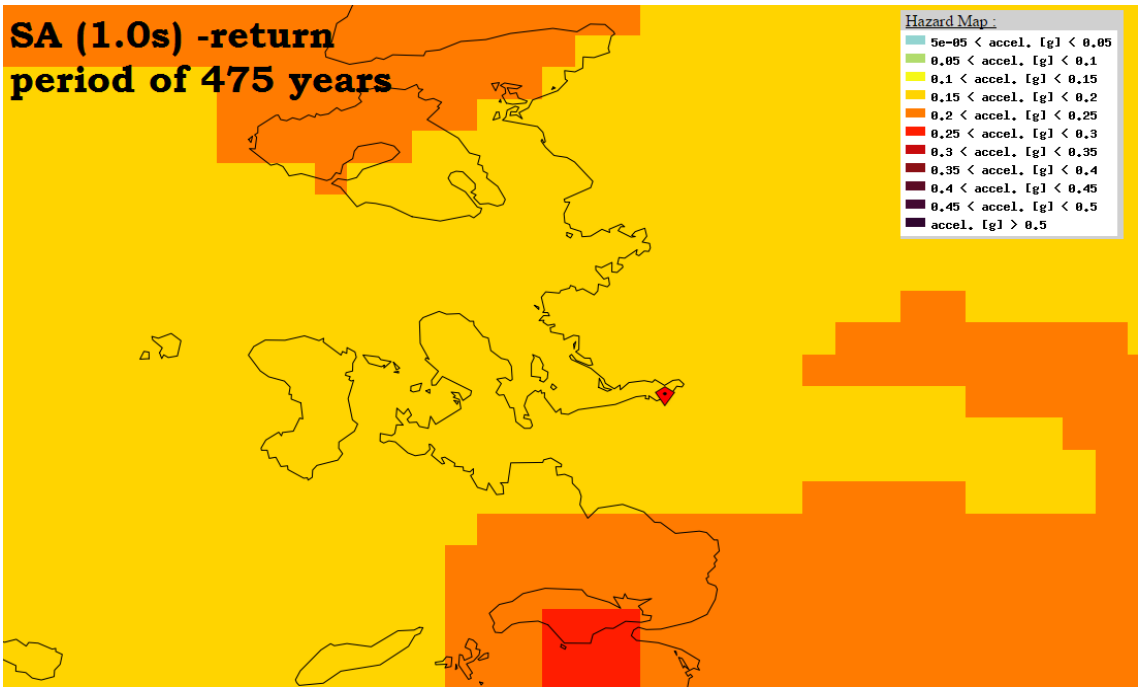

Fig. 6.1.3. SA values using a period of 1.0s and a return period of 475 years from EFEHR, (2015).

EFEHR (2015) estimated a PGA value of about 0.35g, by using a return period of 475 years in the area between Manisa, Akhisar and Salihli. This value is similar to the values found in the thesis, and it is therefore reasonably to conclude that this area have a significant high hazard. For the Karaburun Peninsula, EFEHR (2015) estimated a PGA value of about 0.30g for the whole peninsula. This is higher than in the thesis, but the hazard map from EFEHR is gathered for more regional maps, and do not show local variations that well.

The same pattern, with higher PGA values than in the thesis is found using the same return period in other areas such as the area northeast of Akhisar, the west coast north of Dikili, in the mountain region south of Büyük Menderes graben, in Menderes graben, on Chios Island and on Samos Island.

6.4 Stochastic ground motion results and comparison of previous studies

Several stochastic ground motion simulations are carried out for the Izmir fault, the Manisa fault, the Karaburun fault, the Seferihisar fault, the Tuzla fault, and the Samos fault. The reference scenario magnitudes for the various faults in these simulations are set to M_W = 6.8, 6.5, 6.9, 6.6, 6.9, and 6.9, respectively. The simulations for the Seferihisar fault is carried out by using two different stress drops and two different dip's as seen in fig. 5.2.2 and fig. 5.2.3. The output is the maximal ground motion from large specific hypothetical earthquakes.

The faults with highest ground motions are the Karaburun fault, the Seferihisar fault, and the Tuzla fault, with a PGA of about 0.5g as seen in fig. 5.2.2, 5.2.3 and 5.2.4, respectively. All these have significant high PGA values, much higher than what was found, by using a return period of 475 years in the PSHA. The stochastic simulations uses a stress drop value of about 80 bars, and the faults have relatively high reference scenario magnitudes.

A comparable fault in source dimensions is the Izmir fault seen in fig. 5.2.1. This fault produce a maximum PGA value of about 0.3g. Therefore, it is interesting to look how lower stress drops will affect the PGA value. For a similar simulation, by only changing the stress drop from 80 to 30 bars, the Seferihisar fault reduced its maximum PGA value from about 0.5g to 0.2g. Stress drop changes affects the PGA values in stochastic ground motion simulations, which is realistic having more energy release from larger ruptures.

All stress drop values used in this thesis, was retrieved from the study by Bjerrum and Atakan (2008). PGA values of 0.2g was found from the Manisa and Samos fault, similar to what was found in the PSHA study.

Another simulation from the Seferihisar fault, using a dip of 60˚ instead of 80˚ gives interesting results. Then, the PGA value increases from 0.5g to above 0.6g, because of a concentrating of the energy, more upwards. Decreasing the dip and increasing the stress drop will increase the maximum ground motion from the fault.

- Comparison with previous studies

Other studies have been carried out by Bjerrum and Atakan (2008) and Bjerrum et al. (2013), looking at the ground motion simulations from larger faults in the study area. In this thesis, the reference scenario magnitudes are derived from Bjerrum and Atakan (2008), and Bjerrum et al. (2013). The simulated ground motions are highly dependent on input parameters such as the size of the reference scenario earthquake, stress drop, and on other fault parameters.

Bjerrum and Atakan (2008) estimated a PGA of 0.44g from the Izmir fault, while Bjerrum et al. (2013) estimated a value of 0.60g. This is significantly higher than the 0.3g value found in the thesis. Bjerrum and Atakan (2008) estimated a PGA of 0.56g from the Karaburun fault, which was similar to the value found using a stress drop of 80 bars in the thesis. Bjerrum and Atakan (2008) found similar PGA values as was found in the thesis, with maximal ground motion values of 0.57g in the Tuzla fault, 0.53g in the Seferihisar fault, and 0.27g in the Manisa fault.

This similarity of PGA values is not a coincidence, since many of the parameters used in the stochastic simulation such as stress drop and reference scenario magnitudes are the same as in the study by Bjerrum and Atakan (2008) as seen in table 4.2.2.

7 Conclusion

The aim of this thesis was to do a broad seismic hazard analysis in the region surrounding Izmir, identify and evaluate areas with the highest hazard levels. For each area identified with high seismic hazard, there is worked out a description, which describes the causes for these high values.

Empirical data based on previous history, evidences of several destructive earthquakes, emphasizes the importance of carrying out a seismic hazard analysis of this region. This thesis have identified three main areas with significant hazard values. These are the area including the Izmir metropolitan, the area between the cities of Manisa, Akhisar and Salihli, and the northern part of the Karaburun Peninsula.

- The metropolitan of Izmir is one of the locations with a significant seismic hazard. By using a return period of 475 years, PGA values up to 0.27g are estimated. The stochastic simulation from the Izmir fault, using a reference earthquake of M_W = 6.8 gives a maximum PGA value of 0.3g, which is a significant seismic hazard. In the past, there have been several destructive earthquakes in Izmir, indicating the same. In Izmir, the high seismic hazard is a result of a large maximum magnitude and high seismicity.

- The area with highest seismic hazard is located between the cities of Manisa, Akhisar and Salihli in the Gediz graben. By using a return period of 475 years, the highest PGA value is estimated to be 0.33g. This high seismic hazard seems reasonable based on several large faults, a large maximum magnitude and a relatively high seismicity.

- The third location with significant high hazard is the northern part of the Karaburun Peninsula. The PGA values are considerably higher in the north than in south peninsula, due to higher seismicity in north, possible from a large amount of faults. By using a return period of 475 years, the highest PGA value is estimated to be 0.28g. By using a stochastic simulation, a maximum PGA value of 0.5g was found, by using a reference earthquake of M_W = 6.9 on the Karaburun fault, indicating that the seismic hazard in fact could be even higher. The high seismic hazard is a result of a large maximum magnitude and high seismicity.

- Generally, the PGA, and SA values by using a period of 0.3s, gives lower estimated values than previous result from other studies in the study area. Identified SA values by using a period of 1.0s gives in fact a relatively low seismic hazard, similar to the seismic hazard identified in other studies.

- The seismic hazard identified by using the GMPE from BA08 gives higher values than by using the GMPE from CB08. Based on a comparison from previous studies, it seems like the results from BA08 are the most realistic. It is important to choose the most conservative estimate regarding seismic hazard analyses, because it is important to be precautionary.

- The maximum PGA values found by using the stochastic ground motion simulations are high on all the faults. The values ranges from 0.2g on the Manisa fault too values of 0.6g on the Seferihisar fault. The parameters used in the simulations affects the ground motion values. By increasing the dip, the ground motion decreases. By reducing the stress drop, the ground motion decreases significantly. In overall, the ground motions from the stochastic simulations are generally higher than the ground motions from the PSHA, because the PSHA uses a fixed probability, while the stochastic model give the highest possible values.

References

Akinci, A., D`Amico, S., Malagnini, L., and Mercuri, A. (2013). Scaling earthquake ground motions in western Anatolia, Turkey. *Physics and chemistry of the earth* 63 (2013) 124-135.

AFAD, The Disaster and Emergency Management Authority. Available at: http://www.deprem.gov.tr/sarbis/Shared/Default.aspx. Last accessed 02.04.15

Ambrayseys, N. N., and Finkel, C. F. (1995). The seismicity of Turkey and adjacent areas - A historical review, 1500-1800. *EREN Yayıncılık ve Kitapçılık Ltd. Şti.,* (1995). No: 34

Aktuğ, B., and Kılıçoğlu, A. (2006). Recent crustal deformation of Izmir, Western Anatolia and surrounding regions as deduced from repeated GPS measurements and strain field. *Journal of Geophysical Research, 41* (2006), 471-484. doi:10.1016/j.jog.2006.01.004

Benetatos, C., Kiratzi, A., Ganas, A., Ziazia, M., Plessa, A., and Drakatos, G. (2006). Strike-slip motions in the Gulf of Sığacık (western Turkey): Properties of the 17 October 2005 earthquake seismic sequence. *Tectonophysics*, 426(3-4), 263–279. doi:10.1016/j.tecto.2006.08.003

Beresnev, I.A., and Atkinson, G,M. (1997). Modelling finite-fault radiation from the Ψ^2 spectrum. *Bulletin of the Seismological Society of America*, Vol 87, No. 1, pp. 67-84.

Beresnev, I.A., and Atkinson, G.M. (1998). FINSIM – a FORTRAN program for simulating stochastic acceleration time histories from finite faults. *Seismological research letters*, vol. 69, No. 1.

BGS, British Geological Survey. A guide to seismic hazard. Available at: http://www.earthquakes.bgs.ac.uk/hazard/haz_guide/determinism.html Last accessed 14.05.15

Bjerrum, L. W., and Atakan, K. (2008). Scenario based ground motion simulations for assessing the seismic hazard in İzmir, Turkey, 1-8. *The 14th World Conference on Earthquake Engineering October 12-17, 2008, Beijing, China*

Bjerrum, L.W., Sørensen, M.B., Ottemöller, L., and Atakan, K. (2013). Ground motion simulations for Izmir, Turkey: parameter uncertainty. *J Seismol* 17:1223-1252. DOI 10.1007/s10950-013-9389-0

Bjerrum, L.W., Bjørge, Å.O., Sørensen, M.B., Ottemöller, L., Sari, C., and Atakan, K. (2014a). Building vulnerability and seismic risk assessment for Izmir, Turkey. *Second European conference on earthquake engineering and seismology, Istanbul Aug. 25-29, 2014*

Bjerrum, L.W., Lutro, T., Sørensen, M.B., Ottemöller, L., Sari, C., and Atakan, K. (2014b). Simulated ground motions with site effects potential evaluated through transfer functions and H/V measurements: case study for Izmir, Turkey. *Second European conference on earthquake engineering and seismology, Istanbul Aug. 25-29, 2014*

Boore, D.M., and Atkinson, G.M. (2008). Ground-motion prediction equations for average horizontal component of PGA, PGV, and 5%- damped PSA at spectral periods between 0.01 s and 10.0 s. *Earthquake Spectra*, Volume 24, No. 1, pages 99–138, Earthquake Engineering Research Institute. DOI: 10.1193/1.2830434.

Boore, D.M. (2009). Comparing stochastic point-source and finite-source ground-motion simulations: SMSIM and EXSIM. *Bulletin of the Seismological Society of America*, VOL 99, No. 6, pp. 3202-3216.

Bozkurt, E. (2001). Neotectonics of Turkey – A synthesis. Tectonic Research Unit, Department of Geological Engineering, Middle East Technical University, *Geodinamica Acta* 14, 3-30. doi:10.1016/S0985-3111(01)01066-X

Campbell, K.W., and Bozorgnia, Y. (2008). NGA ground motion model for the geometric mean horizontal component of PGA, PGC, PGD and 5% damped linear elastic response spectra for periods ranging from 0.01 to 10 s. *Earthquake Spectra*, Volume 24, No. 1, pages 139–171, Earthquake Engineering Research Institute. DOI: 10.1193/1.2857546.

Cornell, C.A. (1968). Engineering seismic risk analysis. *Bulleting of the seismological society of America*. Vol. 58, No. 5, pp. 1583-1606.

Deniz, A. (2006). Estimation of earthquake insurance premium rates based on stochastic methods. *M.Sc. Thesis*, Middle East Technical University, Ankara.

Deniz, A., Korkmaz, K.A., and Irfanoglu, A. (2010). Probabilistic seismic hazard assessment for Izmir, Turkey. *Pure and Applied Geophysics*, 167, 1475-1484. Doi:10.1007/s00024-010-0129-6

Duval, B., Dercourt, J., and Le Pichon, X. (1977). From the Tethys Ocean to the Mediterranean Seas: A plate tectonic model of the evolution of the western Alpine system. *Editions technip*, Paris 1977, pp. 143-164

EFEHR, European Facility for Earthquake Hazard & Risk. Available at: http://www.efehr.org:8080/jetspeed/portal/HazardMaps.psml. Last accessed 14.05.15

Emre, Ö., Özalp, S., Doğan, A., Özaksoy, V., Yildirim, C., and Göktaş, F. 2005 (in Turkish). İzmir yakın çevresinin diri fayları ve deprem potensiyelleri. *Maden Tetkik Arama Enstitusu, Jeoloji Etütleri Dairesi*, MTA Rapor No. 10754. 86p.

Gok, E., and Polat, O. (2014). An assessment of the microseismic activity and focal mechanisms of the Izmir (Smyrna) area from a new local network (IzmirNET). *Tectonophysics*, 635, 154–164. doi:10.1016/j.tecto.2014.08.003

Grünthal, G., and Wahlström, R. (2009). The unified catalogue of earthquakes in central, northern, and northwestern Europe (CENEC)-updated and expanded to the last millennium. *Journal of Seismology*, 13 (4), pp. 517-541. DOI 10.1007/s10950-008-9144-9

Havskov, J., and Ottemöller, L. (2014). Seisan: The Earthquake Analysis Software, Version 10.2. Institute of solid earth physics, *University of Bergen*, Norway.

ISC, International Seismological Centre. Available at: http://www.isc.ac.uk/iscbulletin/. Last accessed 02.04.15

Jimenez, M.J., Giardini, D., Grünthal, G., and SESAME Working Group (Ch. Papaioannou, A. Rebez, S. Riad, S. Sellami, A. Shapira, D. Slejko, T. Van Eck, A. El Sayed), 2001. Unified seismic hazard modelling throughout the Mediterranean region. *Bollettino di Geofisica Teorica ed Applicata*. Vol. 42, N. 1-2, PP. 3-18; Mar.-Jun. 2001

Johnston, A. C., and Halchuk, S. (1993). The seismicity database for the Global Seismic Hazard Assessment Program. *Annali di Geofisica*. 36, 133-151.

Jafari, M. A. (2008). Distribution of b-value in different seismic provinces of Iran. *The 14th World Conference on Earthquake Engineering October 12-17, 2008, Beijing, China*

Jolivet, L., Faccenna, C., Huet, B., Labrousse, L., Le Pourhiet, L., Lacombe, O., Lecomte, E., Burov, E., Denèle, Y., Brun, J-P., Philippon, M., Paul, A., Salaün, G., Karabulut, H., Piromallo, C., Monié, P., Gueydan, F., Okay, A., Oberhänsli, R., Pourteau, A., Augier, R., Gadenne, L., and Driussi, O. (2013). Aegean tectonics: Strain localisation, slab tearing and trench retreat. *Tectonophysics*, 597-598, 1–33. doi:10.1016/j.tecto.2012.06.011

KOERI, Kandilli Observatory and Earthquake Research Institute. Available at: http://www.koeri.boun.edu.tr/sismo/2015/earthquake-catalog/. Last accessed 07.03.15

Korkmaz, K.A., Irfanoglu, A., and Kayhan, A.H. (2009). Seismic risk assessment of buildings in Izmir, Turkey. *Springer Science+Business Media B.V.* 54:97–119. DOI 10.1007/s11069-009-9455-3

Metropolitan Municipality of Izmir [MMI], *Izmir Earthquake Master Plan*. http://www.izmir.bel.tr/izmirdeprem/izmirrapor.htm (Metropolitan Municipality of Izmir publication, Izmir, Turkey 2000).

McClusky, S., Balassanian, S., Barka, A., Demir, C., Ergintav, S., Georgiev, I., Gurkan, O., Hamburger, M., Hurst, K., Kahle, H., Kastens, K., Kekelidze, G., King, R., Kotzev, V., Lenk, O., Mahmoud, S., Mishin, A., Nadariya, M., Ouzounis, A., Paradissis, D., Peter, Y., Prilepin, M., Reilinger, R., Sanli, I., Seeger, H., Tealeb, A., Toksöz, and Veis, G. (2000). Global Positioning System constraints on plate kinematics and dynamics in the eastern Mediterranean and Caucasus. *Journal of Geophysical Research*, VOL. 105(1999), pp. 5695-5719.

Motazedian, D., and Atkinson, G.M. (2005). Stochastic Finite- Fault Modeling Based on a Dynamic Corner Frequency. Bulletin of the Seismological Society of America, Vol. 95, No.3, pp. 995-1010, June 2005, doi: 10.178510120030207

Nyst, M., and Thatcher, W. (2004). New constraints on the active tectonic deformation of the Aegean. *Journal of Geophysical Research*: Solid Earth, 109(B11), n/a–n/a. doi:10.1029/2003JB002830

Ocakoğlu, N., Demirbağ, E., and Kuşçu, İ. (2005). Neotectonic structures in İzmir Gulf and

surrounding regions (western Turkey): Evidences of strike-slip faulting with compression in the Aegean extensional regime. *Marine Geology*, 219(2-3), 155–171. doi:10.1016/j.margeo.2005.06.004

RADIUS (1997). Risk assessment tools for diagnosis of urban areas against seismic disaster Izmir earthquake master program, *Bogazici University Kandilli Observatory*, Istanbul, Turkey,

Reilinger, R., McClusky, S., Vernant, P., Lawrence, S., Ergintav, S., Cakmak, R., Ozener, R., Kadirov, F., Guliev, I., Stepanyan, R., Nadariya, M., Hahubia, G., Mahmoud, S., Sakr, K., ArRajehi, A., Paradissis, D., Al-Aydrus, A., Prilepin, M., Guseva, T., Evren, E., Dmitrotsa, A., Filikov, S., Gomez, F., Al-Ghazzi, R., and Karam, G. (2006). GPS constraints on continental deformation in the Africa-Arabia-Eurasia continental collision zone and implications for the dynamics of plate interactions. *Journal of Geophysical Research*, 111(B5), B05411. doi:10.1029/2005JB004051

Reiter, L., Earthquake Hazard Analysis (Columbia University Press, New York, 1990).

Stein, S., and Wysession, M. *An Introduction to Seismology, Earthquakes, and Earth Structure* (Blackwell Scientific, Malden, MA, 2003).

Taymaz, T., Jackson, J., and McKenzie, D. (1991). Active tectonics of the north and central Aegean Sea. *Geophysical Journal International*, 106(2), 433–490. doi:10.1111/j.1365-246X.1991.tb03906.x

Taymaz, T., Yilmaz, Y., and Dilek, Y. (2007). The geodynamics of the Aegean and Anatolia: introduction. *Geological Society*, London, Special Publications, 291(1), 1–16. doi:10.1144/SP291.1

USGS, U.S. Geological Survey. Available at: http://earthquake.usgs.gov/earthquakes/map/doc_aboutdata.php#data-availability. Last accessed 07.04.15

Wells, D. L., and Coppersmith, K. J (1994). New empirical relationships among magnitude, rupture length, rupture width, rupture area, and surface displacement. Bill. Seismol. Soc. Am., 84, 974-1002.

Wiemer, S., Giardini, D., Fäh, D., Deichmann, N., and Sellami, S. 2008. Probabilistic seismic hazard assessment of Switzerland: best estimates and uncertainties. J Seismol, 1313:449-478. DOI 10.1007/s10950-008-9138-7

Appendices

A Results from the probabilistic seismic hazard assessment

A.1 2% probability in 50 years using GMPE from BA08

These seismic hazard values have a return period of 2475 years and are measured in acceleration of gravity.

A.1.1 PGA values

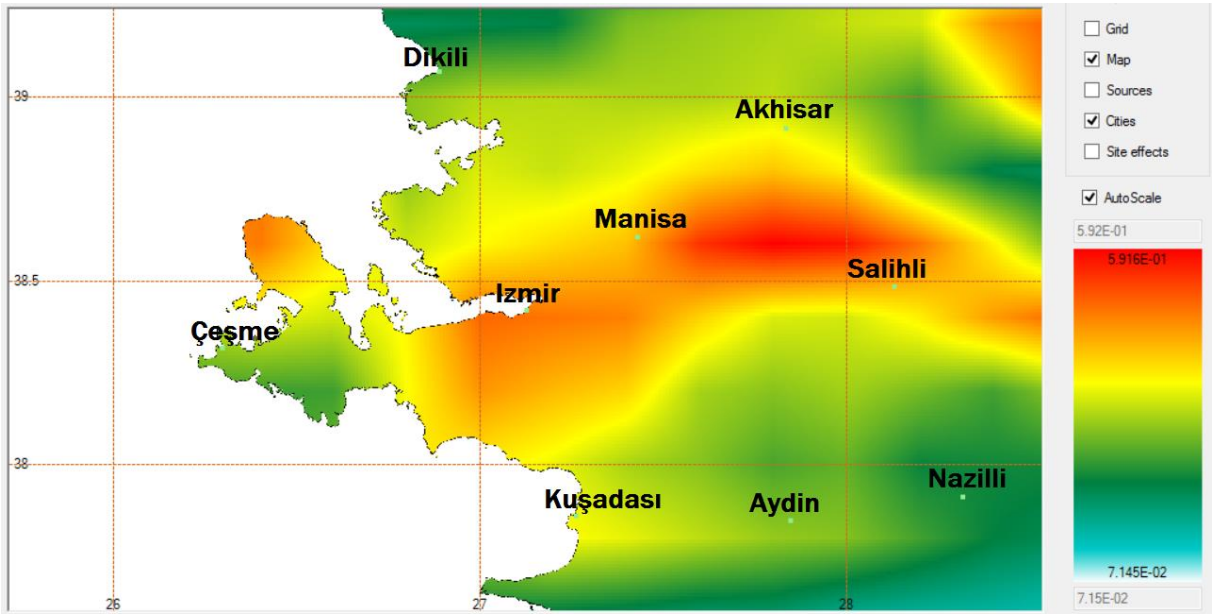

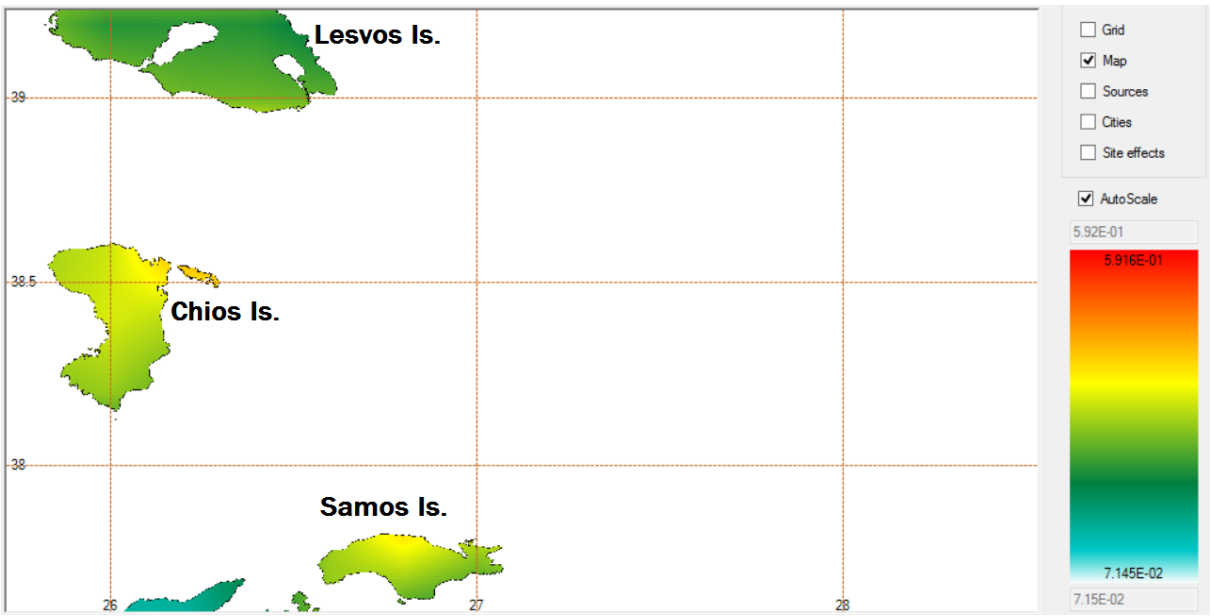

A.1.2 SA values with a period of 0.3s

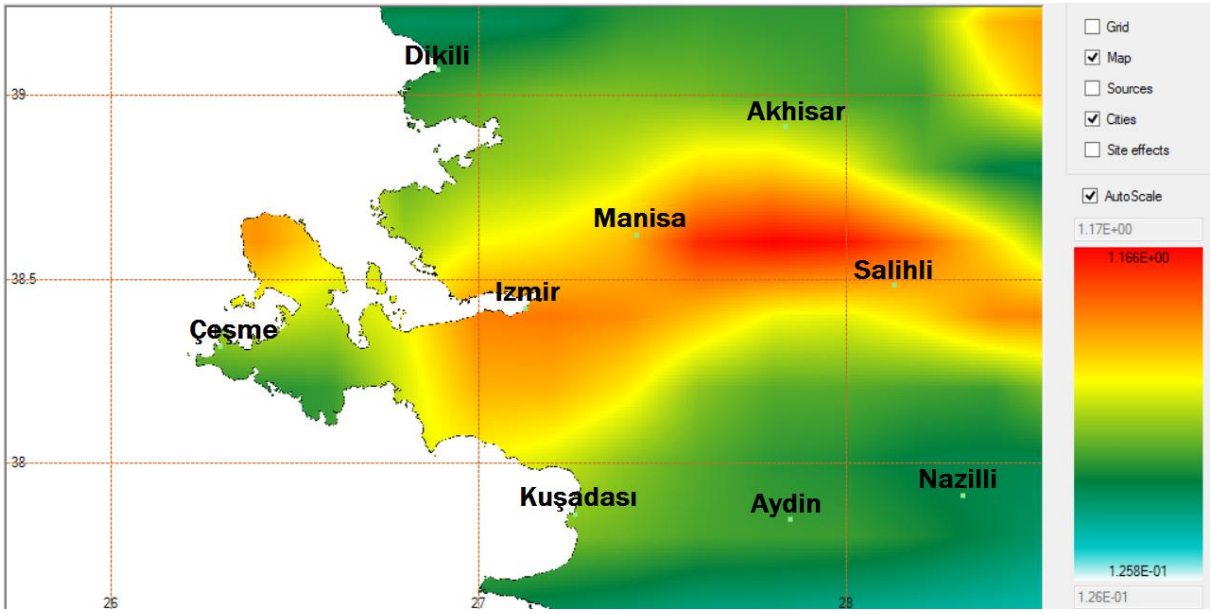

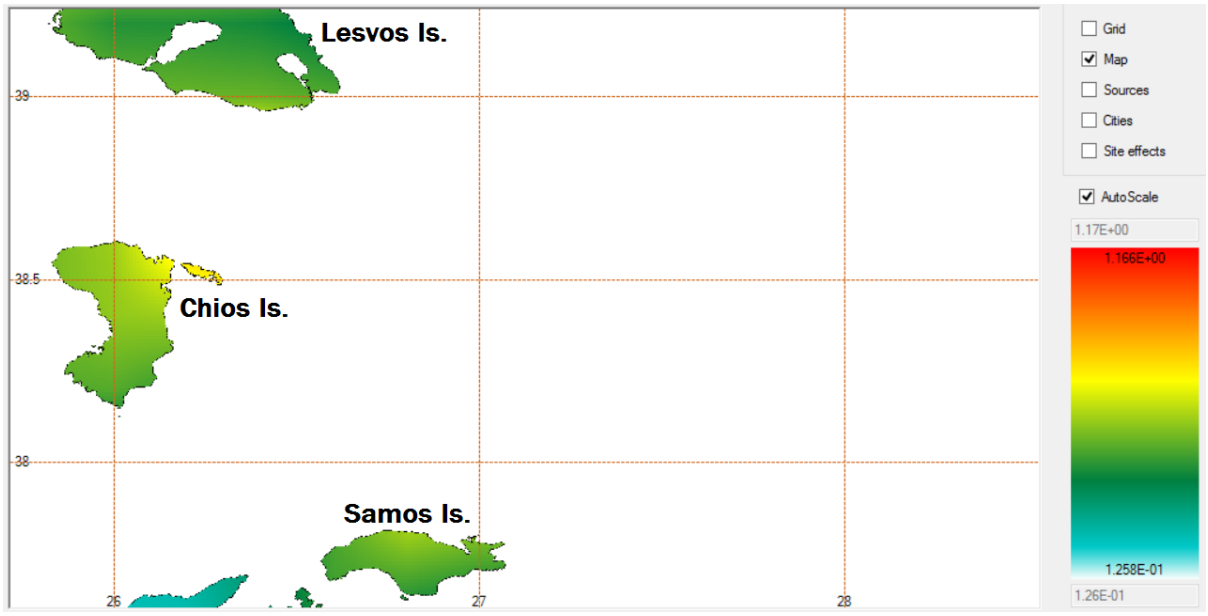

A.1.3 SA values with a period of 1.0s

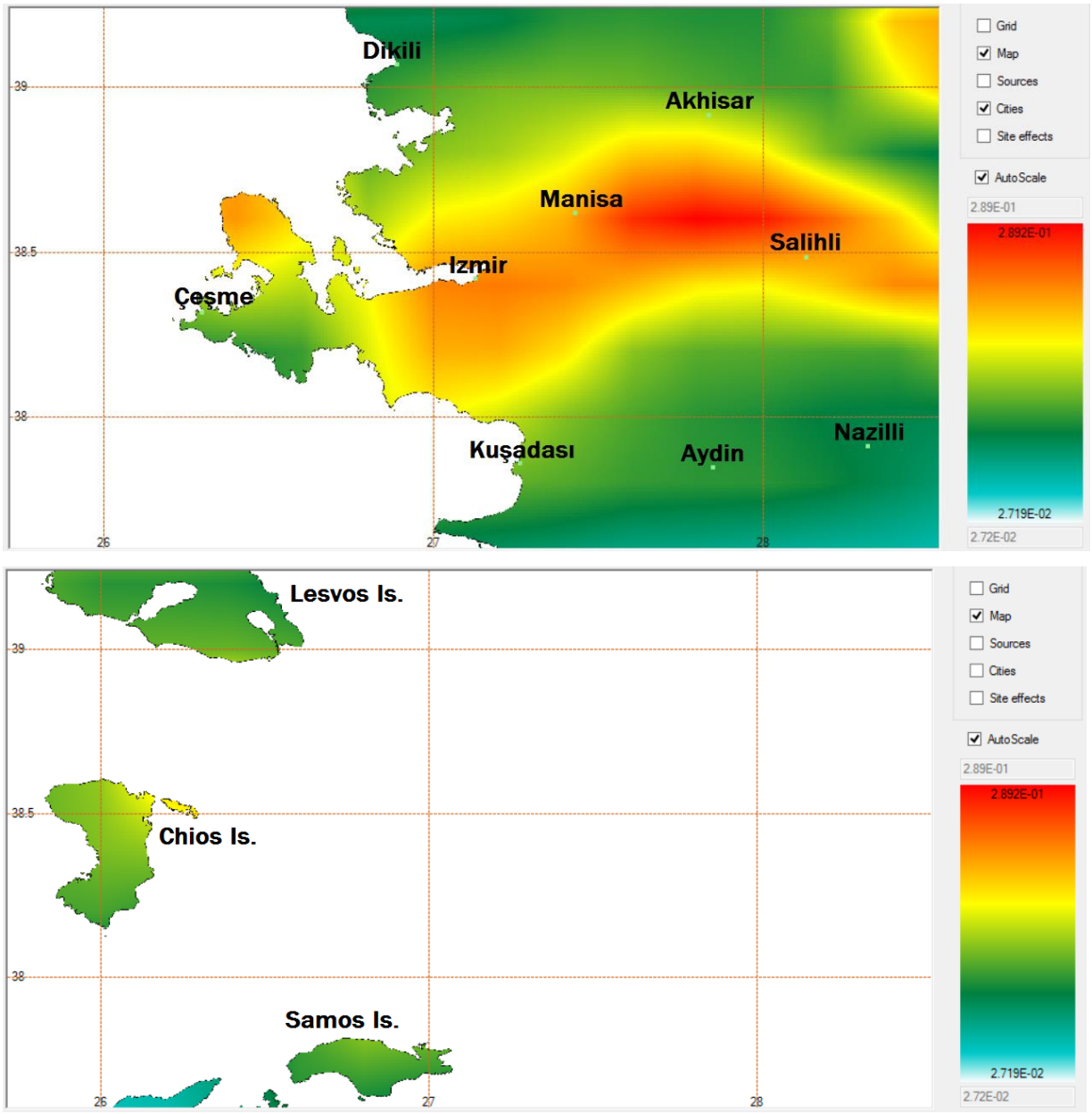

A.2 2% probability in 50 years using GMPE from CB08

These seismic hazard values have a return period of 2475 years and are measured in acceleration of gravity.

A.2.1 PGA values

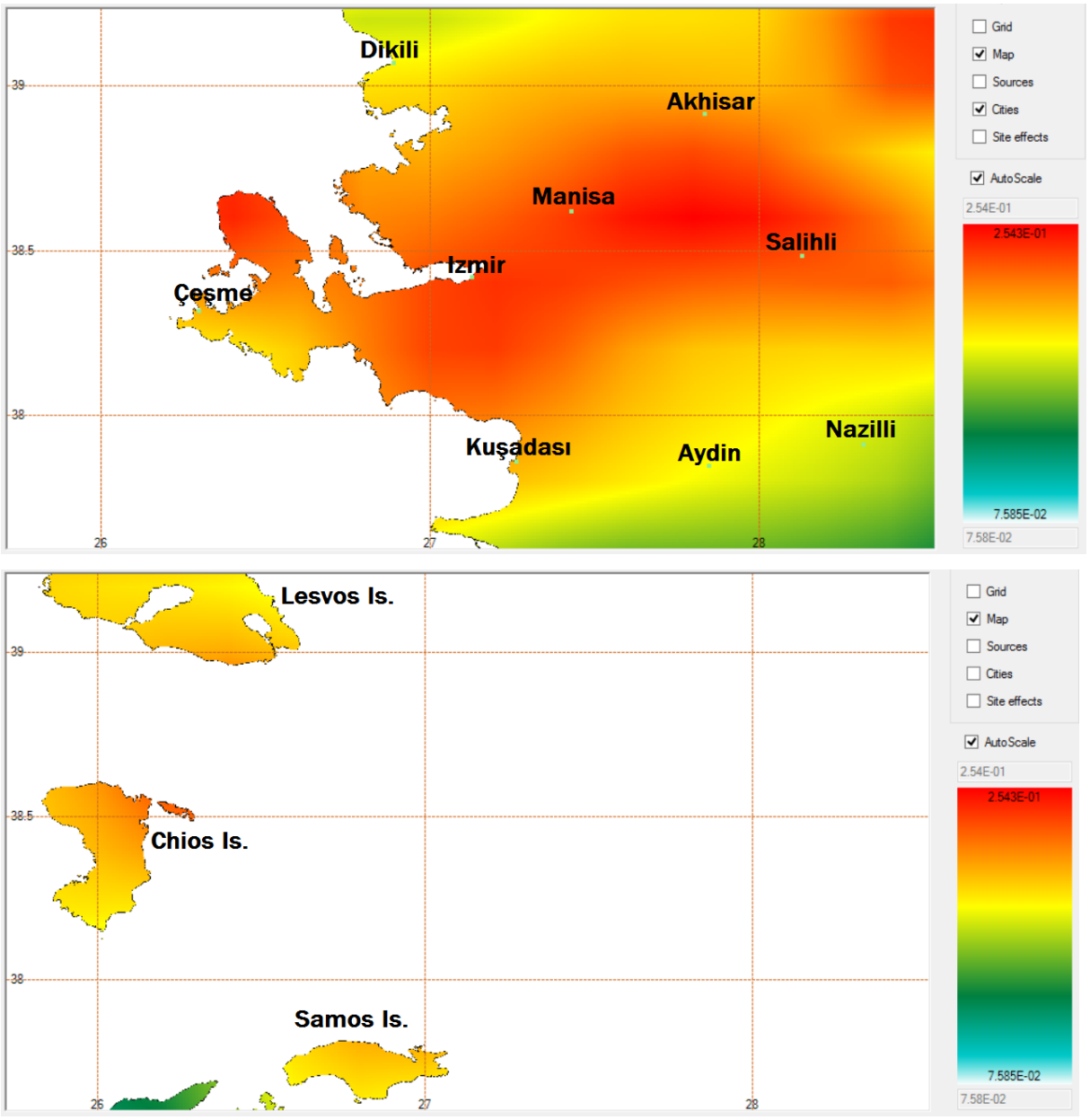

A.2.2 SA values with a period of 0.3s

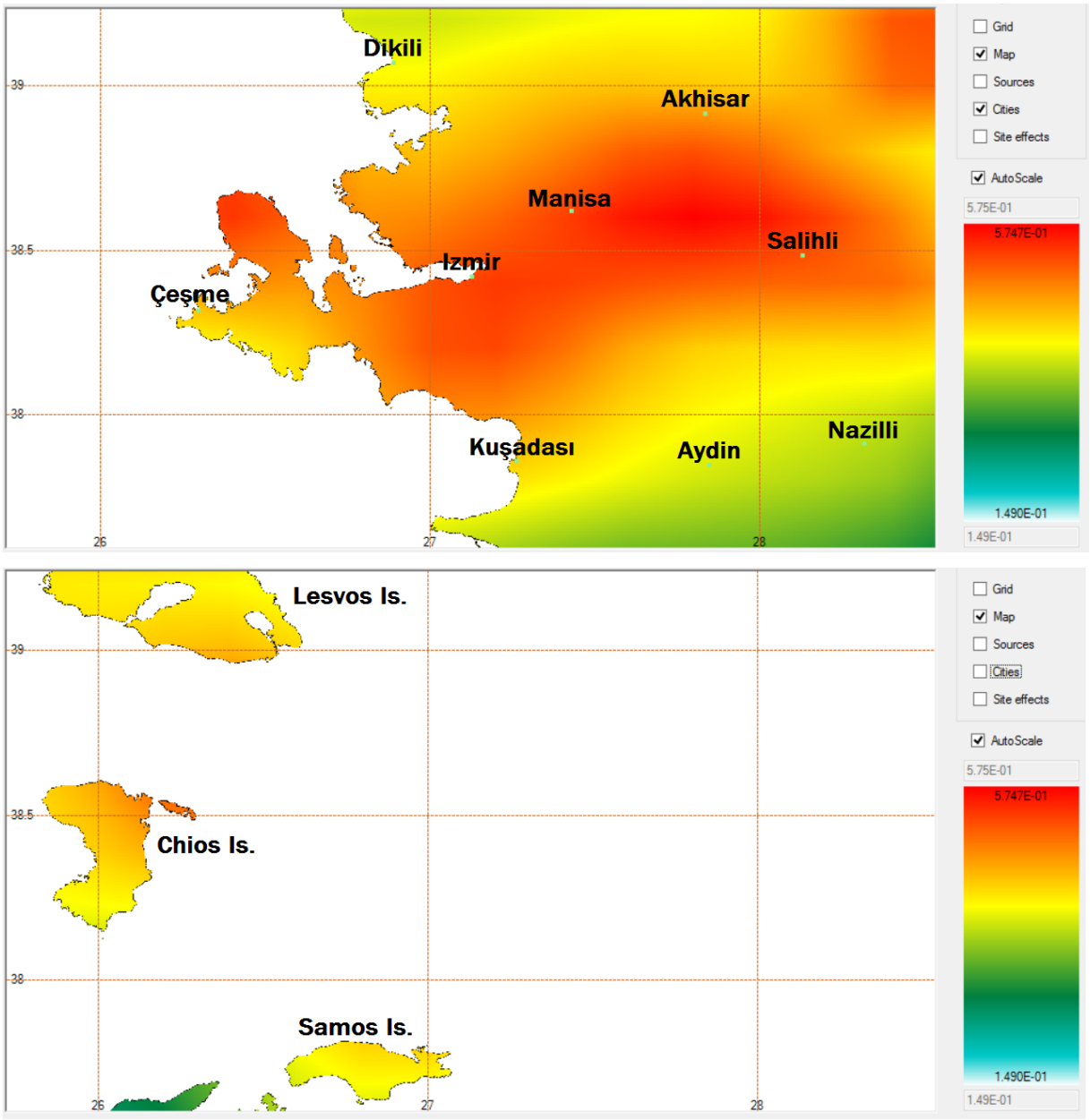

A.2.3 SA values with a period of 1.0s

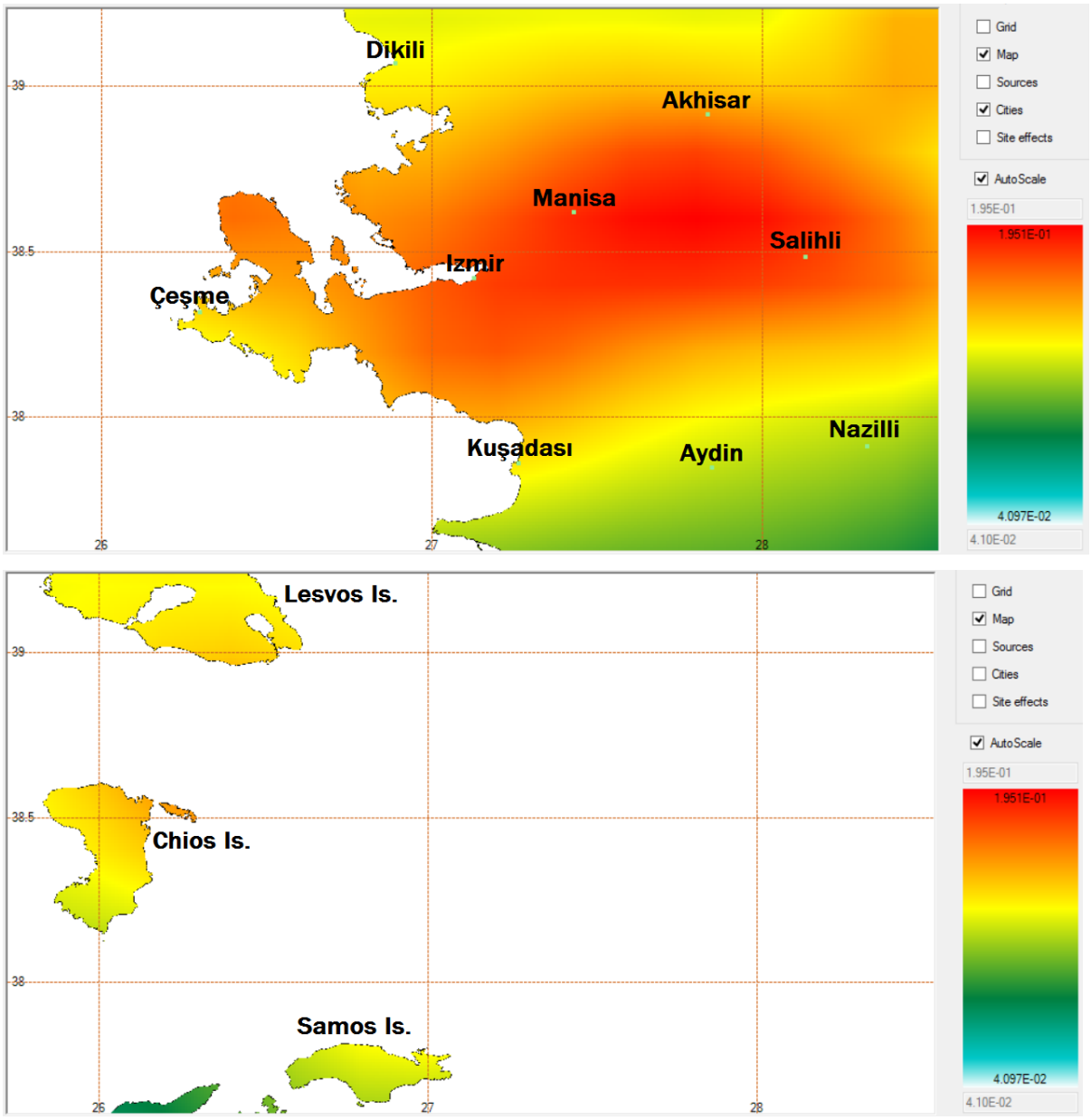

A.3 10% probability in 100 years using GMPE from BA08

These seismic hazard values have a return period of 949 years and are measured in acceleration of gravity.

A.3.1 PGA values

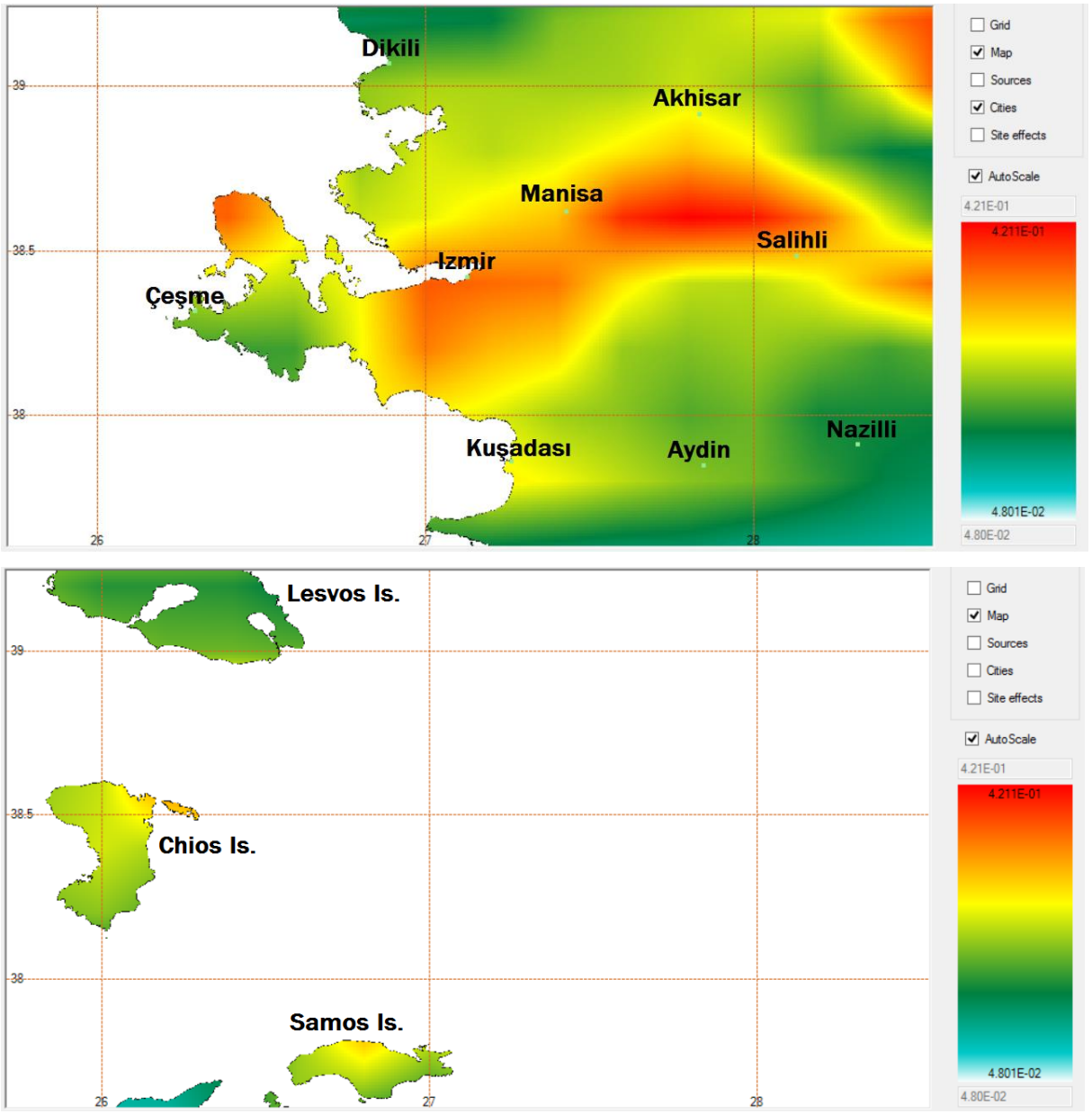

A.3.2 SA values with a period of 0.3s

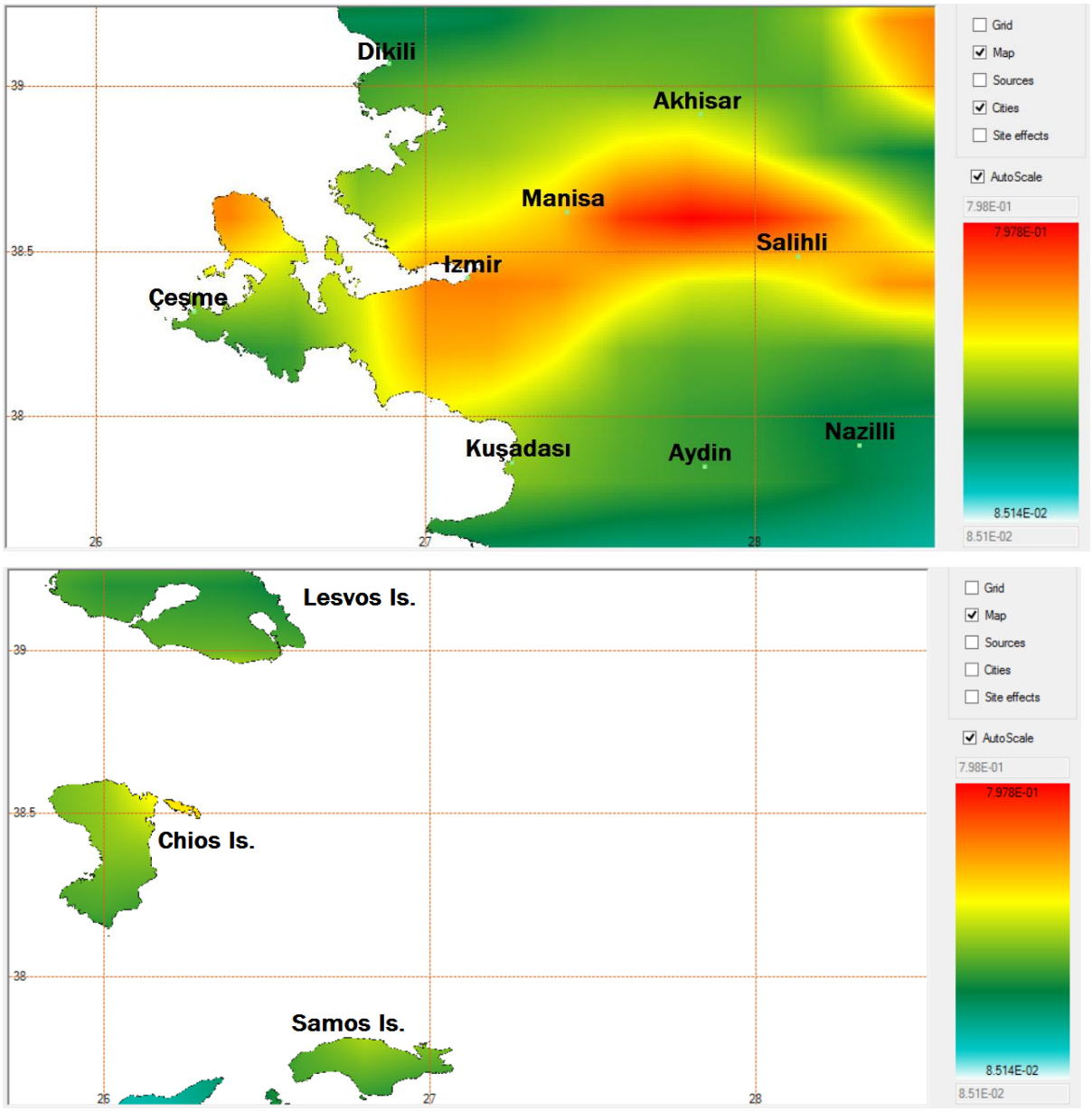

A.3.3 SA values with a period of 1.0s

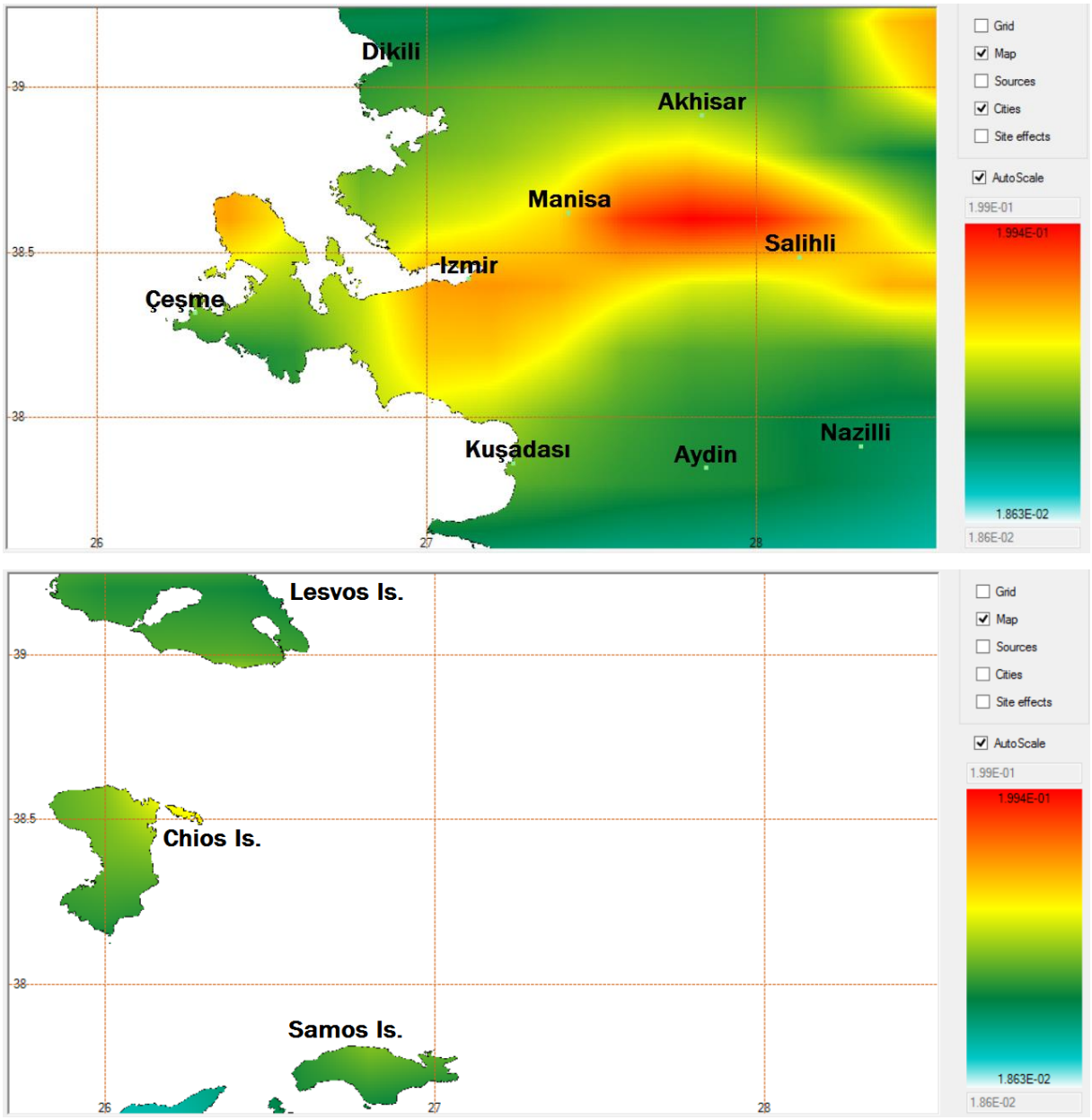

A.4 10% probability in 100 years using GMPE from CB08

These seismic hazard values have a return period of 2475 years and are measured in acceleration of gravity.

A.4.1 PGA values

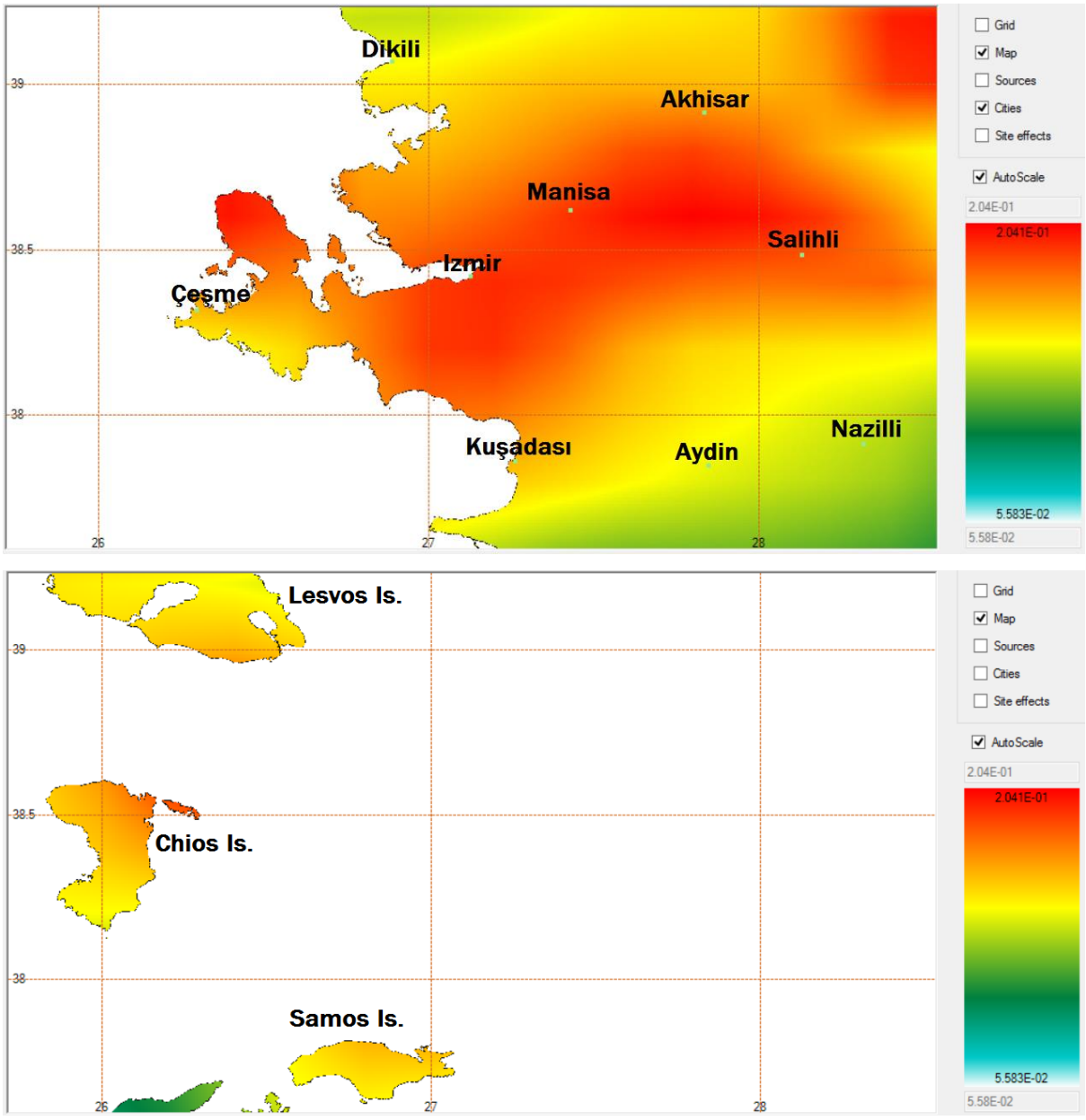

A.4.2 SA values with a period of 0.3s

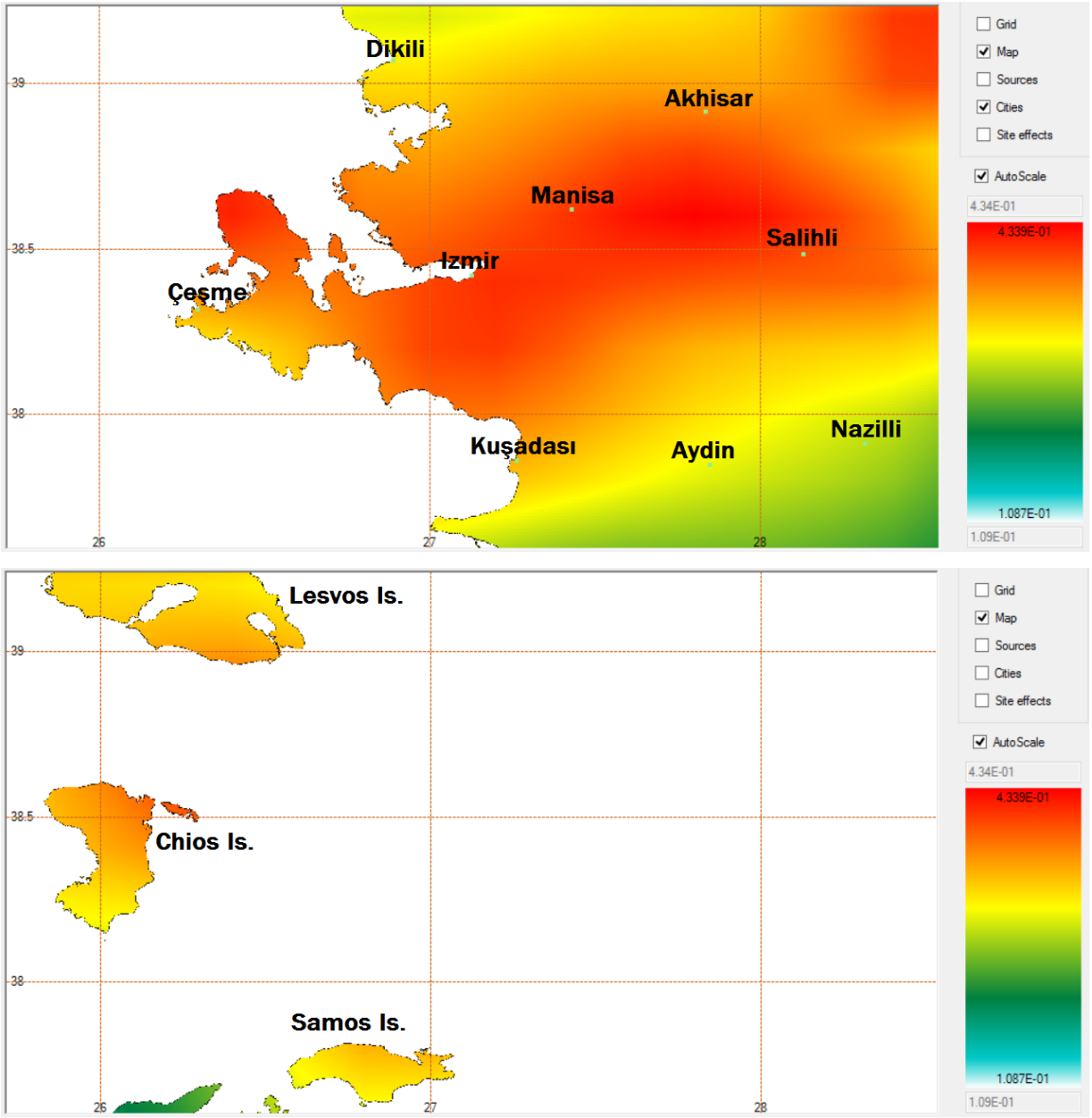

A.4.3 SA values with a period of 1.0s

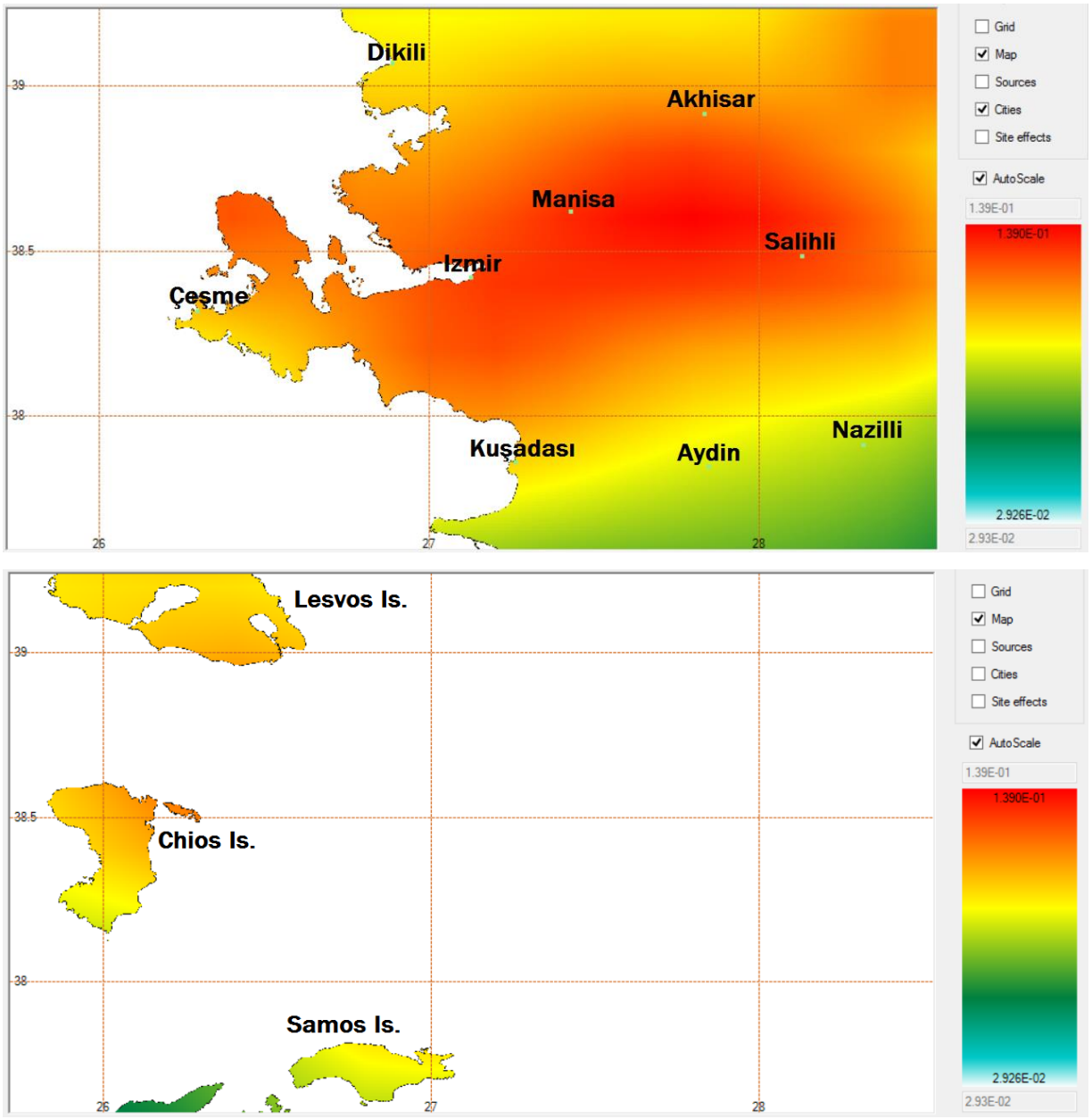

A.5 2% probability in 100 years using GMPE from Boore and Atkinson (2008)

These seismic hazard values have a return period of 4950 years and are measured in acceleration of gravity.

A.5.1 PGA values

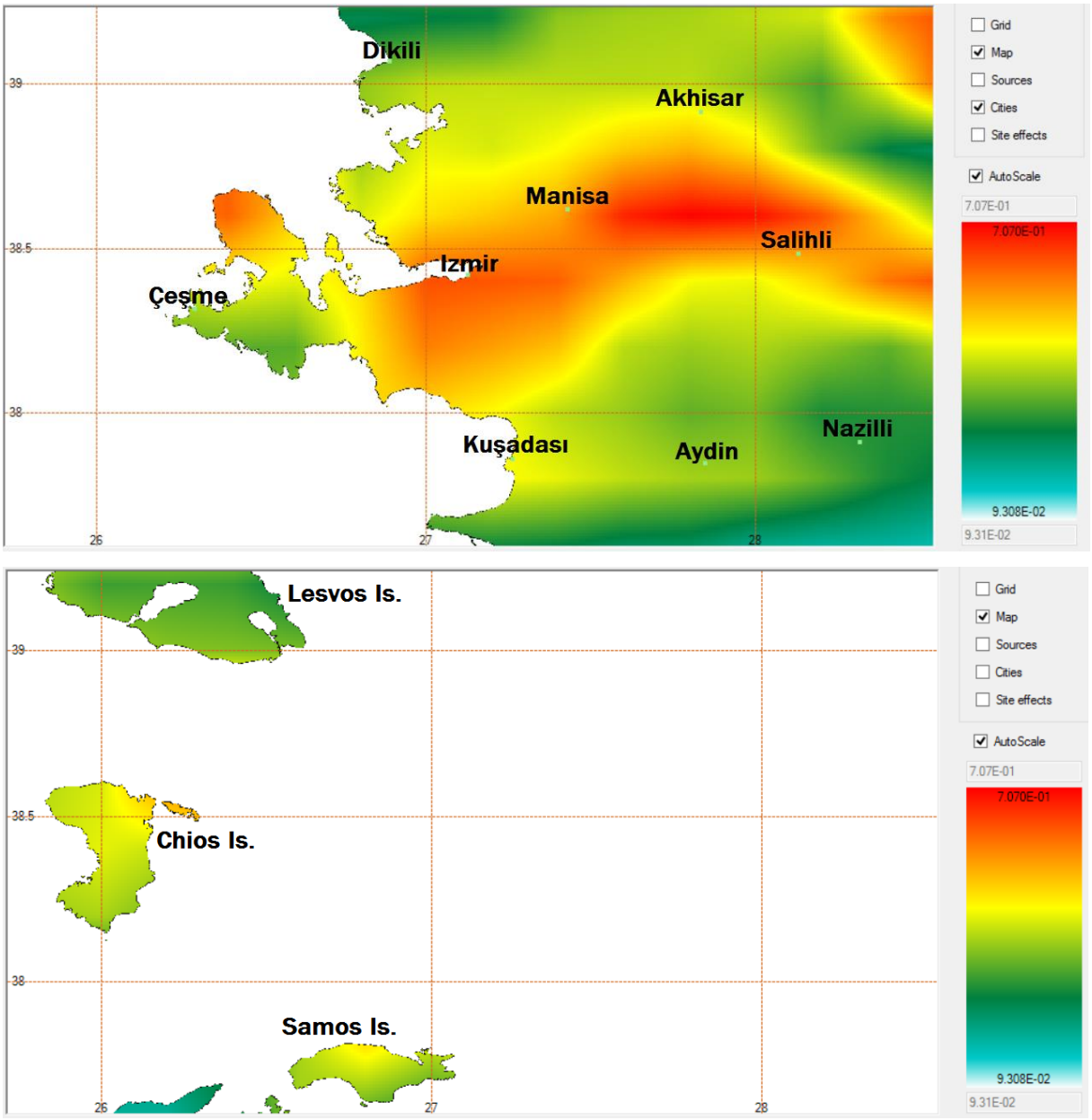

A.5.2 SA values with a period of 0.3s

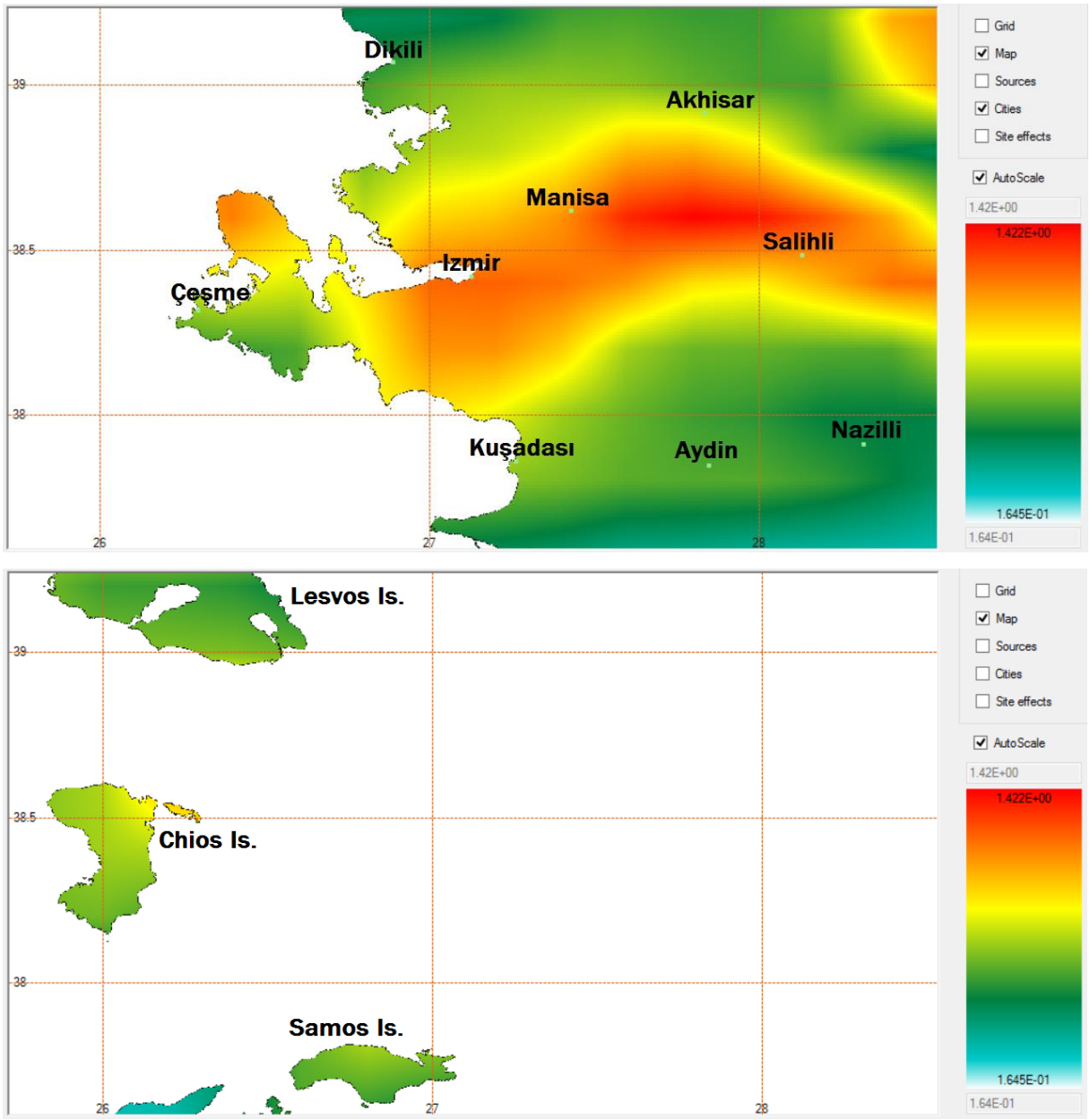

A.5.3 SA values with a period of 1.0s

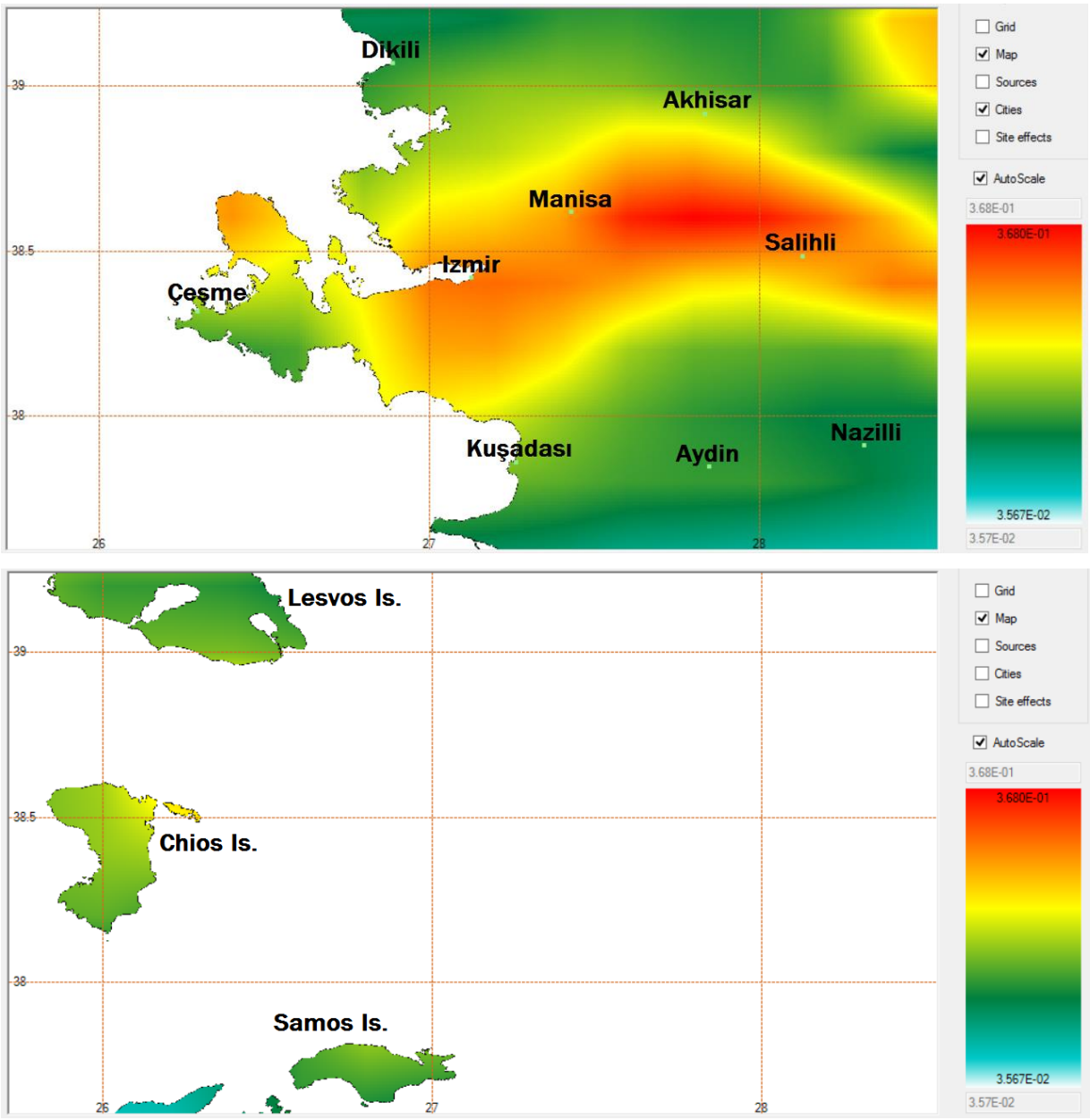

A.6 2% probability in 100 years using GMPE from CB08

These seismic hazard values have a return period of 4950 years and are measured in acceleration of gravity.

A.6.1 PGA values

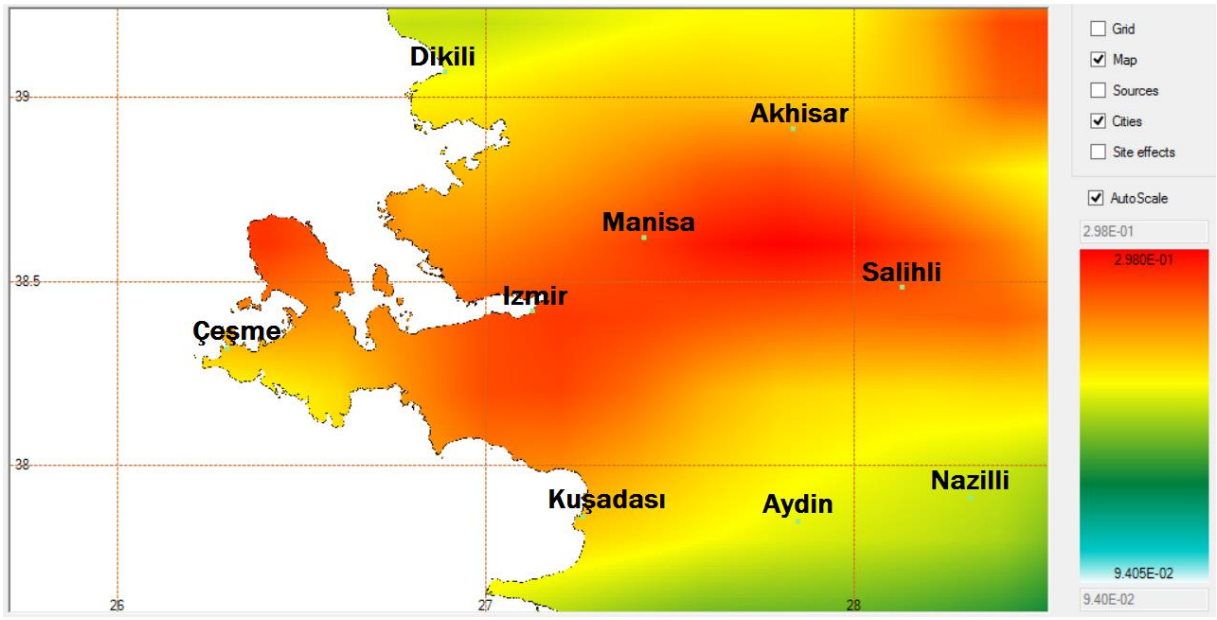

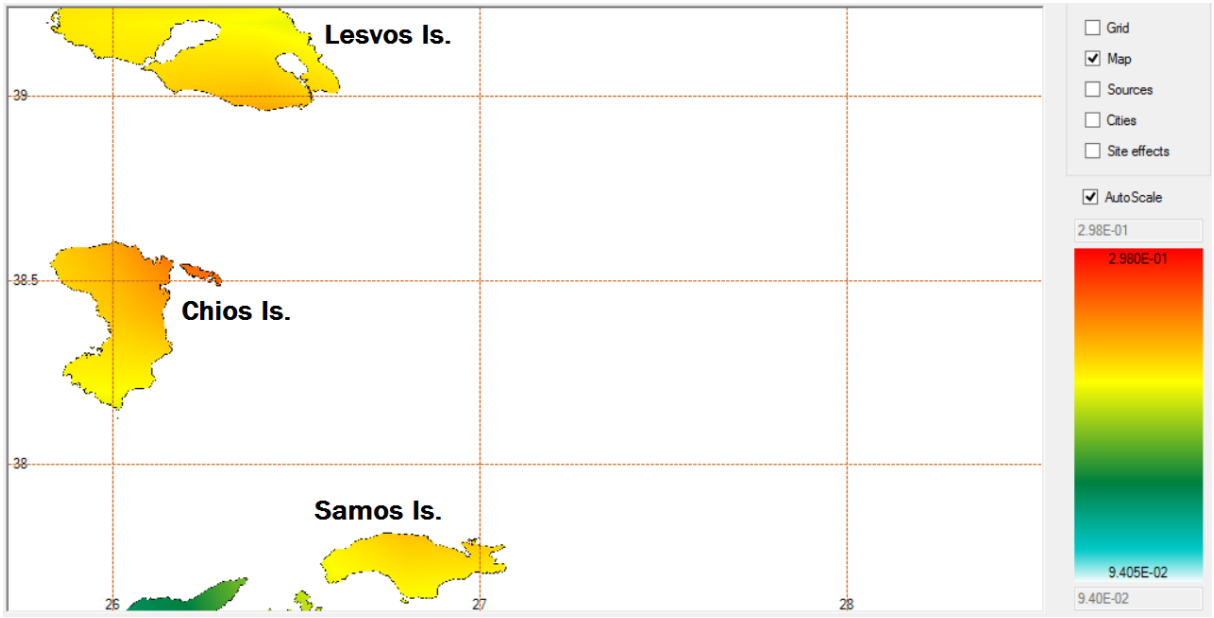

A.6.2 SA values with a period of 0.3s

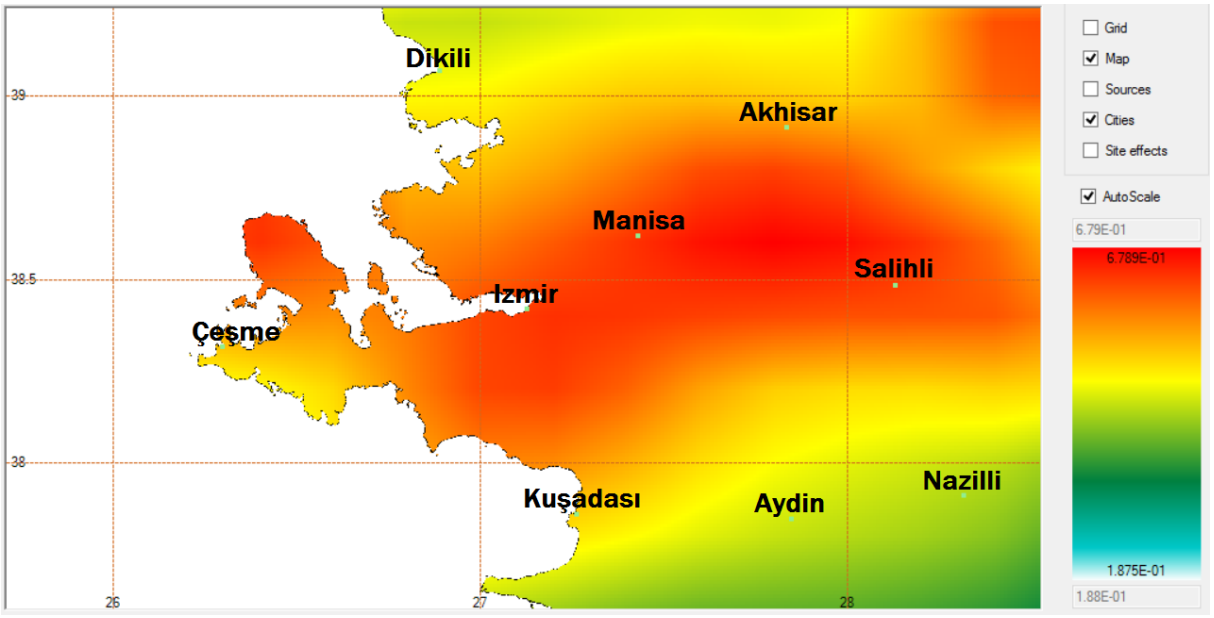

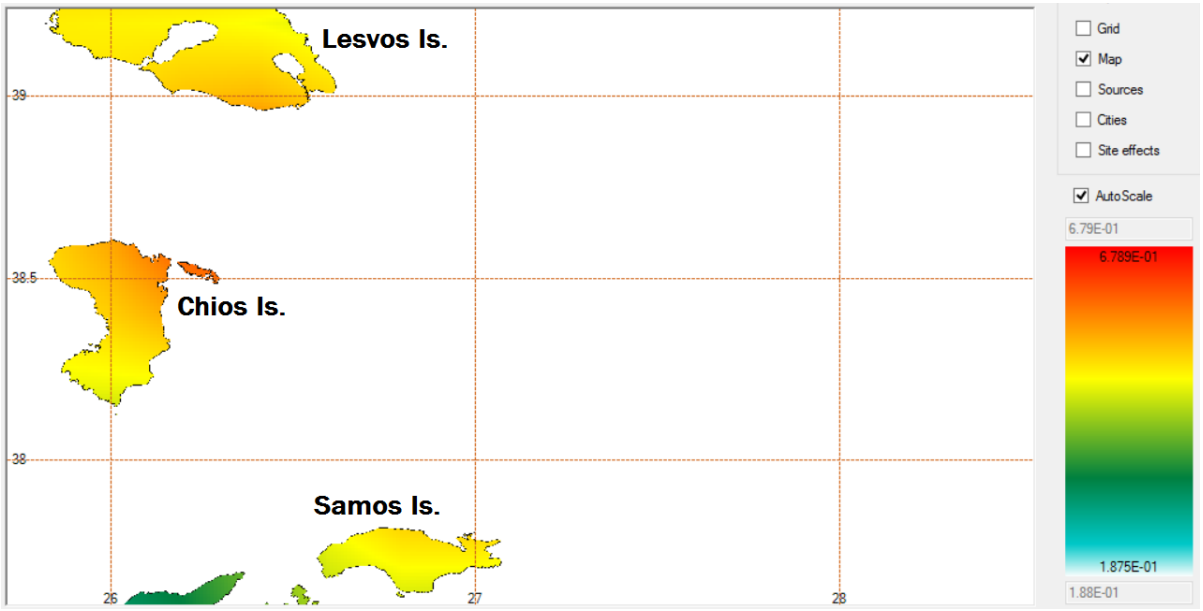

A.6.3 SA values with a period of 1.0s

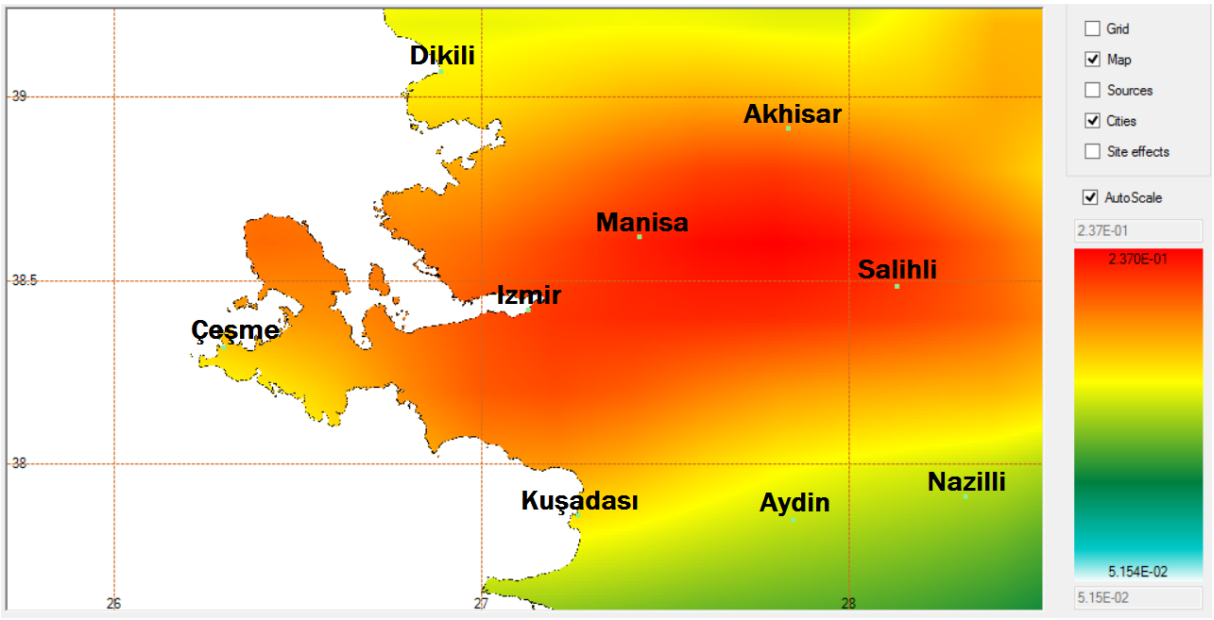

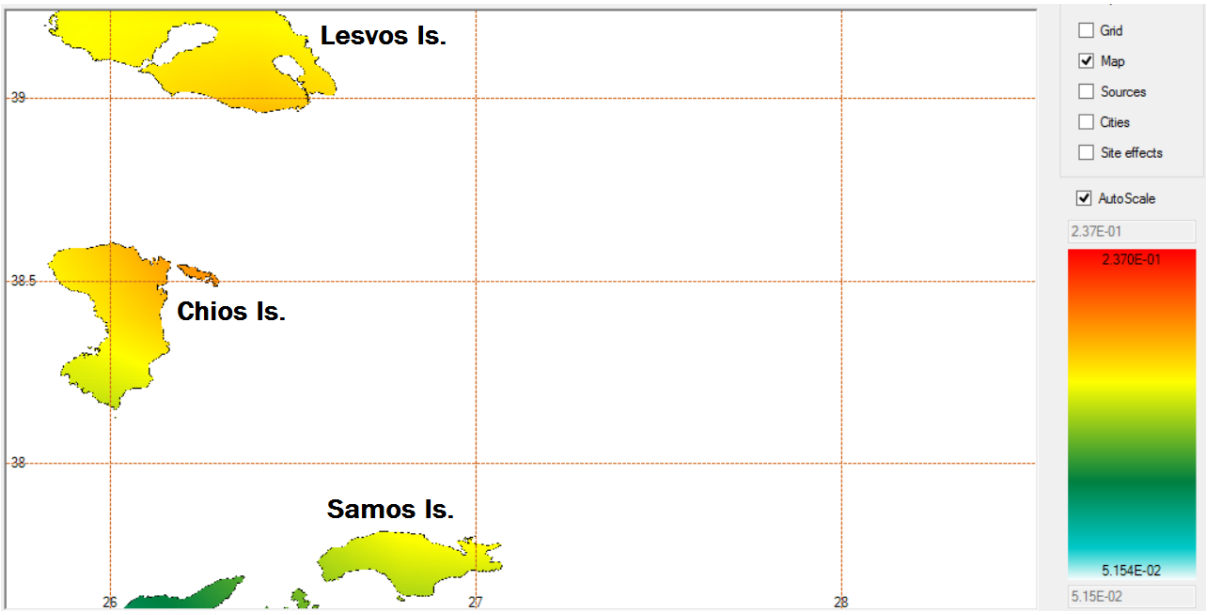

B Mean strike directions

Rose diagrams with mean strike directions from different fault groups.

Akhisar and Alaçatı: Mean direction: 12.3˚, N-S and 101.2˚, E-W

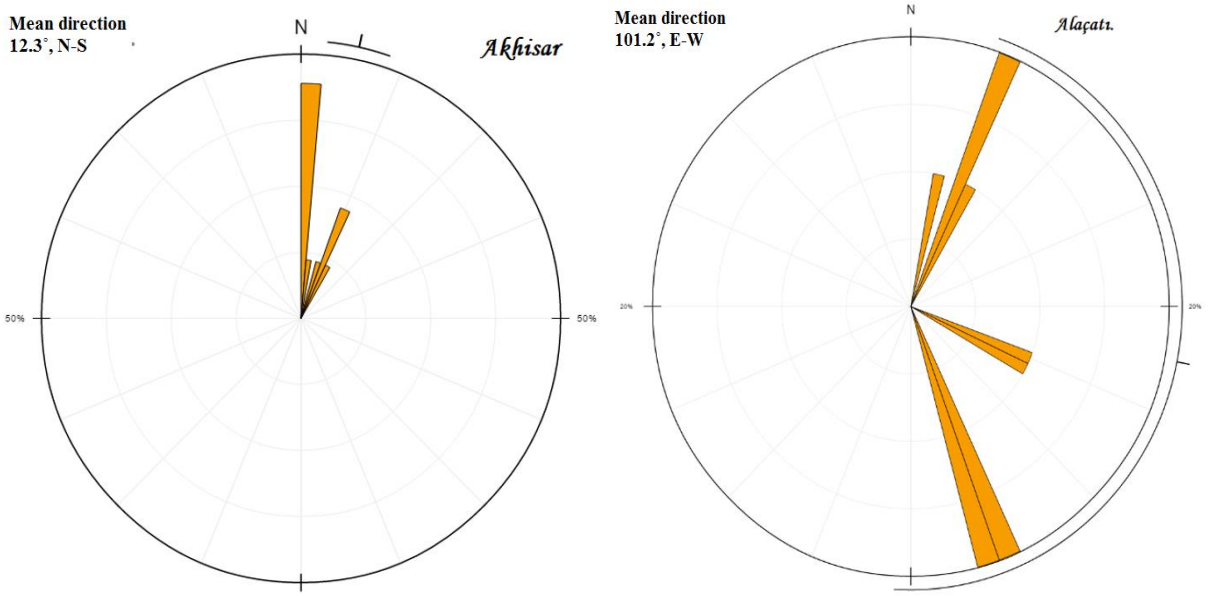

Balıkesir and Büyük-Menderes-Graben-North: Mean direction 78.1˚, E-W and 87.2˚, E-W

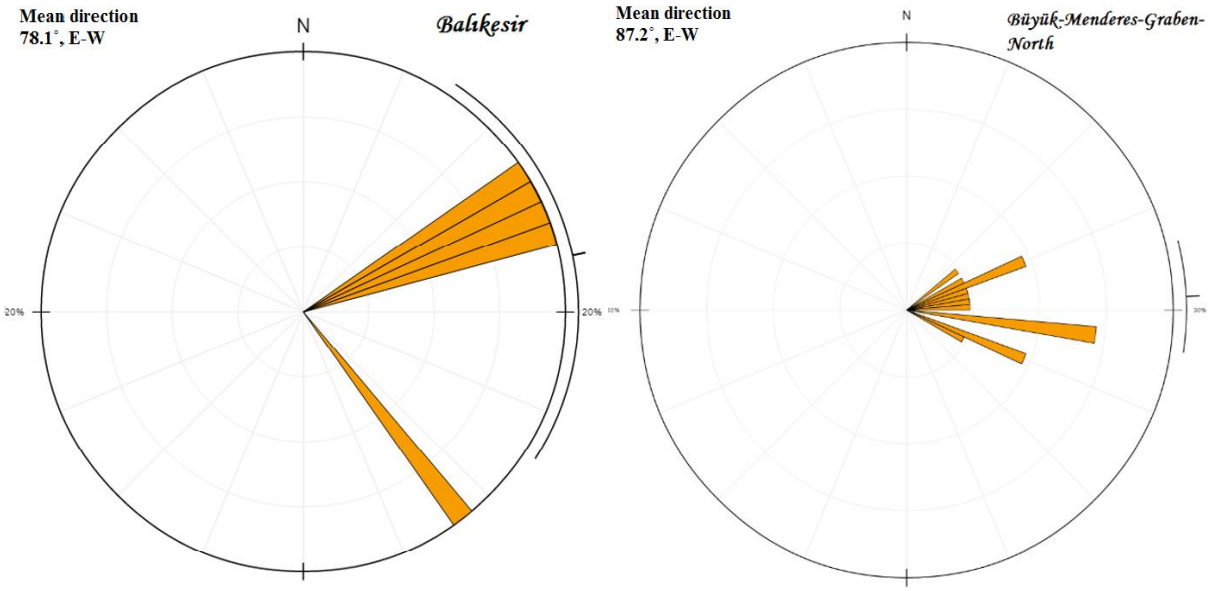

Büyük-Menderes-Graben-South and Chios: Mean direction 80.1˚, E-W and 98˚, E-W

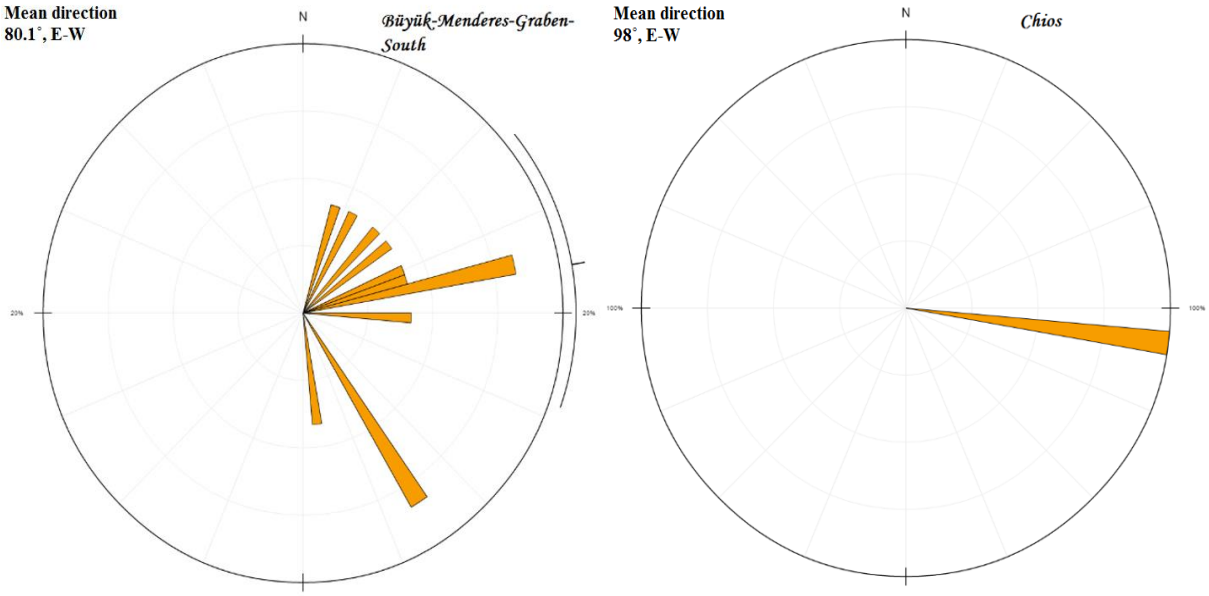

Demirci and Foça-Soma: Mean direction 102.5˚, E-W and 53.3˚, NE-SW

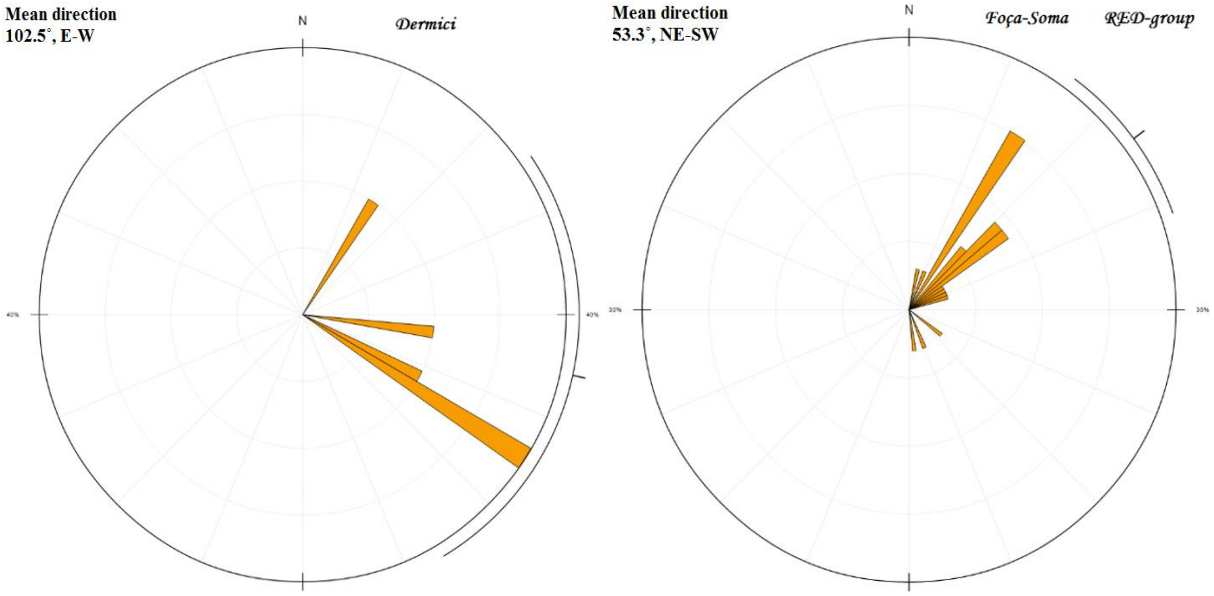

Gediz-Alaşehir-Graben-North and Gediz-Alaşehir-Graben-South: Mean direction 118.1˚, SE-NW and 94.1˚, E-W

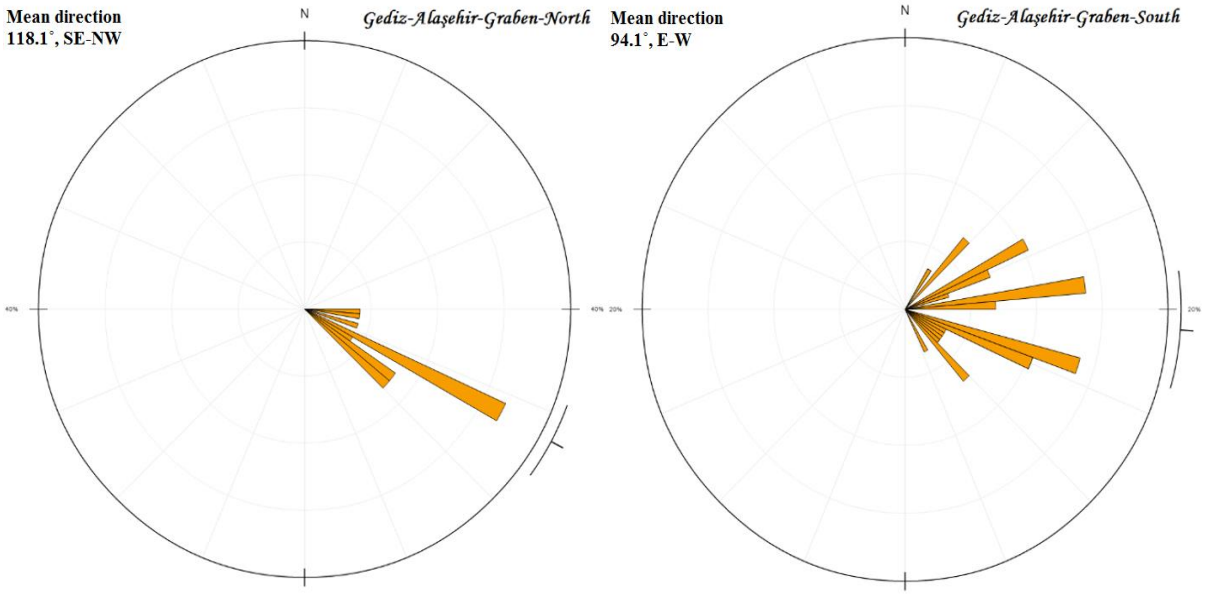

Gökeyüp and Havran: Mean direction 46.0˚, NE-SW and 43.6˚, NE-SW

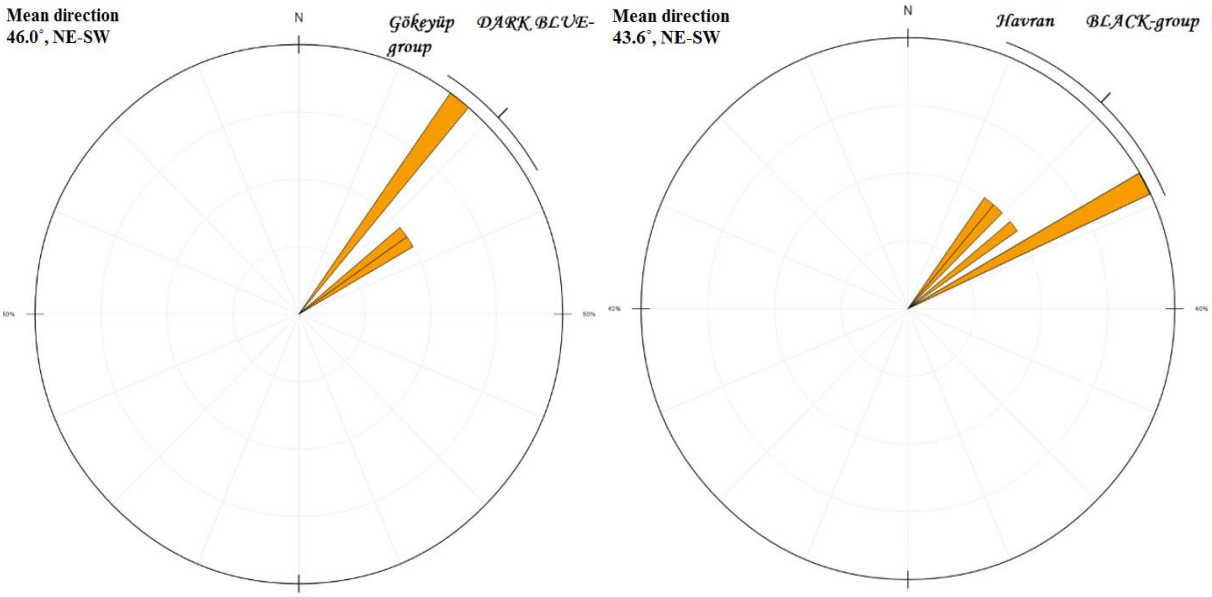

Izmir and KaraburunPeninsula: Mean direction 65.6˚, NE-SW and 28.3˚, NE-SW

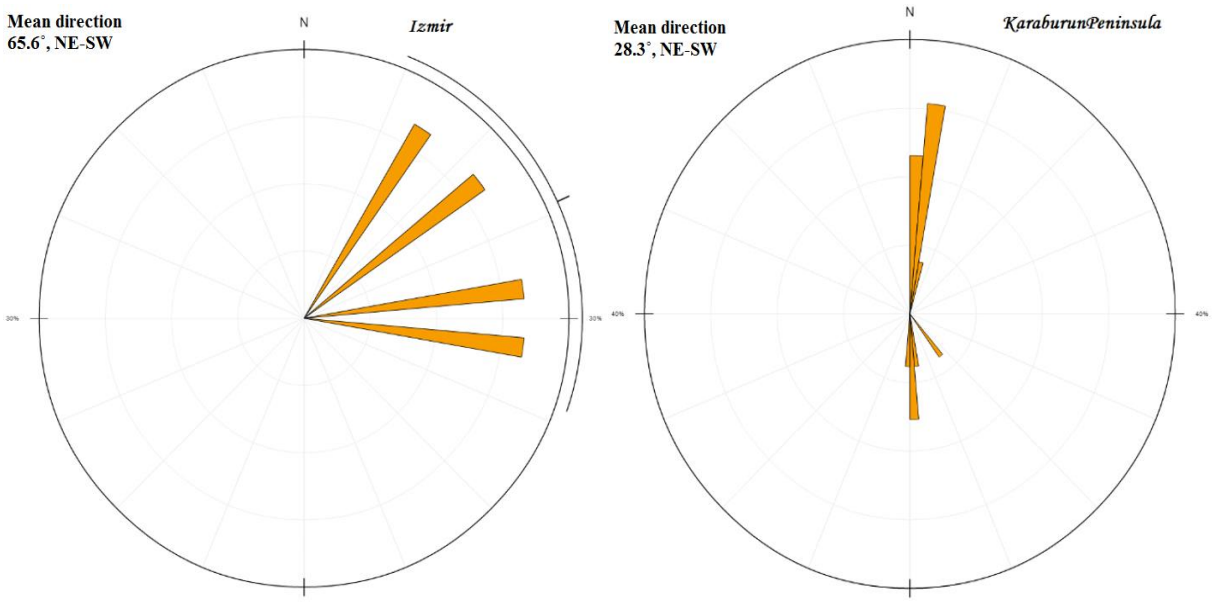

Manisa and Milas: Mean direction 66.4˚, NE-SW and 119.4˚, SE-NW

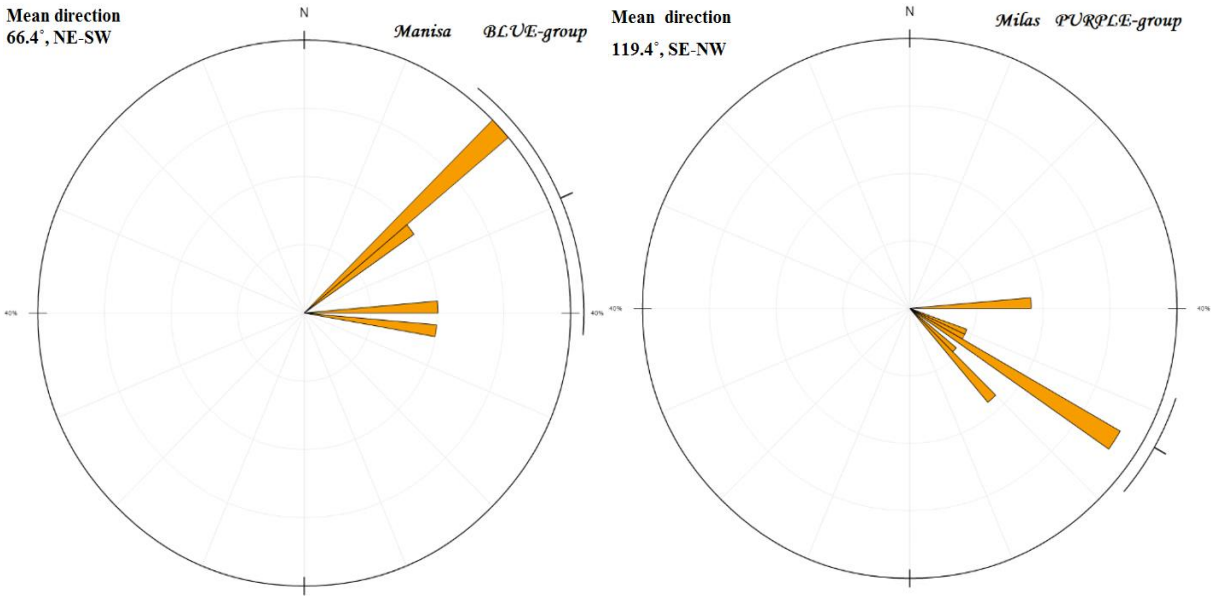

Mügla+Yatağan and Samos: Mean direction 138.0˚, SE-NW and 69.0˚, E-W

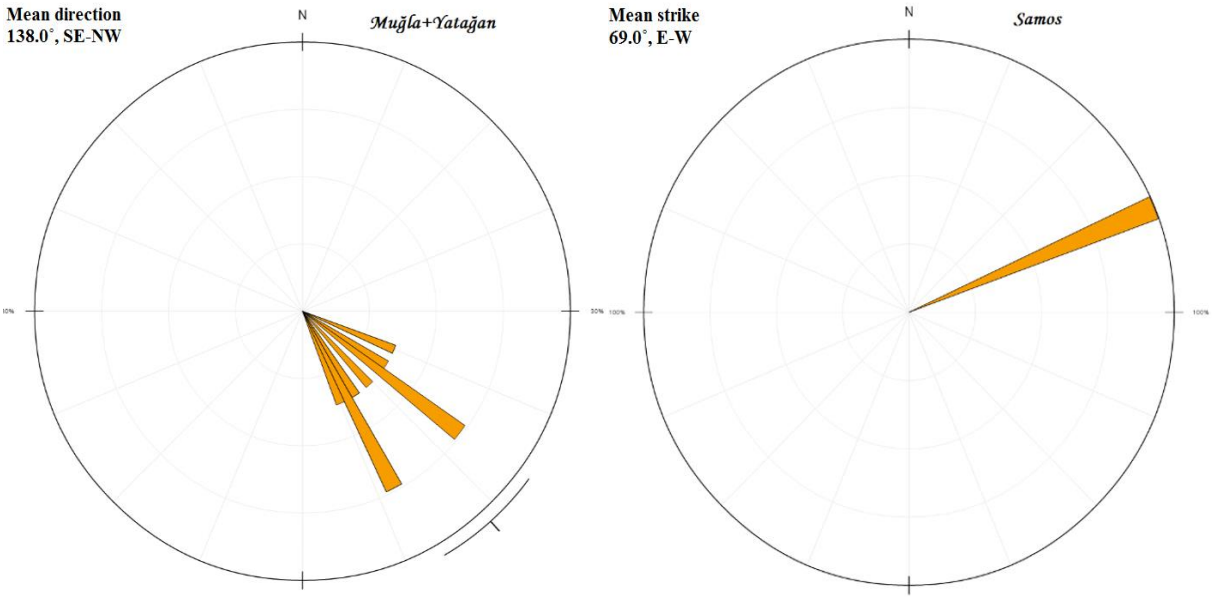

Seferihisar and Sığacık: Mean direction 25.7˚, NE-SW and 81.0˚, E-W

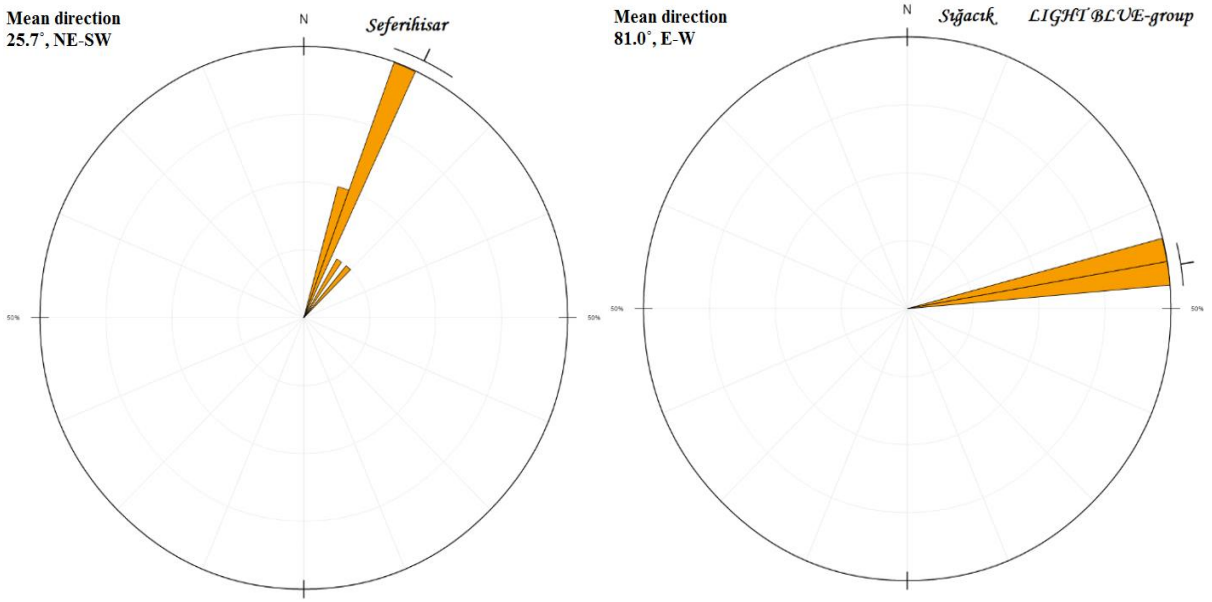

Tuzla and Urla: Mean direction 35.2˚, NE-SW and 59.6˚, NE-SW

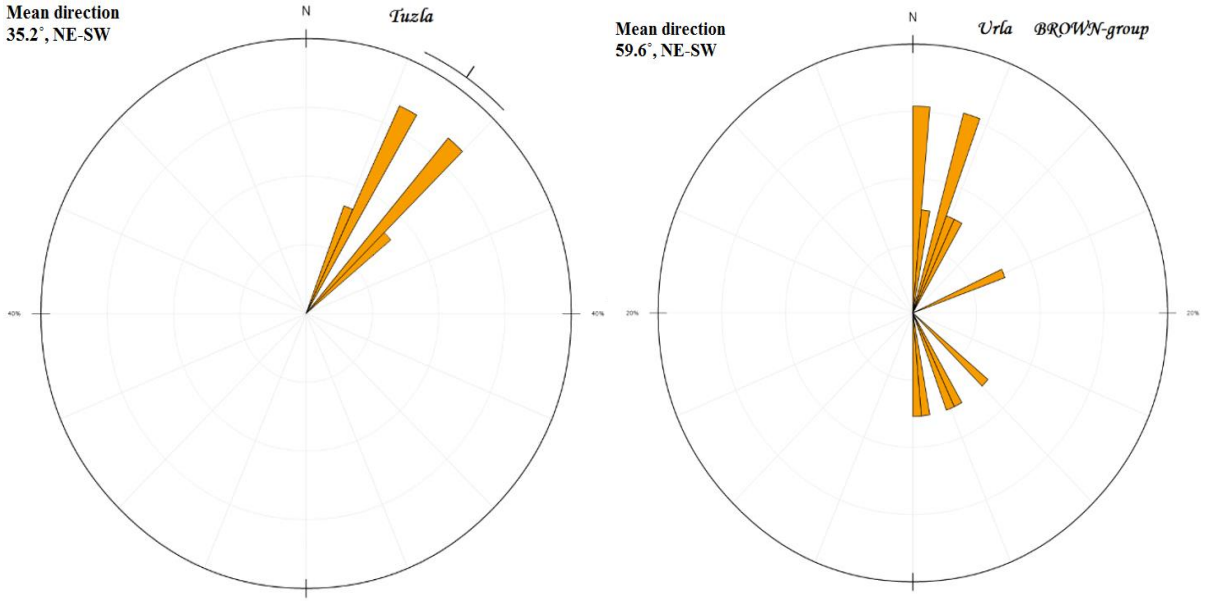

C Magnitude regressions

List of all magnitude regressions used to convert all magnitude scales into moment magnitude.

CKAN to WKAN and LKAN to WKAN

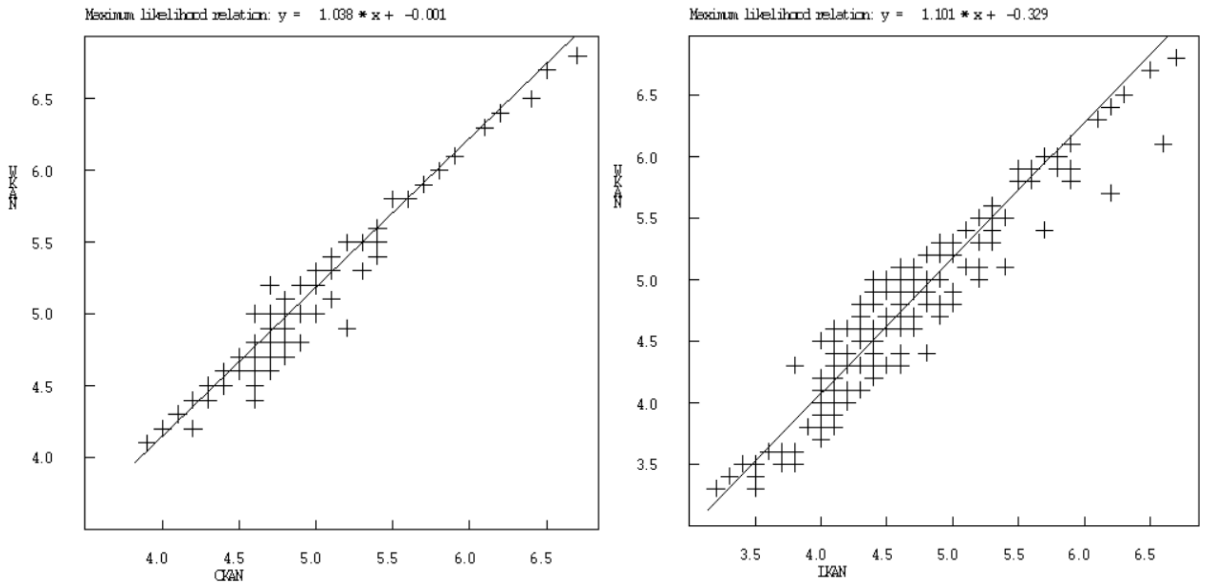

sKAN to WKAN and bKAN to WKAN

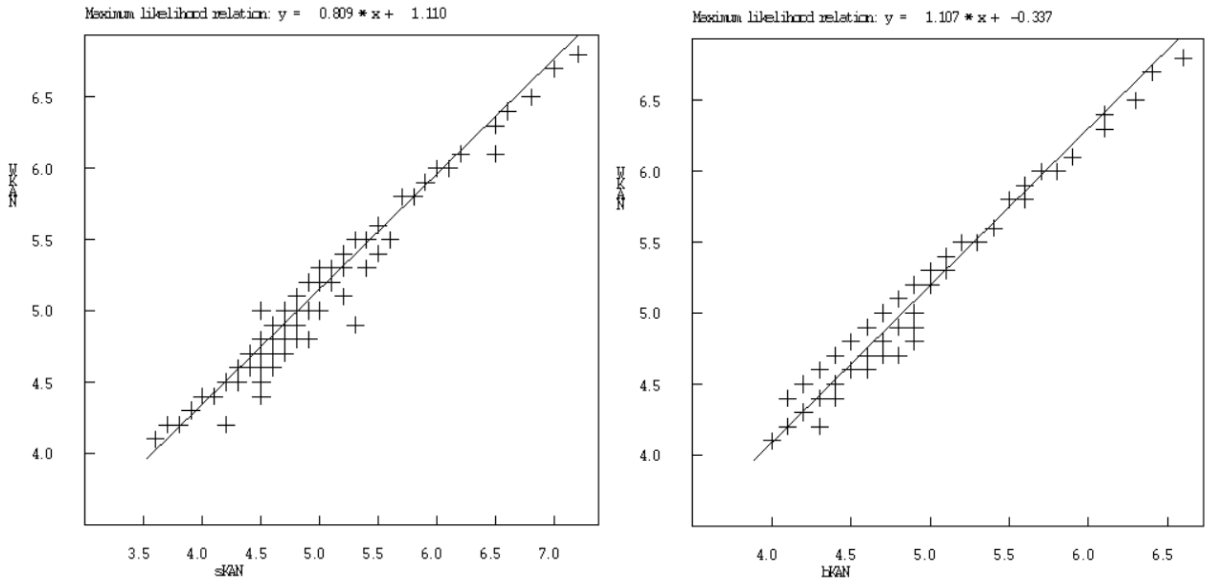

LDDA to CKAN and L to CKAN

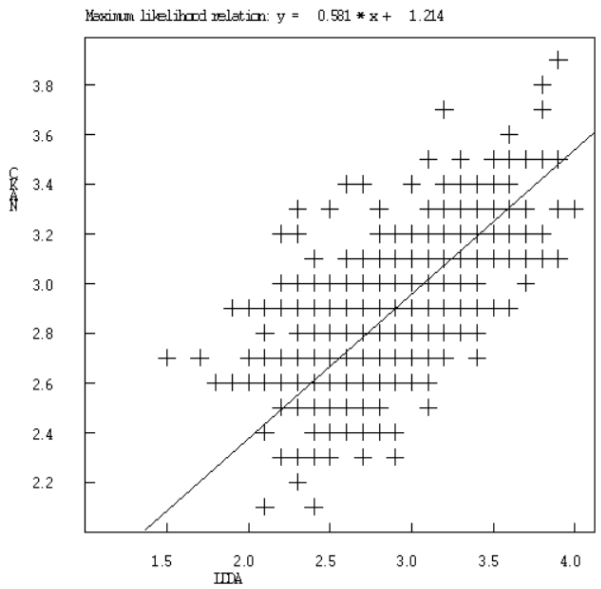

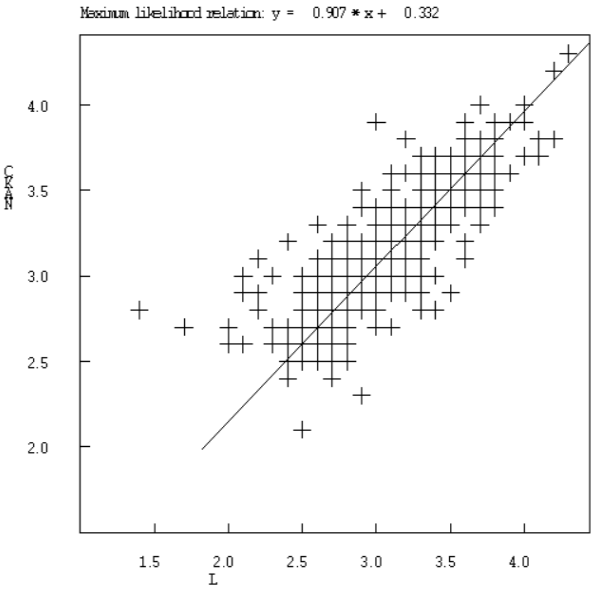

D to CKAN and d to CKAN